On the role of convective motion during dendrite growth:

Experiments under variable gravity

Final Report
NASA Contract # NASA-34605

J. Hallett
Principal Investigator

N. Cho, K. Harrison, A. Lord, E. Wedum, and R. Purcell
Desert Research Institute
Reno, Nevada 89506

C.P.R. Saunders
University of Manchester
Institute of Science and Technology
England

In collaboration with V. Keller, R. Owen and O. Vaughn

Marshall Space Flight Center
Huntsville, Alabama

TABLE OF CONTENTS

TABLE OF CONTENTS (Continued)

Abstract

Experiments show the effect of self-induced convection on individual dendrite growth in uniformly supercooled samples and solidification of the resulting mush under conditions of high (2) and low (.05) g. Convection is visualized by a Schlieren optical system or a Mach Zender interferometer. For ice crystals growing from the vapor in air, a slight reduction in linear growth rate occurs under low g. For ice crystals growing from NaCl solution, dendrite tip velocities are unchanged, but subsequent mush solidification is enhanced through drainage channels under higher g. By contrast, sodium sulfate decahydrate dendrites growing from solution produce convective plumes which lead to higher tip growth rate only as the crystal growth direction approaches that of gravity. Convective plumes are laminar for small (100 μm-mm) crystals under conditions of these experiments; the rise velocity of such plumes is greater than individual vortex rings under identical conditions. Convection effects are only present in solution under a critical supercooling less than about 5°C for sodium sulfate and 2°C for ice in sodium chloride since at higher supercooling the crystallization velocity, proportional to the square of the supercooling, exceeds the convective velocity, proportional to the square root of the supercooling. The role of convective velocity in bulk solidification is to give a large scale flow which under extreme cases may lead to extensive secondary crystal production, which alters the resulting crystal texture of the completely solidified melt. Suggestions are made for further studies under more highly controlled conditions of a shuttle/space station environment. Future experiments for investigating the fundamental aspects of both extreme crystal growth habits and associated fluid motion should utilize a variable g environment from $< 10^{-3}$ to at least 2 g.

1. INTRODUCTION.

Change of phase in any physical system is critically linked to two processes. First, nucleation requires a thermodynamic driving force to overcome a potential barrier to form an embryo large enough to grow rather than dissipate under the ambient conditions. Second, the mass and heat transfer process is limited by both kinetic phenomena at the interface between the two phases and molecular transport processes towards and away from the interface in the bulk of the material. These considerations have general applicability for all phase changes - solid - liquid - vapor, whether as pure materials, as a mixture, or as a solution. A special case arises when mass transport can be neglected, as for example in crystallization from a pure melt or vapor where growth rate is entirely determined by kinetic and heat transport considerations. Even in this case, in practice, trace impurity segregation at the interface may eventually lead to some limitation resulting from mass transport considerations, as in the case of - vapor → liquid → solid (V.L.S.) crystal growth. In a similar way, it is possible that heat transport can be neglected, and the situation be entirely controlled by mass transport or kinetic effects - as in the case of slow glass crystallization. In general, all three aspects of the crystallization process, heat transport, mass transport and interface kinetics must be assessed.

The nucleation process itself is often dominated by the presence of impurity nucleation centers, which prevent the occurrence of substantial supercooling or supersaturation. On occasion however, situations can be contrived where these centers are essentially absent and nucleation occurs by growth from large clusters of atoms and molecules arising by molecular fluctuations. This is homogeneous nucleation of the substance by itself as opposed to heterogeneous nucleation by impurity.

In practice, experimental techniques for the study of this process conveniently follow from the simple process of taking smaller and smaller samples until the probability of having impurity induced heterogeneous nucleation is reduced to insignificant levels. Nature effects this technique very effectively in clouds in the atmosphere, which consist of water droplets some 10 μm diameter, many of which can supercool to temperatures near - 40°C, to freeze by homogeneous nucleation (Mason, 1971). This situation is opposed to that of freezing of a bucket of water which readily occurs at less than a few degrees of supercooling by the chance occurrence somewhere throughout the volume of one impurity nucleus. Similar considerations apply for the solidification of all substances. A second complication arises in the freezing of large volumes in that secondary crystals may be produced in association with the primary growth. These crystals grow and are transported to places elsewhere in the melt either by induced fluid flow or because of their own buoyancy. In freezing rivers, these secondary crystals are readily visible as large numbers of "frazil" ice discs (Daly, 1984), which result in a complex polycrystalline structure of a frozen melt even though its freezing may have been initiated by a single crystal (Estrin, 1975). Similar phenomena and crystal textures occur in crystallizing metal ingots (O'Hara and Tiller, 1967; Garabedian and Strickland-Constable, 1974). A further complication arises at very large supercooling when nucleation of new crystal orientations may occur on a crystal already growing to give a poly-crystalline structure by quite a different physical process (Hallett, 1964; Knight, 1971), electrical effects may enhance the process (Evans, 1973).

The considerations outlined above can readily be carried over to crystallization of other systems. For example, ice and silicon have much in common (both expand on freezing), and the initial crystallization and subsequent freezing of liquid drops have similarities in spite of the difference of melting temperature.

Investigations of these phenomena may be greatly facilitated by study in an environment of low gravity. Particles of one phase in another are usually of different densities, and sediment by buoyancy. While suspension on fibers or a substrate is possible to avoid sedimentation in a gravity environment, such surfaces lead both to undesirable nucleation sites and to additional heat transport during growth. Second, natural convection occurs around particles of different phase because of the density differentials resulting from mass and temperature gradients in the fluid itself (Carruthers, 1976; Hallett and Wedum, 1978; Chen et al., 1979). In high gravity, this motion enhances both mass and heat transfer, and local fluid shears may lead to crystal fragmentation.

In the complete absence of fluid motion, with transport occurring entirely by molecular processes, instabilities develop which interact with the crystallographic anisotropy and lead to growth in non-spherical or non-cylindrical shape (Mullins and Sekerka, 1963). In this case the higher order solutions of the Laplacian of a spherical or the equivalent for a cylindrical diffusion field reinforce periodic variations in the crystal symmetry. Such instabilities are changed further by fluid motion (Glicksman et al., 1984; Fang et al., 1985; Glicksman et al., 1986) inducing periodicities different from or superimposed on those of the crystal structure itself. Similarly, hydrodynamic instability of boundary layer fluctuations when an imposed fluid flow is present may lead to fluctuation in impurity concentration (Carruthers, 1976). In the same way growth of a falling crystal will be influenced by both natural convection of the environment because of fluid density differences resulting from its growth, and its own fall velocity. The ultimate crystalline structure of a frozen melt or an aggregation of crystals grown from the vapor such as a snow pack, and its mechanical and electrical characteristics will be dramatically influenced by the detail of these parameters.

The ultimate structure of the whole aggregate - frozen melt or snow pack depends on two distinct processes. The initial processes result from crystal growth and crystal motion and sedimentation. The second process results from heat transport at the periphery. A supercooled melt begins crystallization by dendrite propagation throughout the volume, freezing a small fraction; f:

$$f = 1 - \frac{\sigma \Delta T}{L}$$

(σ = melt specific heat, L = fusion latent heat)

ΔT = supercooling

at small supercooling, followed by complete solidification from the outside. This may or may not be symmetrical, depending on the symmetry of the heat loss at the outside walls. Prior to complete solidification, bouyant fluid motion may occur within the mush, depending on the cell size (Powers et al., 1985, Huppert and Worster, 1985). Both stages may give rise to impurity distribution and segregation which lead to a complex structure; in the case of a substance which expands on freezing (as ice or silicon) internal pressures often lead to ejection of melt as a spike and possibly mechanical fracture. In the atmosphere or in a shot tower this can lead to drops of simple or complex structure depending on the conditions. The detailed structure of such frozen drops has implication in the use of solidified frozen metal droplets when used, for example, as the basis of material for powder metallurgy or solar cells.

This report describes experiments performed in the laboratory and in a gravity environment controlled by a maneuver of a KC135 aircraft. Experiments utilize short (20s) periods of low g in a parabolic trajectory and higher (1.8) g in pullout over a somewhat longer period. The studies form a basis for experiments which can uniquely utilize long periods of low g available on space station or shuttle environment to enhance our understanding of the role of convection in crystal growth.

2. EXPERIMENTAL.

a. The systems: Two quite distinct systems have been utilized to study growth of dendrites:

1. A volume of liquid is uniformly supercooled (supersaturated)* with respect to the solid phase. This is achieved by taking a tank of volume 10 to 1000 ml, and cooling it to a uniform temperature, such that nucleation does not occur. Uniformity of temperature, investigated by a probe traversing the volume is uniform to $\pm$ 0.1°C in these experiments. Nucleation is achieved in two ways. In the first case, a single crystal of known orientation is slowly inserted into the upper surface of the liquid; the subsequent growth takes place downwards into the liquid and may be single crystalline, isomorphic with the nucleating crystal, or polycrystalline depending on the temperature.

In the second case, nucleation is achieved by moving a small crystal or a liquid nitrogen cooled wire along a narrow tube which has one end above the liquid surface and ends in the bulk of the liquid. Crystals grow from the tube tip into the liquid, and may be single or polycrystalline depending on the nucleation process and the amount of supercooling (Fig. 1).

*FOOTNOTE: Strictly "supercooled" refers to the temperature difference between the actual temperature and the equilibrium crystal-liquid temperature; supersaturated refers to the ratio of excess concentration to equilibrium concentration at the liquid temperature (equivalent to relative humidity for water vapor). Convention uses supercooling for a pure liquid, and the solvent, (for example ice growth in supercooled NaCl solution) supersaturation for a vapor or solute (for example, NaCl crystals growing in a supersaturated NaCl solution). Any solution has the capability of being supercooled with respect to the solvent and supersaturated with respect to the solute. It could, in principle also be superheated with respect to boiling at the same time (Hallett, 1968).

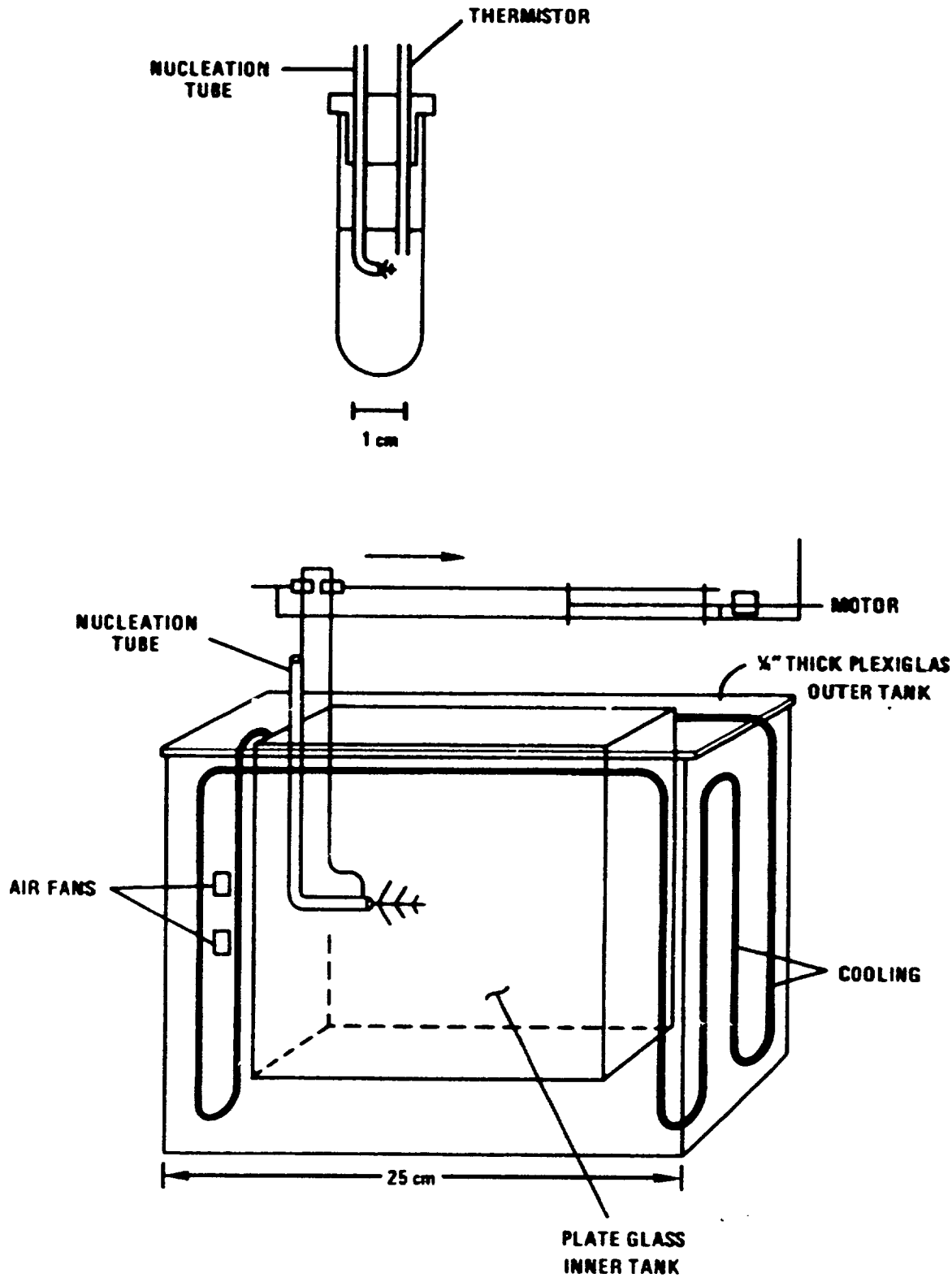

Fig. 1. a, b Containers for investigating crystallization of uniformly supercooled liquids. Nucleation is achieved by injecting a cold wire or a seed crystal into the narrow plastic tube. The larger container (b) enables the growing crystal to be moved at a fixed velocity up to 0.5 cm s^{-1} relative to the liquid. Volume (a) 10 ml, (b) 100 ml.

ii. Steady state supersaturation in a vapor can readily be achieved by using a thermal diffusion chamber. This comprises two horizontal parallel flat plates, both covered uniformly with the material being studied. The upper plate is maintained at a higher temperature compared with the lower plate. Since the vapor density gradient between the plates is approximately linear and the saturated vapor density (Clausius-Clapeyron relation) approximately exponential, the mid-region of the chamber becomes supersaturated, with a maximum just below the center. This value can be calculated in a situation where all aerosol and other growth sites are absent (Fig. 2a). Crystals readily grow on a narrow vertical rod in this region. This may require being cooled with liquid nitrogen to nucleate the crystals, which grow radially outwards. Crystals oriented at 90° to the support eventually outstrip the others to give well defined, individual single crystals. The chamber design is such that wall effects (both thermal and concentration) must be unimportant in the center region where crystals grow. This requires an aspect ratio, width: height > 7:1. [Katz and Mirabel, 1975] Fig. 2b.

In each case crystal growth is recorded by cine camera or VCR, using a long working distance optical system.

b. Ventilation

The effect of fluid flow on growth rate in these systems may be investigated in several ways. In the case of the growth of dendrites in solutions it is convenient to move the dendrites with respect to the stationary solution. This is achieved in practice by moving the tube and dendrites immediately after nucleation by a screw transport (Fig. 1b). In the case of the diffusion chamber, ventilation may be achieved by making the chamber part of a wind tunnel (Fig. 2c) such that air moves in a closed loop horizontally, the upstream length of the chamber being long enough to achieve equilibrium of the vapor density and temperature profile between the plates (Keller and Hallett, 1982).

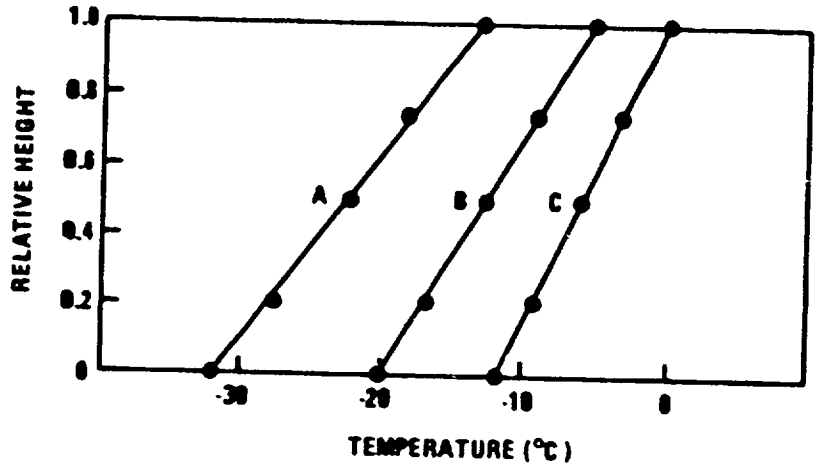

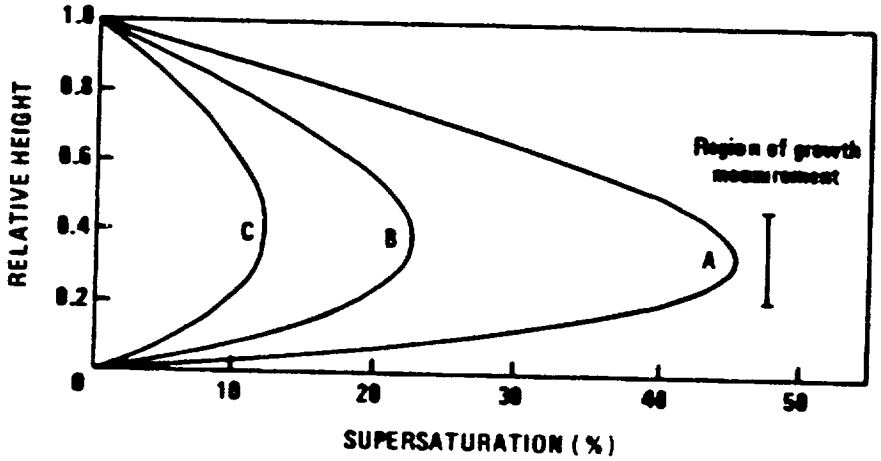

Fig. 2 (a) Thermal diffusion chamber for ice crystal growth from vapor under controlled temperature, and supersaturation. Typical temperature and supersaturation profiles
A 0.59°C mm^{-1} B 0.47°C mm^{-1} C 0.37°C mm^{-1}

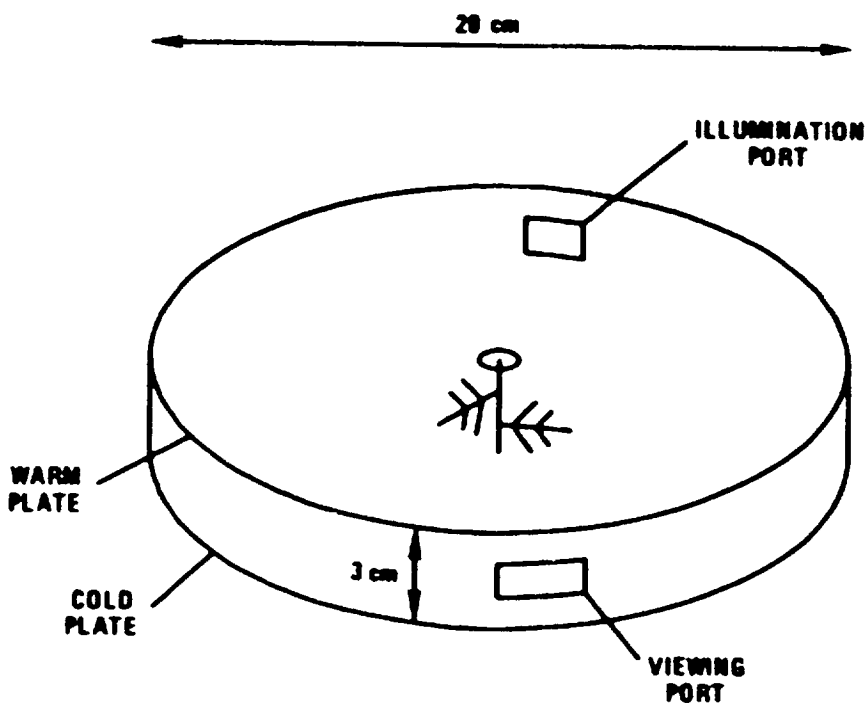

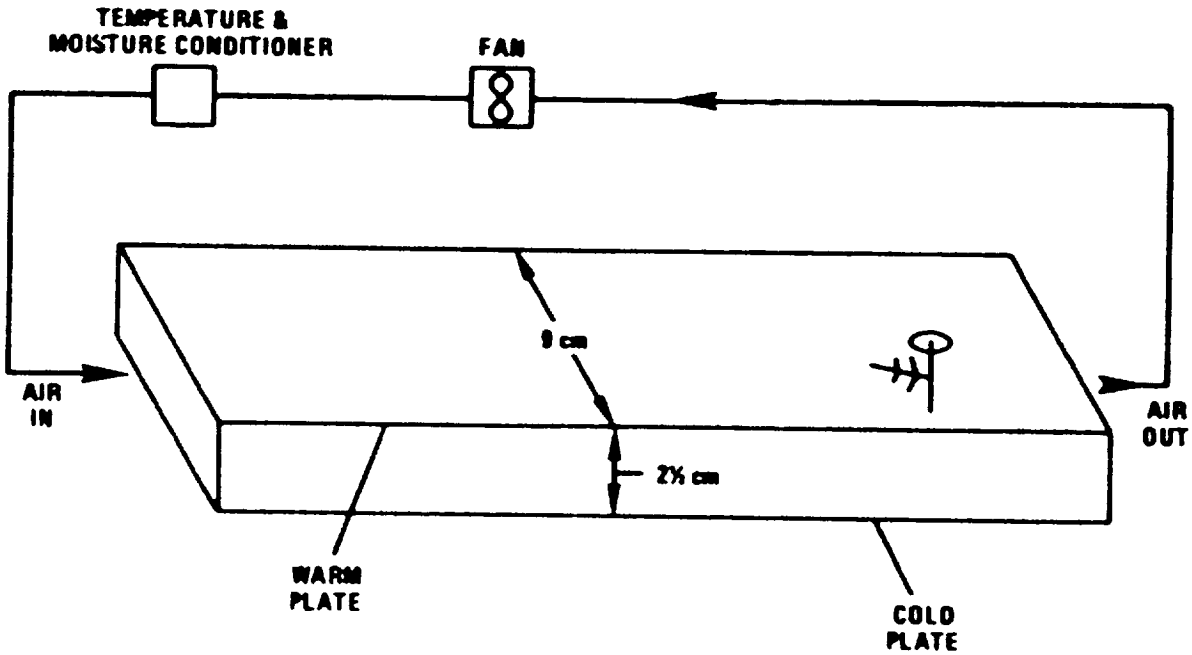

Fig. 2b Thermal diffusion chamber for ice crystal growth from vapor under controlled temperature, and supersaturation.

Fig. 2c The dynamic chamber for controlled ventilation at velocities up to $1/2_{m}$ s^{-1}.

Fluid motion also occurs by buoyant convection in low g. This may take place from the dendrites themselves, since these grow from the ambient fluid and give rise to local concentration and temperature gradients and hence density differences. Motion may also occur from the walls in the thermal diffusion chamber, since in practice, these walls need to be maintained slightly warmer than the linear temperature gradient imposed at the chamber center to prevent crystal growth on the viewing windows.

In the case of an imposed motion, velocity can be measured directly. The crystal orientation with respect to the motion can also be selected by rotating or tilting the rod or tube. The effect of self-induced convection can only be investigated under specific conditions. It is impracticable to use particle tracers for fluid flow visualization (using for example a Doppler velocimeter) since particles will have unknown effects on the crystal growth. Refractive index discontinuities can be visualized using Schlieren optics or a Mach Zender interferometer, the limitation here being that the effect is integrated along the line of sight through the solution, and depends on the integrated refractive index change along this path being great enough. Such an arrangement can display the overall density (refractive index) patterns, and give velocity magnitude and direction should minor perturbations in flow occur. The effect of the flow on growth can be investigated in a non-steady state under conditions of low (0.05) g in KC135 parabola. As soon as low g is reached, motions - both locally near dendrites and overall motions from the chamber walls would be expected to die out with a time constant

$$\sim \frac{d^2}{\nu}, \qquad \begin{array}{l} d \text{ -- system or dendrite size} \\ \nu \text{ - kinematic viscocity} \end{array}$$

with growth continuing after ~ 5 time constants uninfluenced by any further motion.

c. Visualization

Density gradients around a growing crystal can be visualized through the associated gradient of refractive index. A simple technique uses a Schlieren optical system (Fig. 3a). Two large focal length mirrors produce a parallel beam through the growth region, with a point arc lamp as source, and a knife edge at the focus. With uniform medium in the path, no light passes beyond the knife edge; refractive index gradients deflect the light to give bright regions where the effect is greatest (Holden and North, 1956). From a consideration of successive shallow layers thickness dz, refractive index change dn, from the environment n_o we can show that the angular deviation is given approximately by

$$\frac{L}{n_o}\frac{dn}{dz}$$

The actual deviation will depend on the profile of $\frac{dn}{dz}$ in the direction of viewing and will be represented by an integration over L of the above expression.

The geometry of the layer is obviously very important. A flat slab gives no deviation to the beam whereas a wedge will give a deviation to be computed from the usual relation for a prism, with, either a greater or lower refractive index than the environment. A better approximation could be achieved with a parabolic profile to represent the usual boundary layer shape. In the experiments to be described, the dimension of the region influenced by the growing crystal is ~ 1 mm. Taking the spot size, d, for a zero magnification with identical mirrors as 3 mm, an effect would be expected for angular deviation of $\frac{d}{f} \sim 0.1°$ (f = mirror focal length 1.54 m in these experiments). This gives $\frac{dn}{dz}$ as $\sim 10^{-3}$ mm^{-1}. This provides a practical lower limitation to the density and hence refractive limitation of plumes that can detected by this technique.

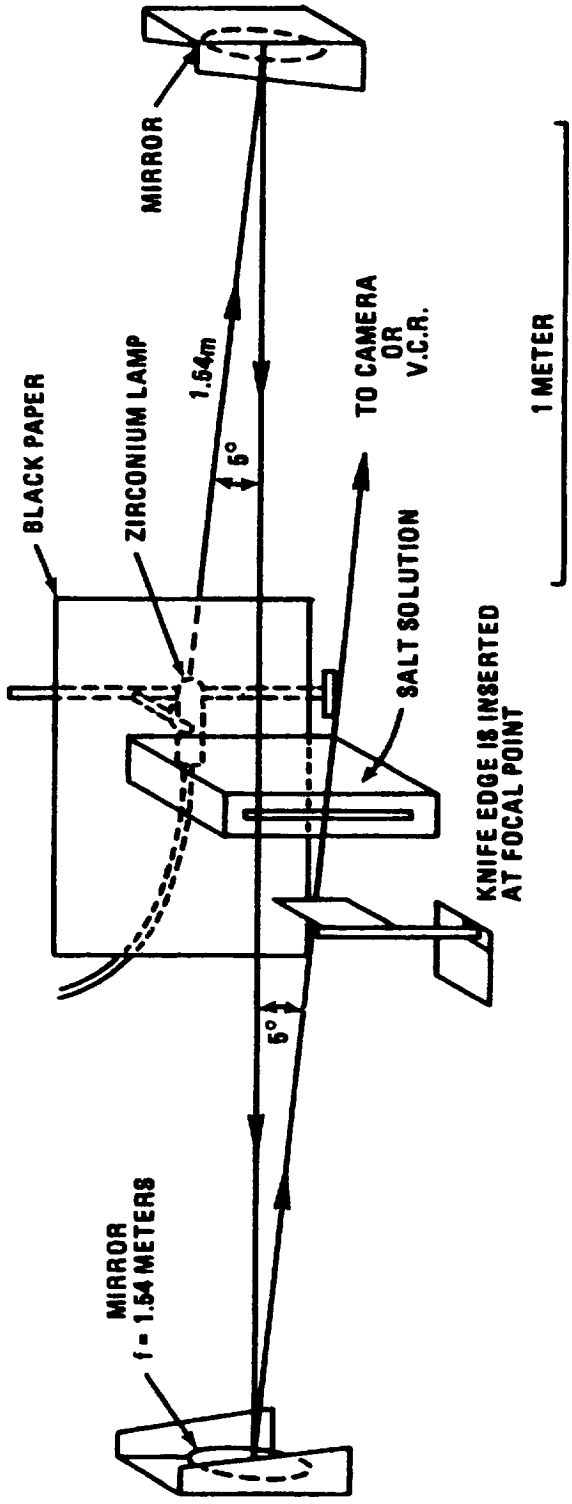

Fig. 3a Schlieren optical system for investigation of crystal growth in solution.

A more precise technique which is capable of direct measurement of path difference uses an interferometer technique. For a large system (capable of holograph recording) the Mach Zender interferometer is set up to give parallel interference fringes using a monochromatic light source, (Owen, 1982) (Fig. 3b). Gradients of refractive index are manifest as deformation of the interference pattern. The interference technique was first used by Humphries-Owen (1949) to investigate the diffusion field around a growing crystal between optical flats; the Mach Zender interferometer gives a much greater working volume well separated from the optical surfaces. For a refractive index difference of Δn over a length L for the one wavelength difference between fringes.

$$\Delta n = \frac{\lambda}{L}$$

λ = wavelength of light.

This gives Δn of 6.3×10^{-4} for $\lambda = 632.8$ nm and L = 1 mm.

The difference between fringes can usually be resolved to better than 1/10 fringe width, so it is clear that the interference technique is capable of considerable precision; the inherent design compensates for environmental temperature changes. The advantage of the Schleiren system is that it is very simple to set-up and record, not too sensitive to vibrations and local air convection currents; it gives a large field of view, although only a qualitative picture of the convection process. In these studies, the Schlieren system was used in the laboratory, and the NASA Mach Zender system in the KC135 studies.

3. THEORETICAL CONSIDERATIONS.

a. Thermal and mass balance.

Some insight into the density differences surrounding growing crystals can be obtained by a simple heat balance analysis. This has been examined in detail by O'Hara and Reid (1973) for solution and Mason (1971) for vapor growth.

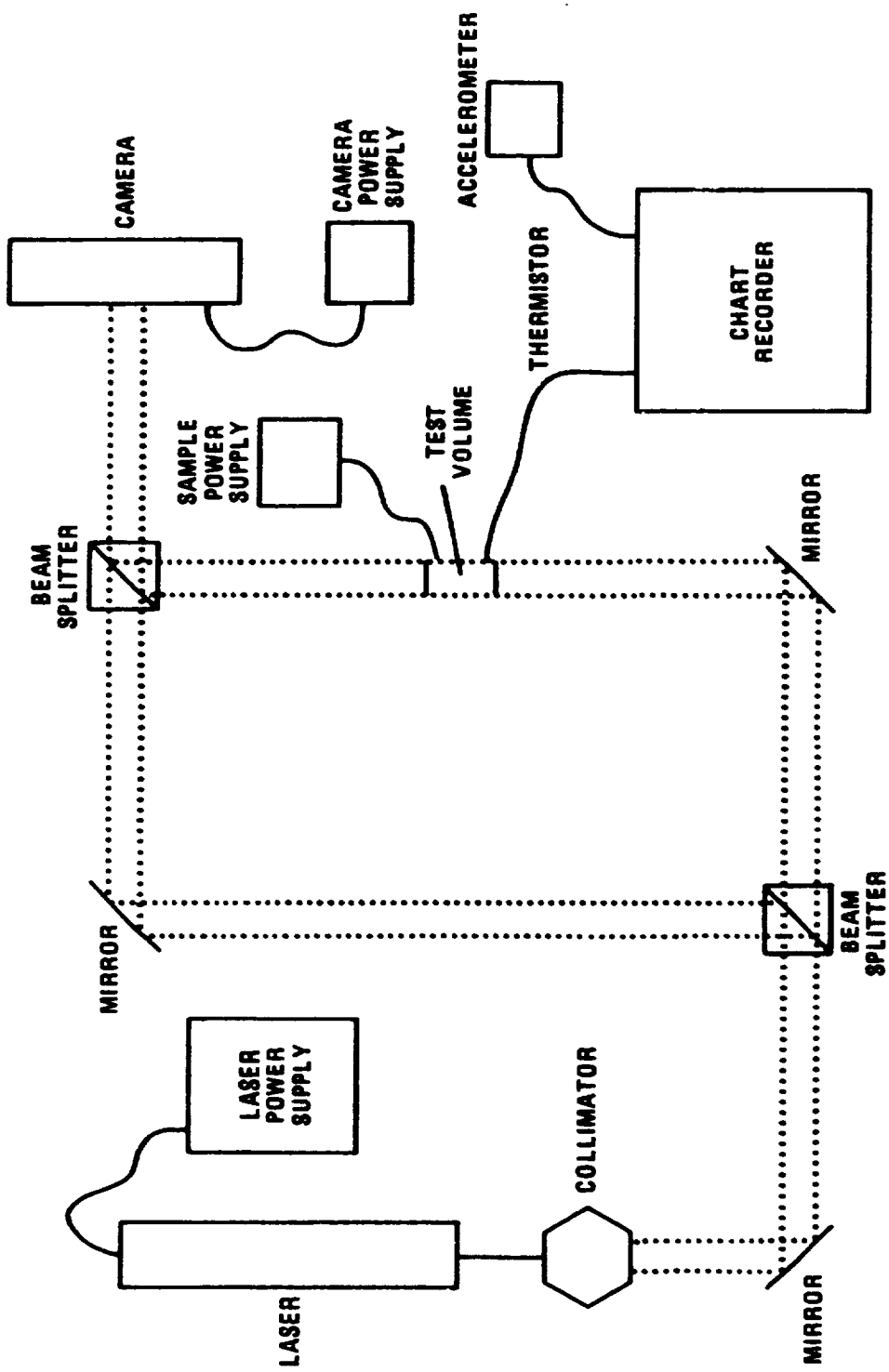

Fig. 3b Mach Zender interferometer for KCl35 solution growth study.

Consider a spherical crystal growing from a supercooled or supersaturated environment. Heat transport can be represented by

$$\frac{dQ}{dt} = - 4\pi r K(T_s - T_\infty) F_H \qquad \ldots\ldots 1$$

Where r, crystal radius, which can be replaced by electrostatic capacitance for non-spherical shapes

T_s, T_∞, surface temperature (considered uniform) and environmental temperature

K, thermal conductivity of the environment

F_H, enhancement by fluid motion

and mass transport by

$$\frac{dm}{dt} = + 4\pi r D(\rho_s - \rho_\infty) F_M \qquad \ldots\ldots 2$$

D, diffusion coefficient

ρ_s, ρ_∞, surface density (considered uniform) and environmental density

F_M, enhancement by fluid motion

As a first approximation, we assume that ρ_s, and T_s are at equilibrium and given by the Clausius-Clapeyron equation. The equations ignore crystallographic and kinetic effects, which give anisotropy and invalidate the above assumption of equilibrium.

Under steady state conditions, there is a balance between outward heat transport and latent heat released by growth:

$$L \frac{dm}{dt} = \frac{dQ}{dt} \qquad \ldots\ldots 3$$

where L is the appropriate latent heat.

This gives

$$\frac{\rho_s - \rho_\infty}{T_s - T_\infty} = - \frac{K}{LD} \cdot \frac{F_H}{F_M} \qquad \ldots\ldots 4$$

with $F_H = F_M = 1$ for molecular processes without motion.

It is convenient to examine the solution of the equations graphically (Fig. 4). The full line here represents the equilibrium relation between the concentration (solution) and vapor density (gas). The point T_∞, ρ_∞ represents the environmental conditions, which are assumed to remain unchanged during the experiment. Equation (4) represents the equation of a straight line, which passes through this point and intercepts the curve at T_s, ρ_s the surface conditions of the crystal. Extreme cases arise for small diffusion coefficient $LD \ll K$, making the line nearly vertical - there is no significant increase of temperature; density difference is given directly by $\rho_s (T_\infty) - \rho_\infty$ (Fig. 4). For large $LD \gg K$ on the other hand and for a pure material, the slope approaches zero, and the surface temperature increases to that where the vapor pressure is close to that of the environment, which limits the rate of growth.

For ice crystals growing from the vapor in air at 1 atmosphere, $LD \approx K$ so that the surface temperature lies somewhere between. In practice the surface temperature of the growing crystal is also influenced by the effective curvature through the Kelvin effect and the molecular kinetics of the surface. These are orientation dependent for a crystal which implies that the actual growth rate and surface temperature are orientation dependent which requires a much deeper level of analysis and is currently an important topic in crystal growth [Huang and Glicksman, 1981a,b; Glicksman, 1984; Laxmanan, 1985 a,b,c; Tewari and Laxmanan, 1987]. Strictly, this analysis is applicable to a solid sphere, and to a first approximation a dendrite tip and the local fluid can be so considered. The analysis cannot be applied directly to an array of dendrites, where liquid between the dendrites is heated towards the equilibrium point. Under these conditions, the environmental temperature rises successively as crystal growth continues through the bulk of the liquid (Fig. 5) until it approaches the equilibrium point and crystallization ceases (adiabatic crystallization).

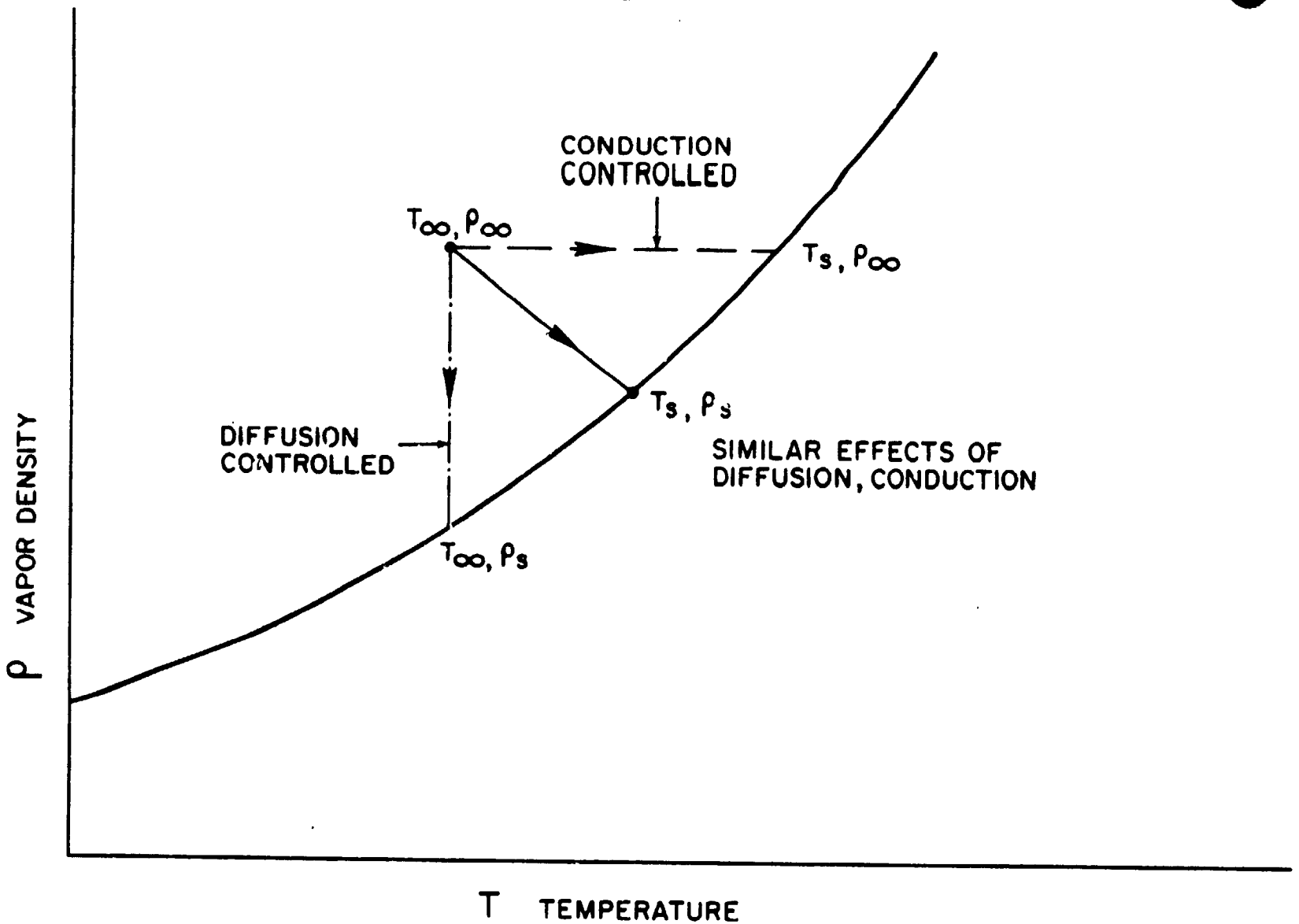

Fig. 4 Growth condition in a vapor with variable carrier gas diffusivity. Conduction dominates in the absence of a carrier gas, and the crystal surface temperature approaches that for a vapor pressure at the environmental temperature. When diffusion dominates (carrier gas at high pressure) the crystal and environment are almost isothermal.

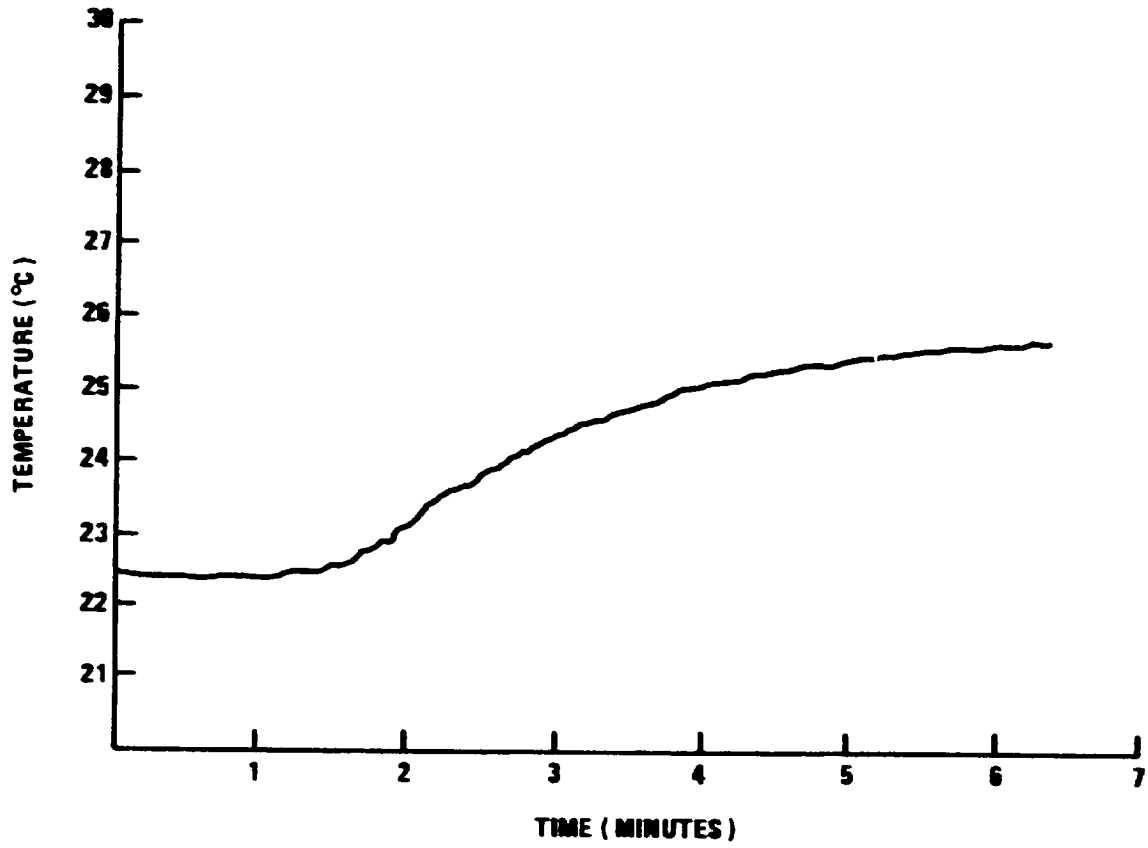

Fig. 5 Increase of Temperature with Time during Adiabatic Crystallization of Sodium Sulfate decahydrate from solution. Trace of temperature recorded by thermocouple shown in Fig. 1a. Crystallization appeared complete after 2 minutes, but final temperature was not reached until 4 minutes later.

In the case of growth in a pure liquid, latent heat from the growth of an individual dendrite passes into the environment to inhibit the growth of neighboring crystals, giving rise to a specific dendrite and dendrite arm separation. Under these conditions, a mushy system ensues (called spongy ice for water) in which a fraction $1 - \frac{\sigma\Delta T}{L_f}$ remains liquid and in which the temperature has risen to a value approaching T_o, coming to equilibrium at a mean Kelvin radius of the crystals. The equilibrium temperature in this case (ice - solution) is not that of the original solution, since, some ice has formed and rejected ions to give a higher concentration, and a corresponding further lowering of the equilibrium temperature (Fig. 6). It is clear that the time for this crystallization, (as ice in water or solution) is much shorter than for sodium sulfate (Fig. 6). This demonstrates the role of crystal kinetics during solidification; there is evidently a rate limiting process for decahydrate growth at a few degrees supercooling (growth on screw dislocations) which is absent for ice growth (growth on a molecularly rough surface). Temperature changes over a long time (1000 s) on the scale of 0.01°C result from changes of equilibrium radii of the crystals (Glicksman and Voorhees, 1985). If such a system is large (a magma chamber, a supercooled tank or lake) the interior regions may be isolated thermally and diffusionally form the outside, the mechanical structure of the crystals inhibiting significant fluid motions when the interstice size is small. In the case of growth from a pure vapor, (density $\sim 10^{-3}$ liquid) the ambient vapor presure can lie below or above that of the triple point. In the former case, growth may occur in skeletal crystal form, similar to the liquid but at a much slower rate; in the latter case the crystal surface temperature can rise by released latent heat above the triple point and all crystals melt.

In summary, the crystallization of a vapor/liquid is limited by the presence of a diffusing medium and by the way in which crystals grow. The density excess

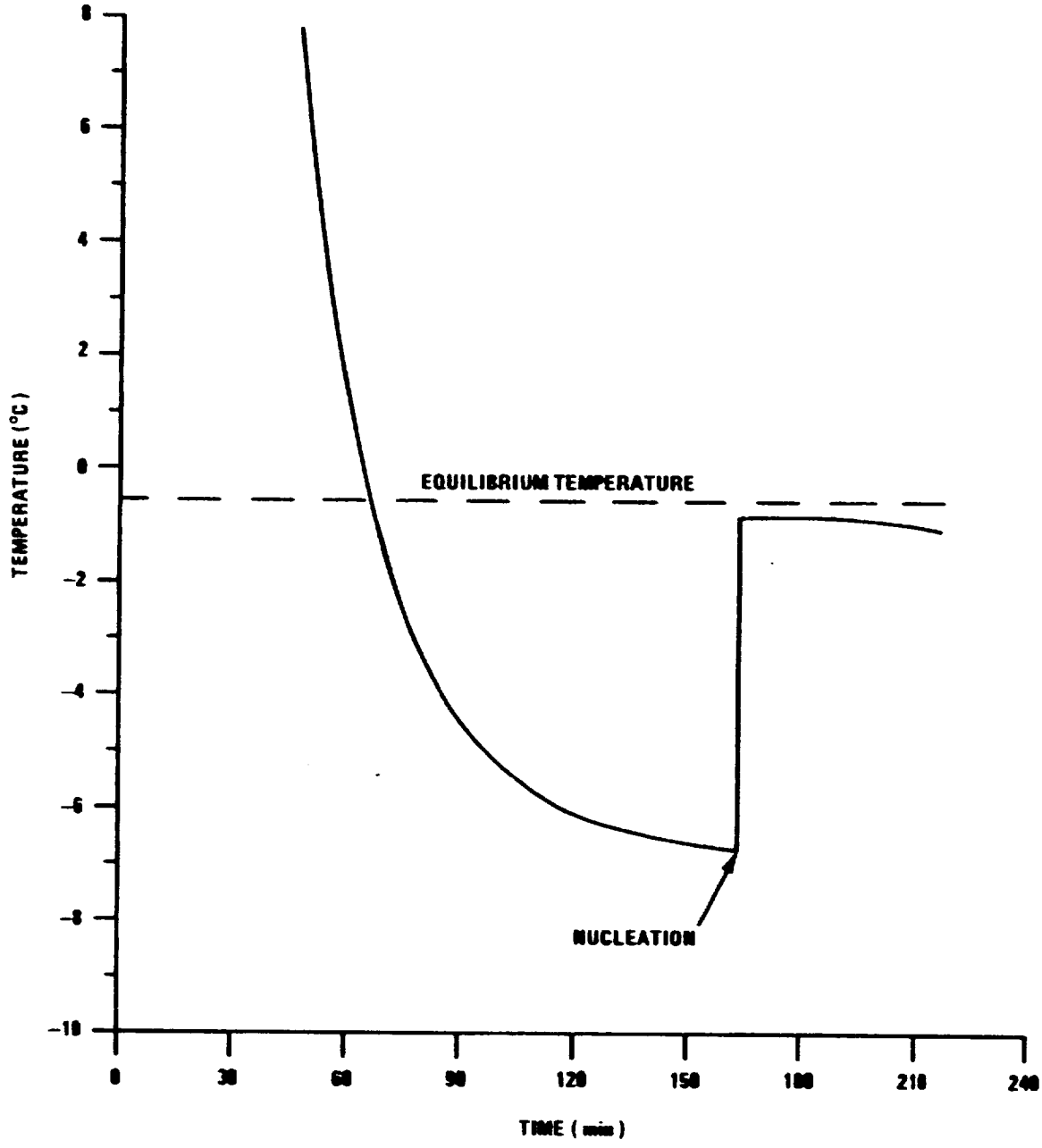

Fig. 6 Increase of temperature following adiabatic crystallization of ice from NaCl solution. Note that the initial temperature of the solution is 0.25°C below that of the equilibrium temperature of the original solution; resulting from solute rejection during ice crystal growth.

around the growing tips cannot be computed from first principles, since estimating the feedback of the environmental conditions on the shape and kinetics of the crystals is beyond our current ability. The studies reported here are designed to investigate some aspects of the growth systems from the viewpoint of giving insight into the physical parameters of importance.

b. Role of fluid motion in crystal growth.

When a phase change takes place, with one or both phases a fluid, density differences in the fluid resulting either from changes of composition or differences of temperature through latent heat release, as described in the last section, lead to local buoyant convection. In addition, more organized motion may exist which results from an overall driving force - for example dendrites grow into a cooling melt with an overall cellular circulation of the dimension of the melt induced by cooling at the upper interface (Gilpin, 1976).

In general, the onset of convection is given by the Raleigh number, $Ra = \frac{\Delta\rho g}{\rho} \frac{d^3}{\kappa\nu}$ where, $\frac{\Delta\rho g}{\rho}$ is the buoyancy in a system diameter d, thermal diffusivity κ, and kinematic viscosity ν. This parameter represents the ratio of buoyant and viscous forces in a fluid such that a parcel of fluid will traverse a distance d before significant diffusion of heat and momentum to the environment takes place. For convection between horizontal surfaces experimental studies show that convection cells begin for $Ra > 650$; for a tilted or vertical surface some influence of convection would be expected for values of $Ra > 1$ (Turner, 1973).

In the case of crystals growing in a fluid the idealization of a plane horizontal surface is clearly not applicable. It is necessary to specify first the geometry of the growth interface and the associated buoyancy excess; the work to be described later examines this problem experimentally. In the case of natural convection, with a specified buoyancy excess, the heat transfer can be related

to a Grashoff number, $Gr = \frac{Ra}{Pr}$; (Pr = Prandtl number $\frac{\upsilon}{k}$ and the Nusselt number Nu, ($\equiv F_H$, F_M,) selected by dimensional considerations:

$$Nu \alpha Gr^{1/4}$$

For forced ventilation on the other hand with a prescribed velocity, the heat transfer can be related to a Reynolds number Re,

$$Nu \alpha Re^{1/2} \alpha Velocity^{1/2}$$

If we assume that a buoyant force is balanced by the drag force for large Reynolds number, with dominant inertial forces, we have:

$$\frac{4}{3} \pi d^3 \Delta\rho g = 1/2 \rho U^2 C_D \pi d^2 \quad . \quad . \quad . \quad . \quad . \quad 5$$

Hence,

$$U \alpha \left(\frac{\Delta\rho g}{\rho} \frac{d}{C_D}\right)^{1/2}$$

where C_D is the drag coefficient of the buoyant fluid parcel.

Conversely, for small Reynolds number and dominant viscous forces

$$\Delta\rho g \delta^3 = \frac{\mu U}{\delta} \quad . \quad . \quad . \quad . \quad . \quad 6$$

$$U \alpha \frac{\Delta\rho g \delta^2}{\mu} \quad \text{or} \quad \alpha \frac{\Delta\rho g d^2}{\mu}$$

Where δ = flow dimension ~ d crystal dimension and μ is the fluid viscosity.

From these dimensional considerations, the convection velocity dependence changes as the individual flow becomes turbulent. In the case of a naturally convecting system with increasing ventilation, a general relationship

$$Nu \alpha Gr^{1/4} Re^{1/2}$$

would be expected in the transition regime

One other parameter of interest is the time constant for initiation of a convective plume. This may be computed to sufficient approximation by assuming a coherent sphere (radius d) of fluid of appropriate excess density starting from rest at the growing crystal. For viscous force domination this can be

written

$$\frac{4}{3}\pi d^3\rho \frac{dv}{dt} = 6\pi\eta dV - \frac{4}{3}\pi d^3(\rho - \rho_g)g \quad . . . . 7$$

where V is the changing velocity in time t, ρ, ρ_g density of the fluid surrounding the sphere and of the environment, of viscosity μ. The solution gives a velocity increasing exponentially to a limit

$$V = \frac{2}{9} d^2 \frac{(\rho - \rho_g)}{\eta} g \quad . . . . . 8$$

with a time constant

$$\tau = \frac{2d^2\rho}{9\eta}$$

Approximate values are shown in Table 1 for different situations. Reynolds numbers are computed from observed convective velocities and indicate a lack of turbulence in the convective phase. The small values of Re indicate no induced convection at a horizontal surface; however, convection obviously occurs at a sloping or vertical surface (Re > 1) when these criteria do not apply, although little could be expected for the case of ice in air for smaller crystals under the specific conditions of Table 1.

In the case of flow at larger buoyancy, giving larger velocity and higher Reynolds number we may write

$$\frac{4}{3}\pi d^3(\rho - \rho_g) g = \frac{1}{2} \rho U^2 \pi d^2 C_D \quad . . . . 9$$

where C_D is an empirical drag coefficient and a function of Reynolds number. In this case

$$U \alpha \sqrt{\frac{(\rho - \rho_g) gd}{\rho C_D}} \quad . . . . . 10$$

This is to be compared with the direct dependence on $(\rho - \rho_g)$ g for viscous flow.

TABLE 1

Quantity	Re		Gr		Ra		τ (s)	
Dimension	cm	mm	cm	mm	cm	mm	cm	mm
Ice crystal in Air σ = 10%	0.5	0.05	100	0.1	100	0.1	1	10^{-2}
Ice crystal in water (large tank)	50	5	50	0.05	0.5	0.005	13	0.13
Sodium Sulfate deca-hydrate from solution (2M) ΔT = 5°C	2	0.2	3×10^{5}	300	9×10^{5}	900	7	0.07
Sea Water ΔT = 2°C	5	0.05	5×10^{6}	5×10^{3}	5×10^{7}	5×10^{4}	10	0.1
Freezing Drop in Air ΔT = 15°C	50	5	10^{4}	10	10^{4}	10	1	0.01

A comparison of characteristic quantities for a sphere of indicated diameter growing under specified conditions in vapor and liquid. The Reynolds Number is computed from an observed convective velocity and a plume dimension; such low values indicate laminar flow in all cases. Raleigh Number, Ra < 1 indicates lack of any influence of convective motion on heat transport. τ is the computed time constant to initiate convection of the given dimension for a sudden change of gravity. Cm dimension is typical of the growth cell; mm of the crystal.

4. DIMENSIONAL AND PRACTICAL CONSIDERATIONS IN CRYSTALLIZER DESIGN.

a. Diffusion chamber - steady state system.

A crystal growing in the center of the chamber under conditions of these experiments has a growth rate up to 10 $\mu m\ s^{-1}$, and grows up to 1 - 2 cm long. Individual crystals are selected for measurements, growing horizontally: excess crystals may be removed by shaking and once one crystal is ahead of the others, it is favored for growth. The chamber achieves steady state, once the temperatures are set with time constant

$$\tau_H \sim \frac{x^2}{\kappa}$$

Where κ is the water vapor or thermal diffusivity of the system $\sim 0.2\ cm^2\ s^{-1}$

With $x = 1\frac{1}{2}$ cm, $\tau_H \sim 10$ s

A more practical consideration is that on start-up, nuclei in the chamber need to be rained out, so that the air is quite particle free and will enable a supersaturation to be achieved. This takes 10–20 minutes and can be monitored separately by a laser scattering experiment. The time constant for internal convection in the chamber - caused by heat flow from the warmer sidewalls towards the chamber interior is similarly

$$\frac{d^2}{\nu}$$

With $\nu \sim 0.2\ cm^2\ s^{-1}$ and $d \sim 3$ cm gives $\tau_m \sim 50$ s. This means that large scale (chamber size) convection will die out with this time constant. In this experiment, this scale of motion will not be eliminated during the typical low g of 20 s - it may be reduced by a factor of 0.25 to 0.75. Motion around a dendrite tip on the other hand, with much smaller size (< 0.5 cm), would die away with a time constant of < 1 s which can be neglected.

b. Solution growth.

Residual convection in the chamber is neglected with temperature uniformity of $\pm$ 0.05° C. With crystal growth from the chamber center towards the walls, two limiting interactions are possible. First, a thermal wave may spread out to the walls, and the whole system may warm up, changing conditions for subsequent crystal growth so the situation is no longer adiabatic.

The time for this to occur is

$$\tau = \frac{x^2}{\kappa}$$

$x = 1$ cm

κ water $\sim 10^{-3}$ cm s^{-1} ~ 1000 s

This can evidently be neglected in any low g experiment. Even in the large tank experiment, $x \sim 10$ cm, with slow growth observed over 100 s, these considerations can be neglected. It is pointed out however that in very slow growth experiments, with crystals growing over several days, these considerations are of major importance, with heat conducted to the chamber walls being removed by the cooling system, so that the adiabatic condition no longer applies.

A further consideration comes from mass transport by diffusion. Crystals growing in the center of the chamber establish an approximate spherical diffusion field, which in the absence of convection reaches steady state in a time $\sim \frac{R^2}{D}$

For a crystal 1 mm - 1 cm diameter, D $\sim 10^{-5} cm^2 s^{-1}$ gives 10^3 to 10^5 s. These times are long for all experiments conducted here; however they are of concern in long periods of slow growth which could be attained in a shuttle or space station environment. The time constant for initiation and stilling of the solution under this condition is $\tau \sim \frac{x^2}{\nu}$

For solution, $\nu \sim 10^{-4}$ cm^2 s^{-1} and $\tau \sim 10^4$ s. Hence under KC135 low g of 20 s, <u>large</u> scale stilling will not occur.

On the other hand, time for initiation of convection from a small buoyant blob is short. This can be assessed by consideration of the sudden release of a buoyant sphere of liquid, and computing the time constant for acceleration.

If we assume that a buoyant force is balanced in steady state by the drag force for large Reynolds number with dominant inertial forces we have:

$$\frac{4}{3}\pi r^3 \Delta\rho g = \frac{1}{2}\rho U^2 C_D \pi r^2 \qquad \ldots\ldots 11$$

Hence,

$$U \propto \left(\frac{\Delta\rho g}{\rho}\frac{r}{C_D}\right)^{1/2}$$

where C_D is the drag coefficient of the buoyant fluid parcel.

For small Reynolds number and dominant viscous forces on the other hand:

$$\frac{4}{3}\pi r^3 \Delta\rho = 6\pi\eta r U \qquad \text{and } U = \frac{9}{2}\frac{\Delta\rho r^2}{\mu}$$

where μ is the fluid viscosity.

Hence, the velocity dependence changes as the individual flow becomes turbulent, the velocity in this case resulting from the buoyancy. The time constant for initiation of a convective plume may be computed to sufficient approximation by assuming a coherent sphere (radius d) of fluid of appropriate excess density starting from rest at the growing crystal and solving the non-steady state equation. For viscous force domination this can be written

$$\frac{4}{3}\pi d^3 \rho \frac{dV}{dt} = 6\pi\eta d V - \frac{4}{3}\pi d^3 (\rho - \rho_E) g \qquad \ldots\ldots 12$$

where V is the changing velocity in time t, ρ, ρ_E fluid density of the fluid surrounding the sphere and of the environment, of viscosity u. The solution gives a velocity increasing exponentially to a limit

$$V = \frac{2}{9} d^2 \frac{(\rho - \rho_E)}{\eta} g \qquad \ldots\ldots 13$$

with a time constant

$$\tau = \frac{2d^2\rho}{9\eta}$$

In the case of flow at larger bouyancy, giving larger velocity and higher Reynolds number we may write

$$\frac{4}{3}\pi a^3 \rho \frac{dv}{dt} = \frac{1}{2}\rho_E V^2 \pi a^2 C_D - \frac{4}{3}\pi a^3 (\rho - \rho_E) g \quad . \quad . \quad . \quad . \quad 14$$

where C_D is an empirical drag coefficient and a function of Reynolds number. In this case the time dependence comes from the solution of

$$\frac{dv}{\frac{3}{8}\frac{\rho_E}{\rho}\frac{C_D}{d}v^2 - \frac{(\rho - \rho_E)}{\rho}} = dt \quad . \quad . \quad . \quad . \quad . \quad . \quad . \quad . \quad 15.$$

For the present case, the Reynolds number is small both for vapor and solution growth. This gives for ice in air cm, mm τ = 1, .01 s; for a sodium sulfate crystal, τ = 7, .07 s.

It follows that the transient for a mm crystal can be neglected in both cases, although for a large crystal in solution, the steady state convection may not be attained.

A further practical conclusion emerges from this analysis, since the plume velocity increases as $(\Delta\rho)^{1/2}$ or as $\Delta\rho$ or $(\Delta T)^{1/2}$ or ΔT and the crystallization velocity for free growth increases approximately as ΔT^2, (Hallett, 1964; Jackson et al. 1965). There is evidently a critical supercooling beyond which self induced convection will not have time to begin. The utility of studies in low g will lie near or below this value of supercooling.

With increase of Grashoff number, and before the transition to turbulence, some oscillation of the convective phase may become evident; (as discussed for example by Carruthers, 1976; Curtis and Dismukes, 1972; Hallett and Wedum, 1978). This could lead to some oscillatory characteristic of the growth and needs to be taken into consideration for these studies under appropriate conditions; indeed it is this oscillation which is used to indicate velocity of a non-steady plume.

These convective effects may, in addition to enhancing mass/heat transport process, also give rise to kinetic changes as manifest by transitions of the kind

discs → plate → dendrite and columns → needle

with increase of supersaturation. [Keller, McKnight and Hallett, 1979]. This transition is expected to occur at a critical supersaturation and could be highly sensitive to the presence of low convective velocities; it is linked closely to the detail of the way in which molecules are transported from the surrounding fluid to the crystal and the thickness of the boundary layer. [Bennema, 1969; Gilmer and Bennema, 1972; Ovinko et al., 1974; Kirkova and Nikolaeva, 1983; Glicksman et al., 1986].

5. THE SYSTEMS.

The purpose of this study is to investigate the effect of imposed and self-induced convection on crystal growth. These systems were chosen for study partly from physical considerations (liquids, vapor, transparency to visible light, visibility of convective phase), partly for convenience (no high/low temperatures) and partly for ease in demonstrating the importance of utilizing a low gravity environment in studying fundamental aspects of crystal growth.

a. Ice crystal growth from the vapor in the presence of a carrier gas.

This situation was investigated using a static thermal diffusion chamber to produce a known temperature and supersaturation and the KC135 to give changes in gravity. Typically, gravity varied from > 1.8 to ± 0.05 g with low g being maintained for ~ 20 s. Temperatures from 0°C to -25°C were available with saturation ratios up to about 1.5. Carrier gas could be changed at will from air to helium at a known pressure. The results could be compared with snow crystal growth in the atmosphere under 1.0 g and in the laboratory both under static and ventilated conditions. The differential optical path was much too short to visualize the motion in these experiments.

b. Sodium sulfate decahydrate crystals in solution.

Sodium sulfate solution can be readily supercooled in large volumes up to 1000 ml. As crystals grow, low concentration solution is produced near the dendrite which leads to upward convection and can readily be viewed optically beyond a critical concentration. Results can be compared with laboratory results in low g and with forced ventilation resulting from moving the growing crystal at known speed through a supersaturated solution.

c. Ice crystals in sodium chloride solution.

Sodium chloride solution can be readily supercooled (as can pure water) in values ~ 10 ml. As ice grows solute is rejected at the interface, the denser solution convecting downwards. Beyond a critical concentration, the plume is readily visible in an optical system.

6. CONDITIONS FOR CONVECTION.

It is evident, for values of Raleigh Number less than unity, (Table 1, p. 25), even in the case of boundaries oriented vertically in a gravitational field, any motions - and their influence on the crystallization process - will be small. With high values of supersaturation, larger values of Raleigh number may be present, and the effect of self-induced convection may become apparent. We examine a number of specific situations; bearing in mind that bouyancy results from both temperature and concentration gradients.

a. Ice crystal growth from vapor.

The excess temperature resulting from latent heat released will always give rise to an upward buoyancy around the crystal; in addition, there will be a difference in water vapor density between crystal and environment which can be expressed as a virtual temperature, the temperature which is required to give the same density if only pure air is present. The cases of ice growth in air and

helium are different since the molecular weight Air: Water vapor: Helium are 29: 18: 4. Hence for growth in air, there is a tendency to lessen the buoyancy caused by temperature increase near the crystal; the converse is true for growth in helium. An upper limit of the temperature excess may be estimated from the equations given earlier:

$$T_s - T_\infty = \frac{L_v}{4\pi Kr}\frac{dm}{dt} = -\frac{L_v D}{K}(\rho_s - \rho_\infty) \quad . \quad . \quad . \quad . \quad 16$$

D is inversely proportional to pressure, and K varies negligibly with pressure; both vary slowly with temperature. Hence the temperature excess varies inversely as the pressure of the carrier gas, and for a given water vapor supersaturation, depends on D/K for the carrier gas. This shows that the temperature difference for air is approximately twice that for helium (Table 2), and is inversely proportional to pressure. The values of temperature difference computed for an excess vapor density supersaturation of 10% (saturation ratio of 1.1) give excess temperatures of + 0.86°C (air) and + 0.49 (Helium). Saturated air at - 5°C has a virtual temperature increment of + 0.4°C compared with dry air; (density of the vapor is 3.24 gm^{-3}). For a saturation ratio of 1.1 this gives a difference of 0.04°C. In helium on the other hand, the increment is of opposite sign and larger by the ratio of the molecular weights (29/4), which give a difference of - 0.29°C. The net effect is + 0.82°C air, + 0.20°C Helium. From these considerations, it would appear that air would be more likely to give a buoyancy effect than helium. The associated Grashoff numbers are in a 2 g environment for a mm crystal, 0.4 and 2 x 10^{-3} and for a cm crystal 200 and 1 respectively. This is to be compared with acceleration noise values 1/100 of this caused by atmospheric turbulence in the KC135 environment (see Fig. 12).

TABLE 2

Physical properties of materials relevant to these studies.

	MWT	D $[H_2O]$ $cm^2\ s^{-1}$ 1000mb, 0°C	κ $cm^2\ s^{-1}$	K (0°C) $cal\ cm^{-1}\ s^{-1}\ °C^{-1}$	ν 0°C $cm\ s^{-1}$	L $cal\ gm^{-1}$	$\frac{D}{K}$ 1000mb, 0°C	Pr $\frac{\nu}{K}$	Sc $\frac{\nu}{D}$
air	29	.226	.187	58×10^{-6}	.135		3900	0.72	0.56
Ar	40	.19		39×10^{-6}			4400		
H_2	2	.687		390×10^{-6}	1.03		1800		1.49
He	4	.770		347×10^{-6}	1.09		2000		1.41
Ice	18	2×10^{-11}	.0115	5300×10^{-6}		(v) 600			
Water	18	10^{-5} (self)	.0014	1440×10^{-6}	.0179	(f) 80		13	1800
NaCl (H_2O)		1.1×10^{-5}							1630
Na_2SO_4 ($10H_2O$)						(f) 45			
Sea Water									

As we have seen earlier, in the case of ice growth, the crystal habit may be extreme - as dendrites or needles - and the mass increase and heat release may take place almost entirely on the crystal extremities. Under these conditions there are significant differences of temperature between different parts of a large (mm) crystal with the growing tips warmer than elsewhere. It is not easy to analyze this situation theoretically. The growth of any point on the crystal depends crucially on a balance between local nucleation at a protruding corner which may be molecularly rough, and, further back from the tip, where growth is by steps growing back to a region of lower local supersaturation (Hallett, 1987). The excess temperature at the tip may be several times that for an equivalent spherical particle, depending on the detailed geometry of the growing crystal, the maximum being expected for a long cylindrical crystal or a narrow dendrite tip. Observations by Gonda and Komabayasi (1970) show that the linear growth rate of crystals in helium exceeds that of air under identical conditions.

In the case of ice, the effect will be greatest at high supersaturation and more extreme habit. These considerations apply near -4°C where the habit is in the form of long columns and needles - the case examined above, and, near -2°C and -15°C, where the habit is in the form of dendrites.

The latter temperature could not be obtained with the system although some laboratory measurements were made near -2°C. The decision to use helium at 1/2 atmosphere was made on the basis of the results of Gonda and our 1 g laboratory studies that growth rates were observed to be highest under these conditions. Maximum practical supersaturation was ~50%, to give linear growth rate ~6 μm s^{-1}; in 10s this gives a distance of 60 μm. Estimate of length with the available optics was ~ $\pm$ 3 μm, which made this particular experiment feasible. Interpretation of self-induced growth enhancement in low g in terms of Grashoff numbers given above only makes sense using a larger dimension, and in any case would

point to a bigger effect in air than helium. Absolute growth rates in air great enough to measure under KC135 conditions were not available in this system (if greater supersaturations were used (> 50%) the growth of crystals from the base plate and the walls was excessive).

b. Crystal growth from solution.

A similar analysis may be carried out for ice growth in supercooled NaCl solution and sodium sulfate decahydrate from solution, using the fusion latent heat and diffusion coefficient of the ions in water. Since all molecular diffusion processes in water are slow the slope of the line is nearly vertical, giving a temperature excess $\sim 10^{-2}$°C, so that its effect on buoyancy can be neglected. The buoyancy in both cases is therefore given approximately by the difference between environment and equilibrium density resulting only from concentration at the supercooling temperature. As pointed out earlier, this neglects kinetic effects at the solid-liquid interface which will reduce the buoyancy somewhat. In these cases, Grashoff number with supercooling of 2°C Grashoff numbers are $\sim 10^{-2}$ for a mm crystal and ~10 for a cm crystal. The same conditions apply from crystal shape and dendrite tip radii as for growth from the vapor (Table 3).

Since quite distinct convection is observed in the case of $Na_2SO_4 \cdot 10H_2O$, the conclusion is reached that a Grashoff number of 10 computed in this way is in excess of that required for self-induced convection. Table 1 gives a comparison of the time constant for initiation of convection for different systems. The time for a crystal tip dimension of mm or less is negligible for systems examined here. However, for larger crystals, ~ cm, the times are significant which is consistent with delays in the plume detachment to be described later (Figs. 19, 39).

Table 3

Comparision of convection parameters for typical growth conditions in liquid.
Gr = Grashoff number; Ra = Rayleigh number; Pr = Prandtl number

	Bouyancy		Kinematic Viscosity	Pr	Tip diameter	Equivalent Gr	Ra = GrPr	Overall crystal length	Equivalent Gr	Ra = GrPr
	$\beta \Delta T g$	$\frac{\Delta\rho}{\rho} g$	$cm^2 s^{-1}$	$\frac{\nu}{\kappa}$	@ΔT	$(g=g_o)$			$(g=g_o)$	
NaCl solution - ice		$\frac{.2}{1.2}$ g	.03	(23)	100 μm @ 2°	0.2	4.6	5 mm	1480	34000
$Na_2SO_4 10H_2O$ - solution		$\frac{0.8}{1.21}$ g	.05	(38)	1 mm @ 5°	26	990	5 mm	3300	125000
Water	10^{-4} 1 g		.017	13	500 μm @ 3°	.13	1.7	5 mm	130	1690
Succinonitrile	$5x10^{-4}$ 1 g		.047	41	50 μm @ 1°	10^{-4}	.004	5 mm	28	1150

7. ICE CRYSTAL GROWTH FROM THE VAPOR.

a. General Considerations: When snow crystals grow in the atmosphere, the observed external form of the crystals is generally hexagonal, the habit (ratio of a/c axis) and the degree of completion of faces (dendritic or needle crystals compared with plates or columns) depends critically on temperature, supersaturation and fall velocity (Hallett, 1987). Whilst at low supersaturation the habit of ice crystals may be determined by the presence of emerging dislocations in preferred directions, under most atmospheric conditions, where the saturation is close to water saturation, growth is determined by surface nucleation and layer spreading and the habit by differential effects on planes perpendicular to a and c axes. Laboratory experiments (Keller and Hallett, 1982; Alena and Hallett, 1987) have shown that transition from plate to dendrite, and column to needle can be initiated by increase of ambient air velocity as well as increase in supersaturation. This occurs in practice as the fall velocity of a crystal exceeds a critical value, or, in the case of a frost crystal, as the surface wind speed exceeds a similar value. These experiments were undertaken to investigate whether changes could be achieved by completely removing any ventilation by growing a crystal under low g. Ice crystal growth under static laboratory conditions may give rise to ventilation either by local convection from the growing crystal itself, or by convection on a larger scale in the chamber in which the crystal is growing. This effect if it is present at all can be readily investigated under low g available in the KC135. Here, it is necessary to utilize the 20 s period of low g available. In order to optimize the conditions under which such a study can be carried out, the maximum linear growth rate of a crystal must be realized. Under ordinary atmospheric conditions this is ~ 1-2 $\mu m\ s^{-1}$ (Ryan, et al., 1976). The growth rate of an ice crystal limited by diffusion and heat condition is given by

$$\frac{dm}{dt} = \rho_i 4\pi r^2 \frac{dr}{dt} = \frac{4\pi C\sigma}{\frac{R\ T_\infty}{e_{sat}(T_\infty) D M_w} + \frac{Ls}{KTs}\frac{L_s M_w - 1}{R\ T_\infty}} \quad . \ . \ 17$$

where C is the electrostatic capacitance of the crystal (= radius for a sphere) and other symbols have their usual meanings. (See Pruppacher and Klett, p. 448). The growth rate can be increased with supersaturation σ, and by increase of D and K. In air at 1 atmosphere and - 10°C the two terms in the denominator are almost equal.

This analysis is applicable to a crystal with uniform surface conditions; in practice this is far from the case as different facets of the crystal are subject to different local supersaturation, since different facets show different kinetics. The result is that a crystal grows in a dendritic or needle (non-faceted) shape where the local supersaturation is greatest and where faceted and layer growth give way to continuous growth on a molecularly rough surface. A thinner crystal (for heat and moisture transport reasons) grows faster.

Laboratory results have shown that increases of D tends to give more faceted crystals (constant K) whereas increase of K (constant D) gives more dendritic crystals (Gonda and Komabayasi, 1971). K can be increased by use of hydrogen/helium as a carrier gas; D can be increased by using a gas at low pressure. Evidently a compromise in choice of carrier gas (Table 2, p. 33) is required to give maximum growth rate. Helium was chosen for safety reasons; the maximum growth rate was found empirically.

b. Chamber design and construction.

The static diffusion chamber is formed by two flat stainless steel plates 28 cm in diameter, spaced 3 cm apart, as shown in Fig. 7. A stainless steel

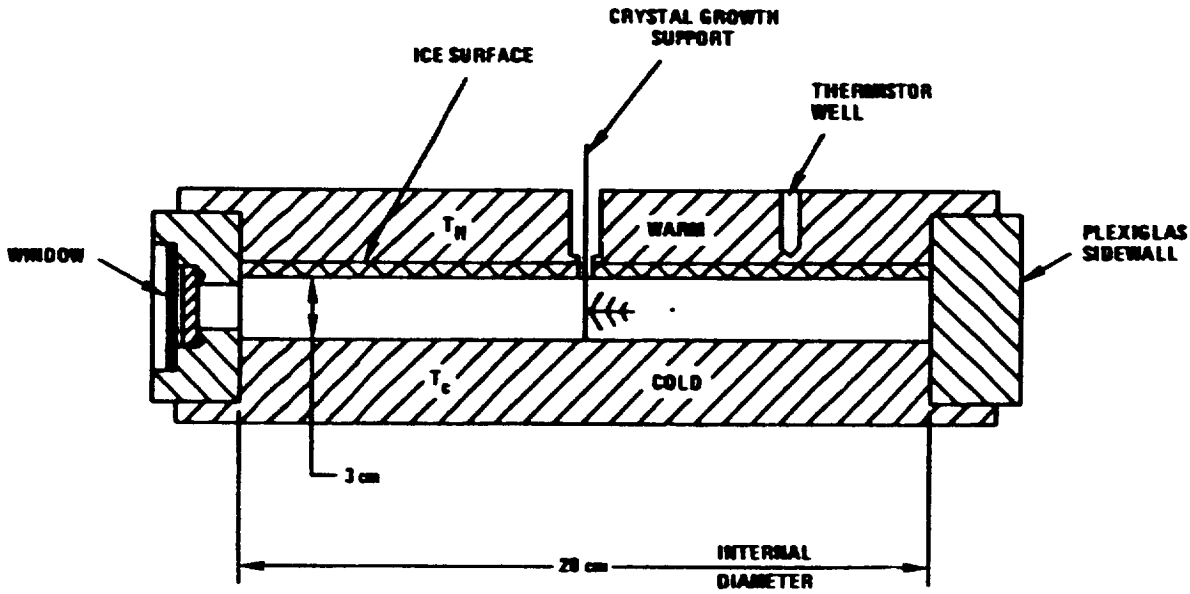

Fig. 7 Cross section of static diffusion chamber for ice crystal growth in air or helium at controlled pressure.

wicking material is diffusionally bonded to the top surface to act as a water source. This wick is 0.1 cm thick, with a capacity of at least 0.07 gm/cm^2 of water. For operation at low vapor pressure, the wick is filled with water at room temperature and then allowed to freeze. The chamber sidewall is constructed of a thick ring of plexiglass. Machined into the sidewall are two access ports, three gas ports, and two window openings. Windows are double pane to minimize heat transfer to the environment. Dry air is circulated between the windows to prevent any water vapor condensation that would impede viewing. The chamber can be flushed, evacuated and filled with other gases, or aerosol as shown in Fig. 8. It is protected from over-pressure by a pressure relief valve. A glass fiber (1/2 mm diameter) with micrometer control of vertical position and rotation is inserted in the top center of the chamber to serve as a nucleation site for ice crystals. It is necessary to nucleate ice crystals for growth above - 10°C by a CO_2/LN_2 cooled probe, otherwise supercooled drops grow on the fiber. Crystals are viewed through a camera window 2 x 7 cm of optical crown glass, treated with a non-reflective coating. A similar window with dimensions as 2 x 11 cm is provided at 180° orientation for using a Vickers high intensity tungsten/iodine microscope lamp with a water filter is provided to reduce infrared heating from this tungsten lamp. The stereo microscope allows simultaneous photography with a 16 mm movie camera or a television camera and VCR, and a 35 mm camera equipped with 250 frame cassettes with motorized drive.

The thermal plates are independently controllable through a temperature range from ambient to - 30°C. Each 2.5 cm thick stainless steel plate has a 0.5 cm thick copper disc brazed to the surface opposite the inside surface. The copper is intended as a thermal buffer to achieve uniform temperatures in the thermal plate. An insulation package equivalent to at least 5.0 cm of air surrounds the chamber to reduce the effects of heat transfer from the environ-

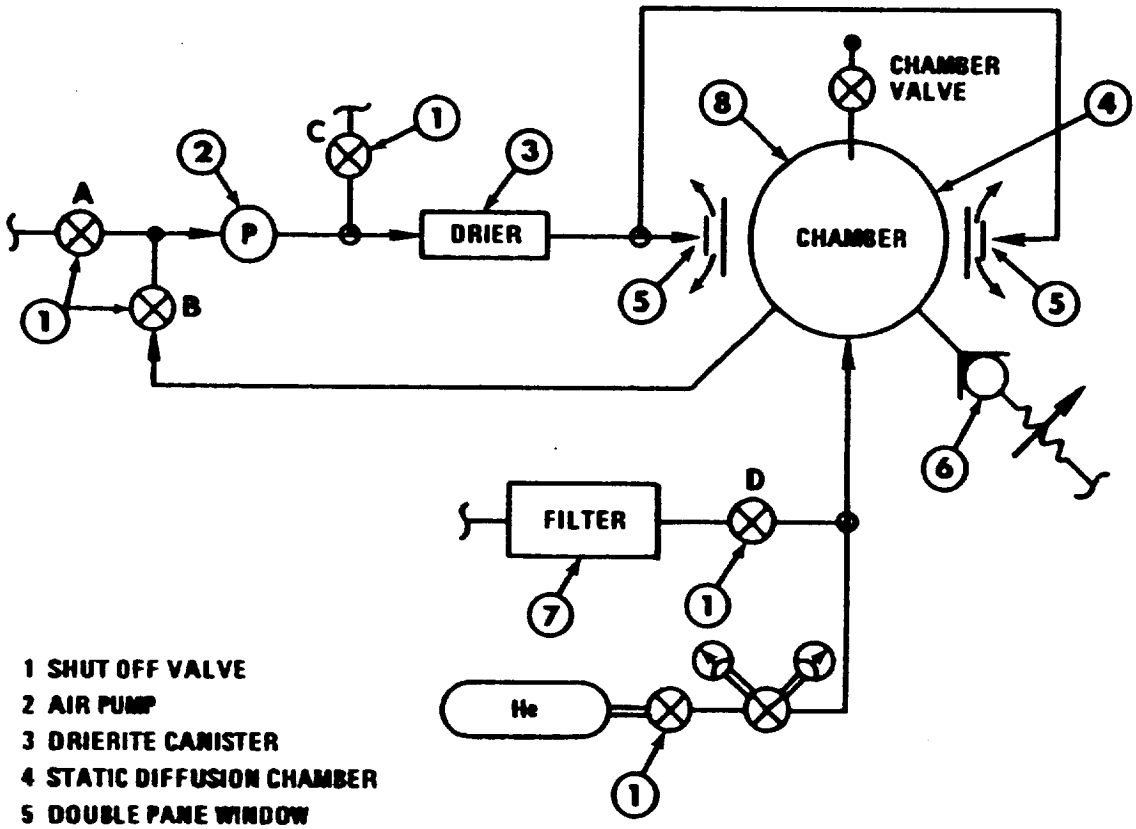

Fig. 8 Chamber filling and flushing connections.

ment. Temperature control is provided by a microprocessor utilizing sampled data servo techniques, utilizing a servo feedback parameter and is provided by a thermistor temperature sensor embedded in the stainless steel plate. The microprocessor incorporates a 12 bit data acquisition system. The plate temperatures are driven by thermo-electric modules which are mounted directly to the copper buffer. A heat exchanger is mounted to the other side of the thermoelectric modules to dissipate waste heat into a water/ice slurry. Acceleration is measured by two accelerometers attached to the chamber which gives vertical and lateral components (sensitivity $\pm$ .01 g); chamber pressure by a piezo electric system through a communicating port.

c. Control System.

Software development for this Z-80 based computer was accomplished using an 8080 assembler program. The procedure for programming the microprocessor consisted of writing the assembly program and downloading the generated machine code directly into a buffered PROM programmer. UV erasable PROMS (INTEL 2716's) were used in our system.

The control system is designed to operate in two working modes. In the STABILIZE mode, servos are updated every 125 ms while temperatures are printed at programmable intervals on a thermal printer. During this mode, the operator may display the output information of any analog channel on the LED display by entering the desired channel number via the keyboard.

In the RUN mode servos are updated every 125 ms, while accelerometer data is plotted at 125 ms intervals on the thermal printer. Again, information from any analog channel can be displayed one channel at a time, on the front panel LED display. When this mode is exited, elapsed time, temperature highs and lows, and acceleration highs and lows are recorded by the thermal printer.

A digital servo was written for this software using sampled data methods. Calibrated temperature feedback information is provided by thermistor temperature sensors. Temperatures are calibrated and displayed in decimal form. This is accomplished by providing a calibration table in memory for each thermistor. The software provides table selection, interpolation, and conversion routines to generate the display of a calibrated decimal number representing temperature.

Because the accelerometer output is essentially linear, the accelerometer signal conditioning circuitry was designed such that a simple offset subtraction could be used on the digitized analog signal. After presenting the number in decimal form, an accelerometer output representing gravity in real units was realized.

d. Control Hardware.

A STD Bus single card processor (PRO-LOG #7803) was selected as the primary control element of this project. Low cost, small physical envelope, and suitability for use in a small dedicated system is inherent with this bus structure.

The single board Z-80 based computer is driven at a clock rate of 2.5 M HZ, and had space for 8K bytes of ROM and 4K bytes of RAM. Our control program utilizes the PRO-LOG monitor, which occupies the first 2K of ROM, and is used for some of the keyboard utility routines that are available in this package. The next 4K bytes of ROM are reserved for the control software, while the remaining 2K bytes of ROM are used for storage of thermistor calibration tables. Less than 1K bytes of RAM are used in our system. Digital I/O is accomplished using a Pro-Log card (#8113) fitted with eight 8-bit input/output ports. Output ports are latched and are capable of readback. Selection of I/O function for each port is done on the card (it is not programmable).

e. Analog Cards.

One 16 channel, 12 bit A/D card (Data Translation #DT-2722) is incorporated to handle conditioned input analog signals from six thermistors, one thermocouple and one accelerometer. Two of the thermistors are used as servo feedback signals as well as temperature monitoring signals; the remaining four thermistors are available as spares. One four channel 12 bit D/A card (Data Transition #DT-2726) is used to provide control signals to the power amplifiers used to drive the TEM heat exchangers. Two of these servo circuits exist and two spare D/A channels are available.

A real time clock card (ENLODE #200-1) is utilized in our package to provide real time in hours, minutes, and seconds. Month, day, and year are also available. The card is equipped with a battery backup, so that the calendar is not lost during power off periods. A hardware timeout function available on the card is used to provide a processor interrupt every 125 ms for clocking the sampling rate of the servo. An I/O card is dedicated to a display and keyboard located on the front panel. A second utility card is also used for a display, along with I/O control of peripheral equipment.

Located separately from the microprocessor bus is the power circuitry incorporated to drive the thermoelectric modules used in the thermal heat exchangers. This circuit consists of two bidirectional power amplifiers; control signals are provided by the microprocessor. Maximum power output is about 15 AMPS at 20 volts for two circuits (combined).

f. Results - Ice crystal growth from the vapor.

The chamber mounted on a palette with computer ready for KC135 installation is shown in Fig. 9. Typical acceleration profiles are shown in Fig. 10. This shows that the limit of low gravity studies are essentially set by the turbulence of the atmosphere in which the aircraft flew. These flights were under-

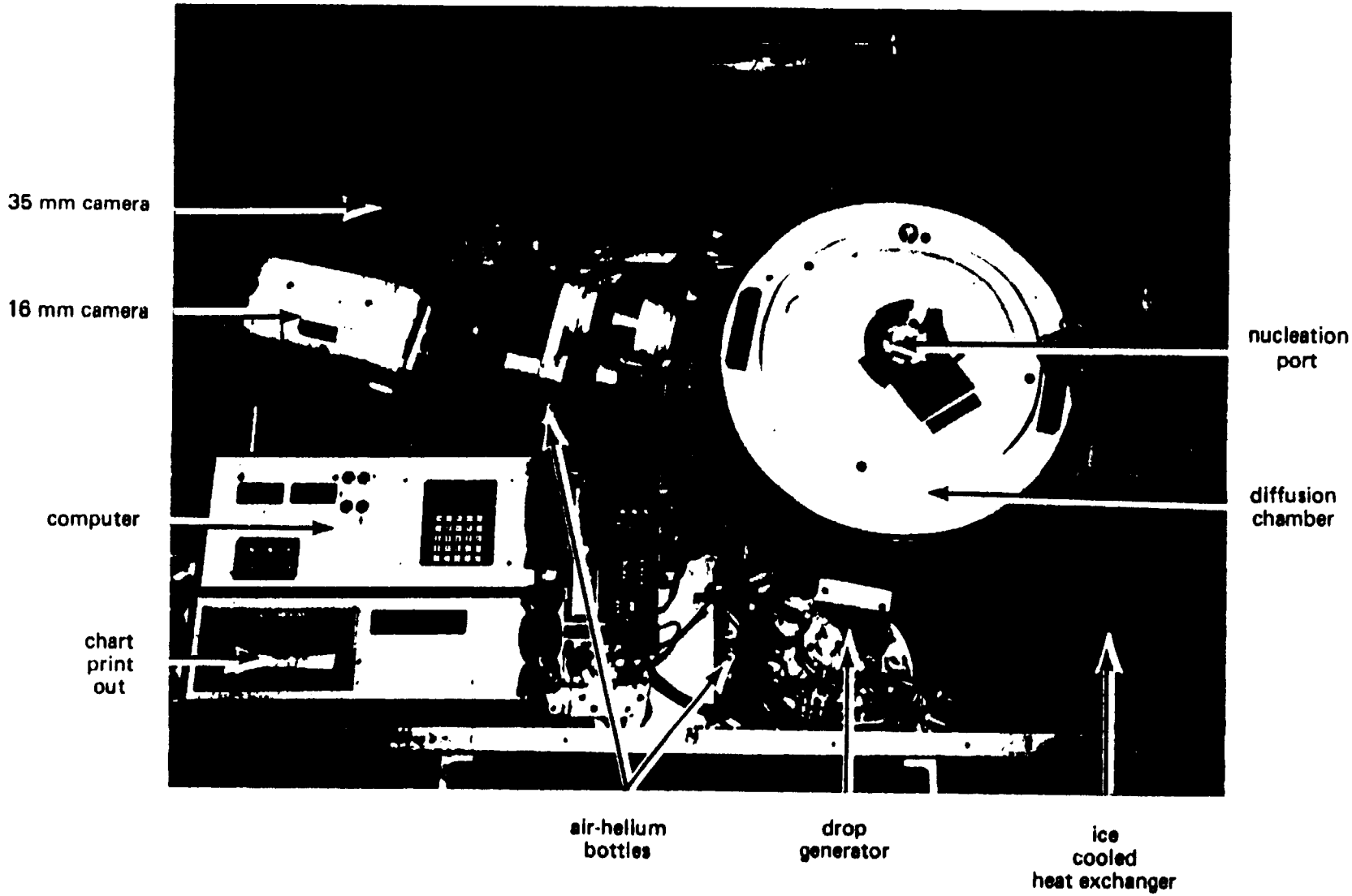

Fig. 9 Layout of static diffusion chamber for ice crystal growth from the vapor. It is mounted in palette ready for KC135 parabolic trajectory flights.

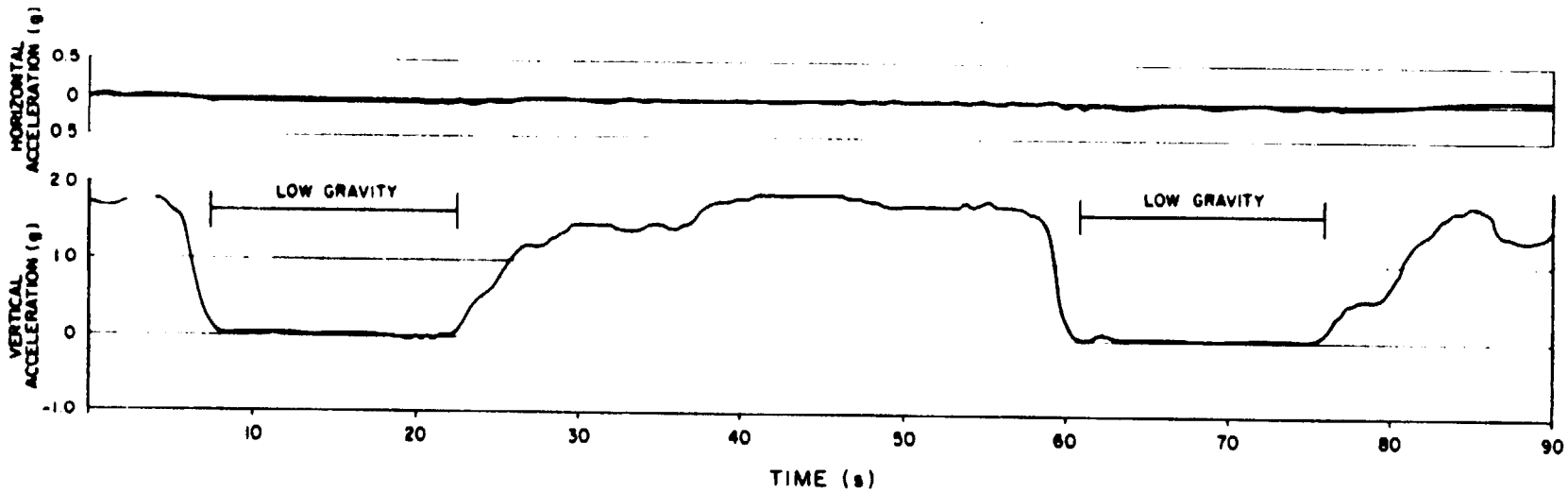

Fig. 10 Vertical and lateral g component during low g KC135 parabola and high g pullout. The effect of turbulence along the flight path gives g uncertainty $\pm$ 0.05 in low g and 1.8 $\pm$ 0.1 in high g with lateral turbulence effects $\pm$ 0.05 g.

taken over the Gulf of Mexico, the aircraft height varying between 20,000 and 30,000 ft. Fig. 10 shows an uncertainty of lateral acceleration $\pm$ 0.05 g and in vertical acceleration of $\pm$ 0.05 g at the parabola tip, but higher uncertainties $> \pm$ 0.1 g during the high period pullout.

In air maximum linear growth rates of ice crystals occur at temperatures where the habit is most extreme. This is at $\sim$ -1.5°C and -15°C for growth as dendrites in the a-axis direction and at - 5°C in the c-axis direction (Hallett, 1987). The growth rate increases with supersaturation. The chamber was operated with central temperature between - 2° to - 6°C with temperature of the plates - 18 to + 8°C; this gives a center temperature of - 5°C. This gives long needles growing radially outward from the support (Fig. 11). Empirically, it was found that the growth rate of needles under identical conditions of supersaturation in 1 g was a maximum for helium pressure of approximately 500 mb. (Fig. 12). This was approximately twice as fast as crystals in air under the same conditions (supersaturation 40 - 50% over ice).

Experiments under these conditions were carried out in KC135 low gravity. Fig. 10 showing accelerometer records typical of such a trajectory, with a low g period of about 16 s. Atmospheric turbulence gives rise to deviations both in vertical and lateral g components, leading to an uncertainty $\pm$ 0.05 g under low g conditions. Somewhat larger uncertainties are present under high g, 1.8 $\pm$ 0.1 g. Measurements of the linear growth of an ice crystal needle during several such trajectories taken continuously are shown in Fig. 13, showing a variation of growth rate between 5.9 $\mu m\ s^{-1}$ (high g) to 2.1 $\mu m\ s^{-1}$ (low g) with a mean growth rate of 3.4 $\mu m\ s^{-1}$. Errors arise from measurement of the location of dendrite and are estimated $\pm$ 0.5 $\mu m\ s^{-1}$.

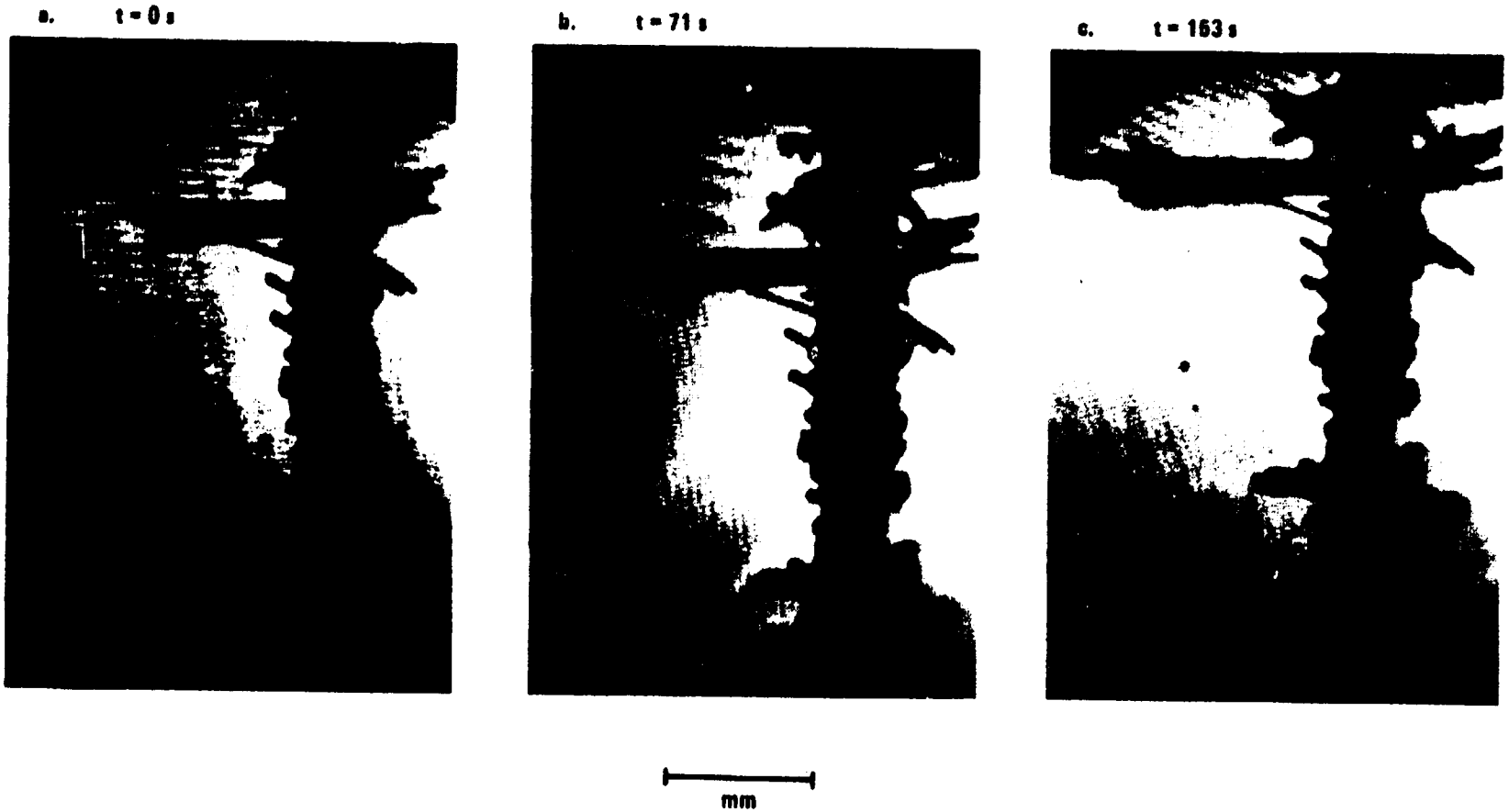

Fig. 11 Ice crystals growing in the static diffusion chamber at temperature - 5° C, ice supersaturation 40% in helium at 500 mb pressure.

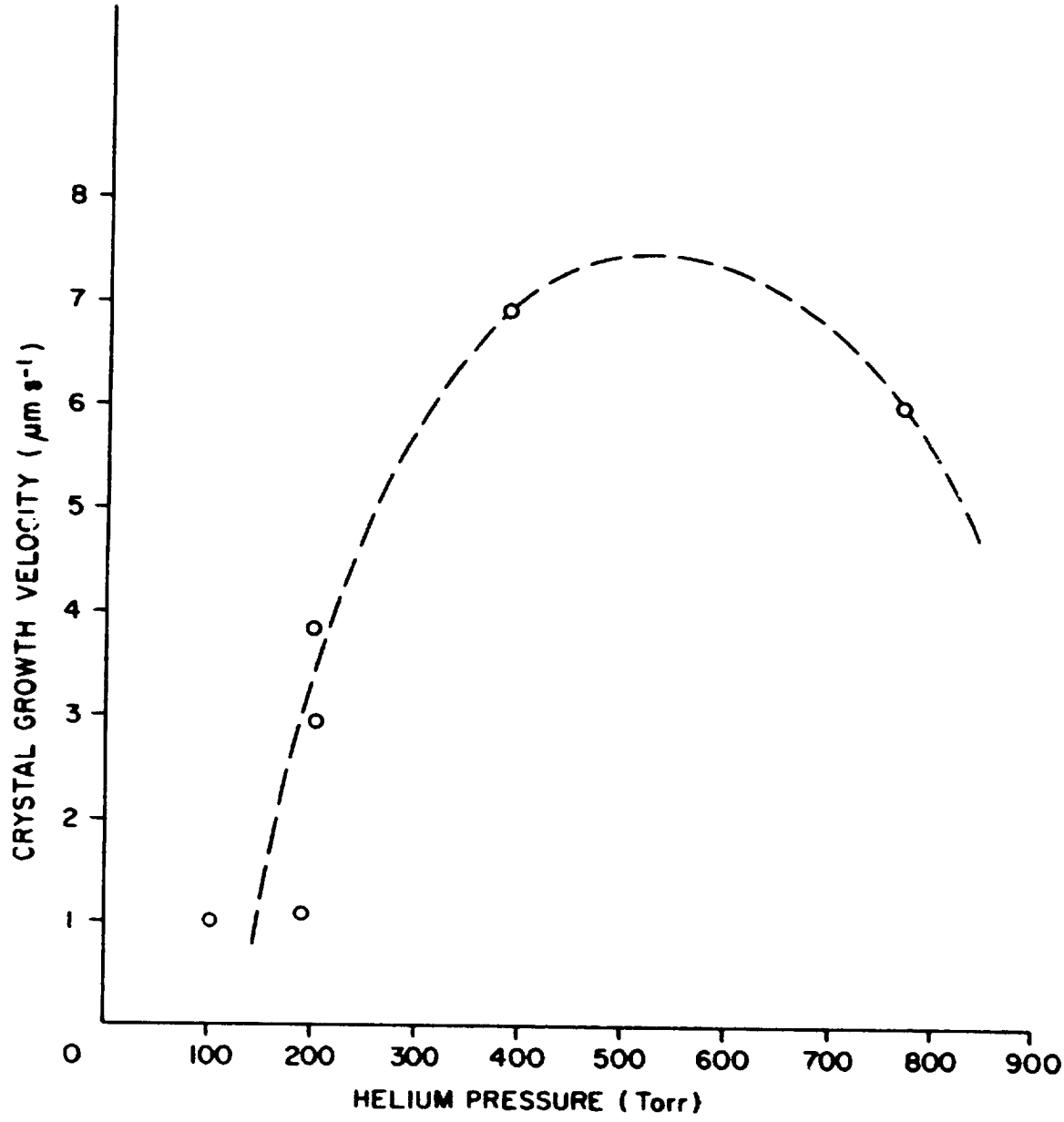

Fig. 12 Linear growth velocity of ice crystals in helium for different pressures.

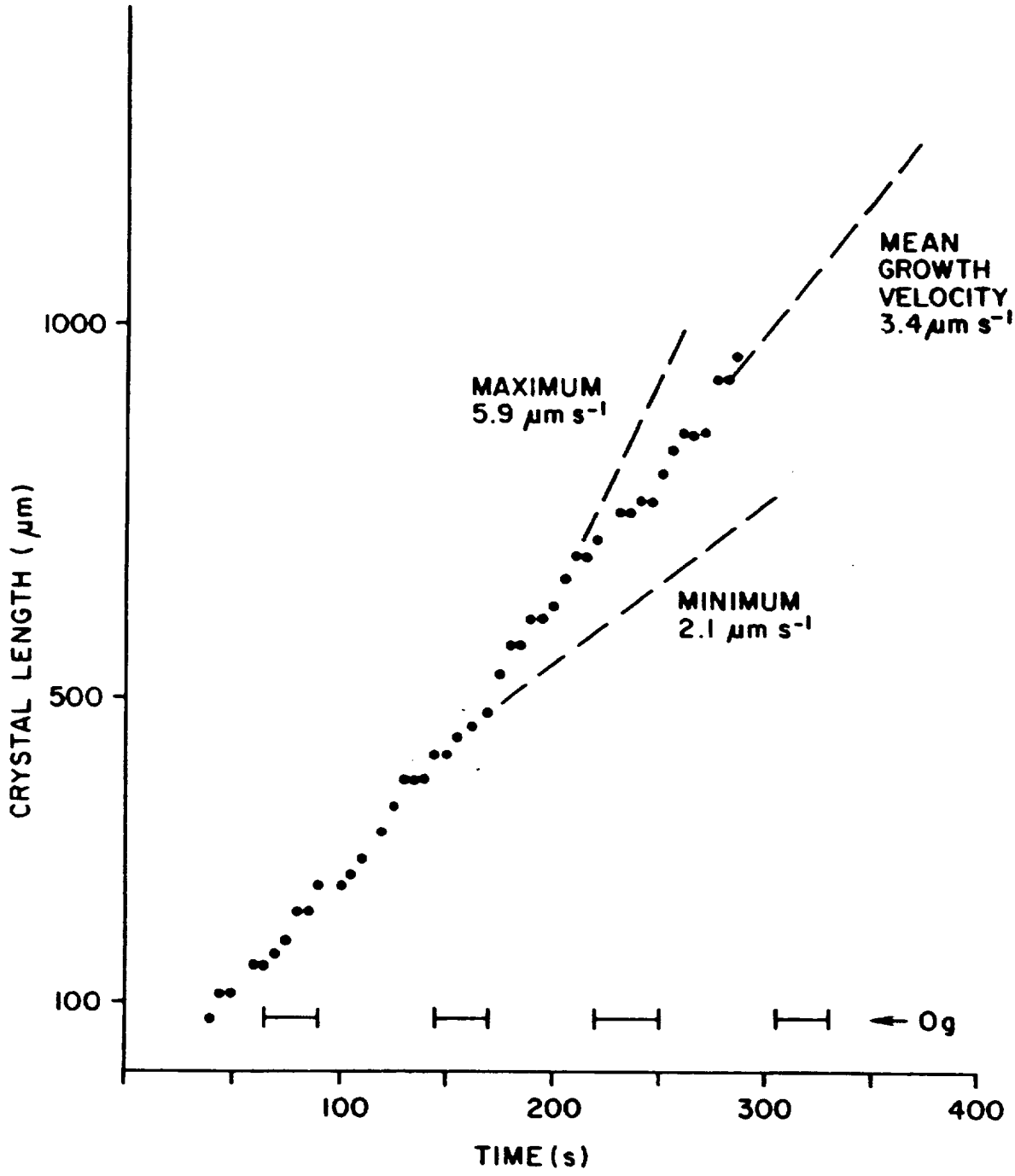

Fig. 13 Growth of ice crystals in helium (500 mb) showing lower growth rate in low g and higher growth rate in high g.

Growth of crystals at very low supersaturation and over much longer periods of time (several hours) shows that at this temperature the habit of the crystal is dependent on supersaturation (Fig. 14). As supersaturation is changed, columns transform to plates and back to columns over the range 1% to 3% ice supersaturation. Since crystal growth rate is strongly dependent on supersaturation, these effects are difficult to observe in the atmosphere where growth takes place under ventilation with a fall velocity ~ 30 cm s^{-1} and often close to water saturation; the crystals which are in fact found are those which grow most quickly and under the most favorable conditions. The role of local convection either around the crystal or on the scale of the chamber itself is not clear. It is of interest that recent laboratory studies using the dynamic diffusion chamber (Fig. 2b) have shown that faceted crystals can be caused to sprout at the corners with increased velocity as little as 2 cm s^{-1}. The growth rate and the shape changes are far too slow however to be studied in the 20 s of the KC135 parabola.

8. CRYSTAL GROWTH FROM SOLUTION.

a. Ground based experiments.

It was found experimentally that convection from growing dendrite tips could be readily observed in the Schlieren system only under quite specific circumstances. No convection could be seen for weak solutions, pure water or pure D_2O. This can be interpreted either as insufficient optical path difference, or as the density difference being too small to initiate convection. It is to be noted that water has a rather flat maximum in refractive index quite close to the melting point (Fig. 15) implying that it would be difficult to visualize ice convective plumes since $\Delta n \equiv \Delta T$, 2° is only ~ 10^{-5}. [Luten, 1934; Tilton and Tugler, 1938; Kirshenbaum, 1959; Mehu et al., 1966; Eisenberg and Kauzmann, 1969]. Conversely, under conditions of high supercooling and correspondingly

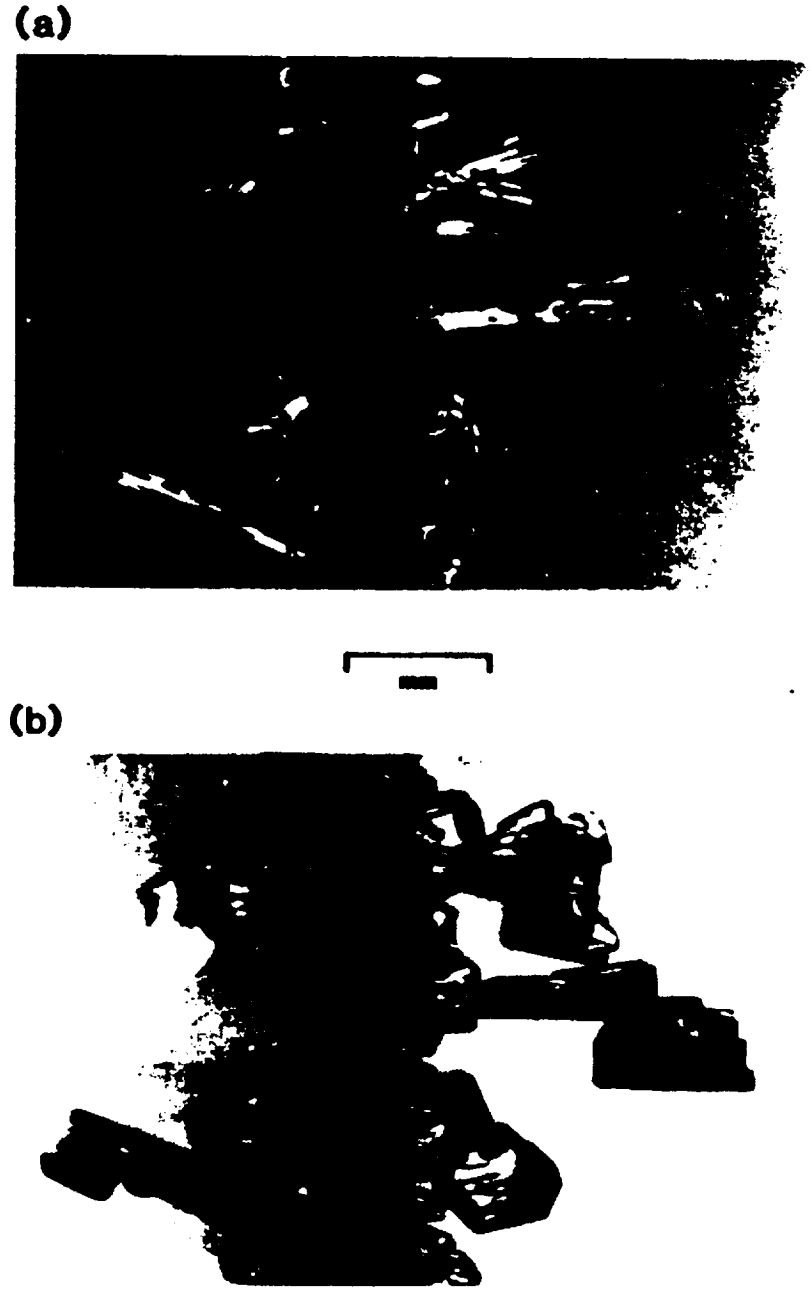

Fig. 14a, b Habit dependence of ice growth from the vapor in air on supersaturation at - 5°C. Initial growth: 12% over ice giving a column; later growth : 1% over ice giving a plate (a); final growth at 5% over ice to give a hollow column (b).

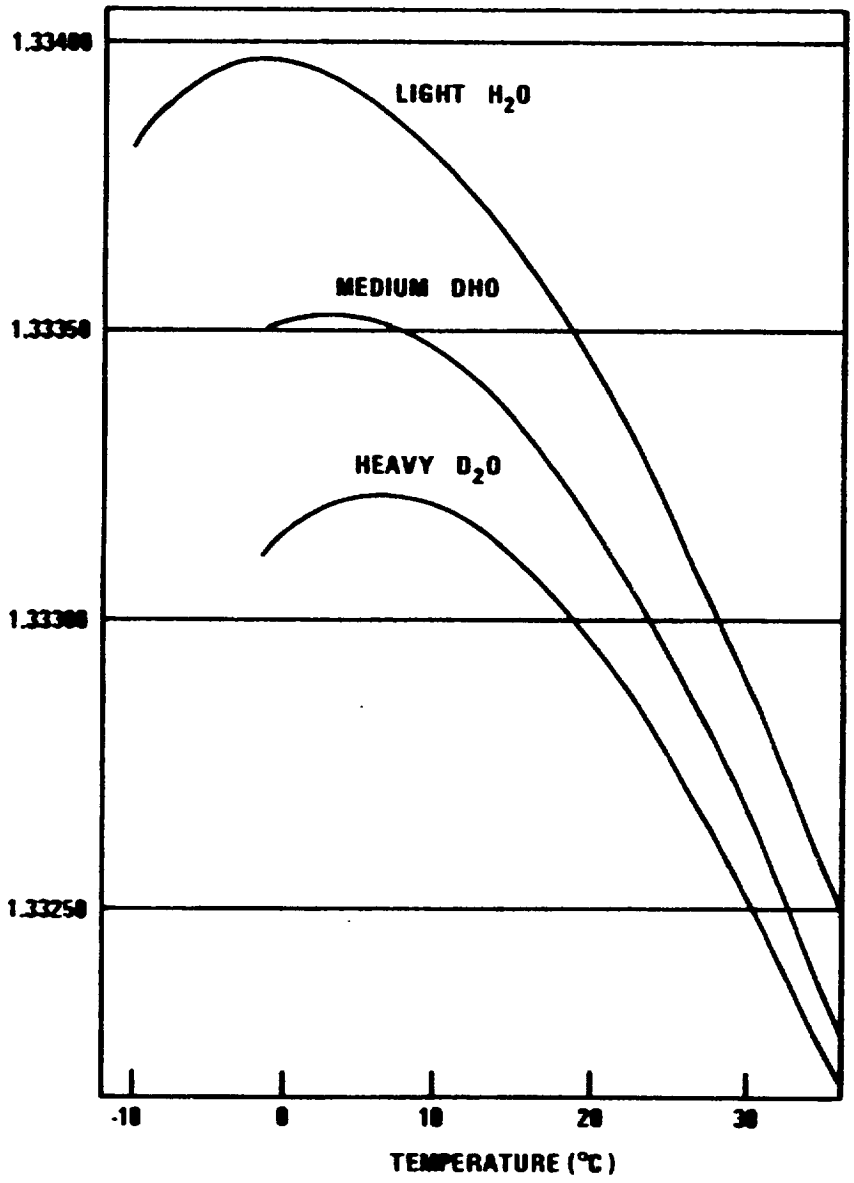

Fig. 15 Refractive index of water shows a flat maximum just below the equilibrium fusion point H_2O, and just above for D_2O. In either case, the difference was not great enough to give visible effects in the Schlieren system.

	Temperature of maximum density	Melting point	Temperature of maximum refractive index
H_2O	+4°C	273.15°C	-2
D_2O	+11°C	276.97°C	+7

high crystal growth the convection did not have time to begin before the crystals grew (Table 1).

1. Sodium Sulfate decahydrate from solution.

Sodium sulfate crystallizes as two forms, heptahydrate and decahydrate, each with quite distinct properties (Fig. 16). The decahydrate is more stable and is used in this study. In order to ensure nucleation of decahydrate, a crystal from a crystal solution mix heated to just below the equilibrium point (+ 32°C) is used as a seed crystal. This ensures that no heptahydrate which decomposes at + 28°C is present. The crystal is inserted into the center of the liquid by pushing it on the end of a flexible coil through the plastic tube until it just emerges from the tip (Fig. 1b). Runs were selected for analysis with an isolated crystal growing in the plane of viewing, either horizontally or at an angle as required. Convection occurs from the dendrite tip, and is readily visible for solutions $M > 1.0$. Since sodium sulfate is removed preferentially from solution, buoyant fluid remains, which convects upwards (Fig. 17). The growth velocity of the dendrite tip, and that of the convecting plume (the starting plume tip or irregularities on the rising plume) is measured directly from the VCR or movie image. This figure shows a plume emerging from the nucleating tube (a) rising straight up, whereas that from the growing dendrite tip is bent as it rises from the growing crystal tip (b). This indicates that the plume is accelerating away from the crystal tip. There is a finite period and distance prior to the plume detaching from the tip (Fig. 18), which increases with concentration and supercooling (Fig. 19a). As the supercooling increases to $> \sim 8°$ C, there comes a distance when the plume fails to detach at all and cannot be observed during the course of the experiment because crystals grow radially out from the nucleating tube and fill the whole volume before convection begins. Crystals growing upwards with the plume grow significantly

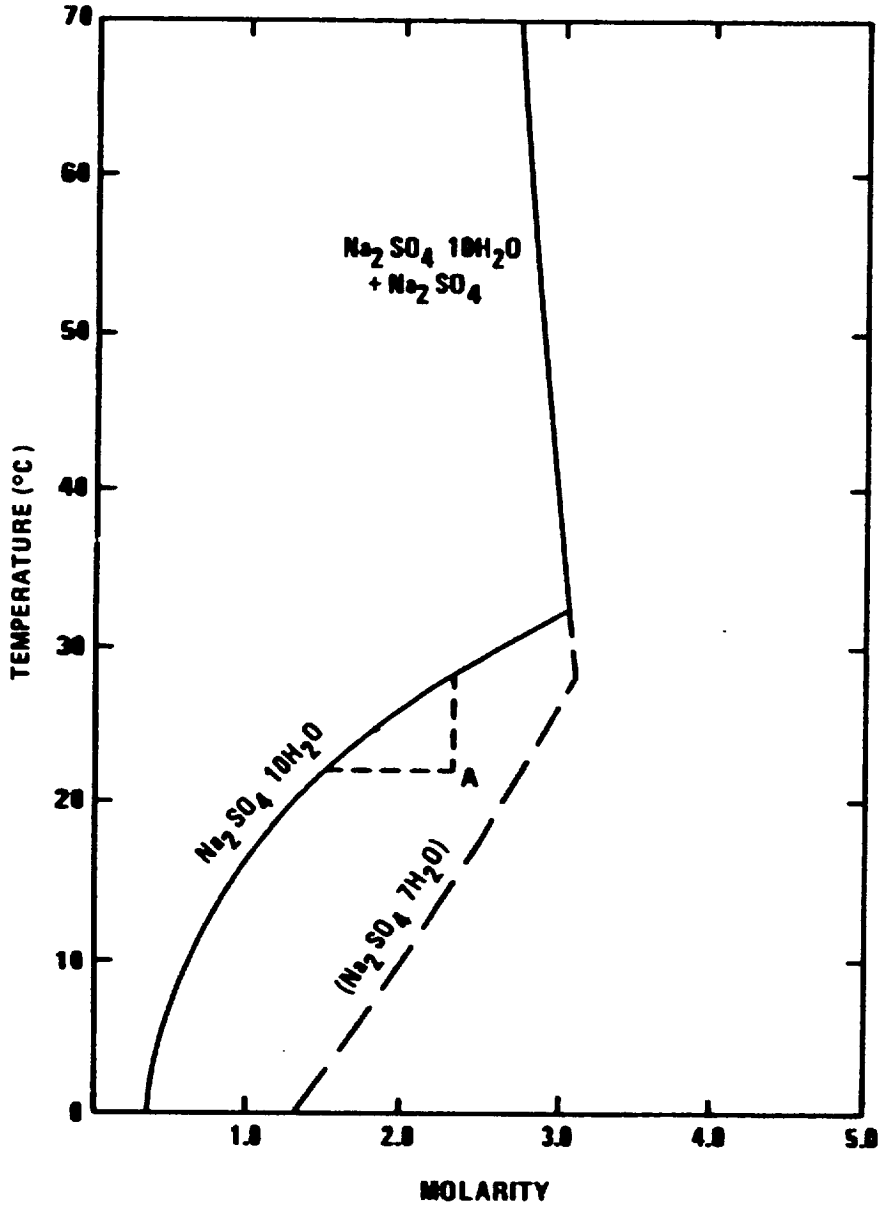

Fig. 16 Phase diagram for sodium sulfate - H_2O solution. Point A represents conditions of a supersaturated solution, 2.2 M; supercooled by 6.9°C. On nucleation, crystals grow with a driving force equivalent to the intersection of the horizontal line with the equilibrium, ΔM = 0.8 M

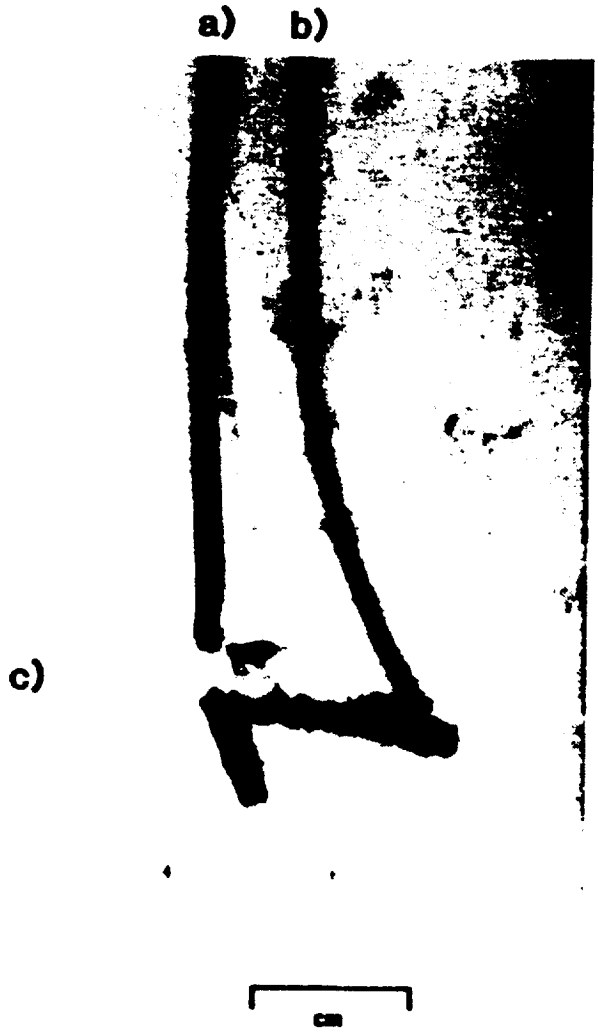

Fig. 17 Sodium Sulfate Decahydrate Crystals Growing into Supersaturated Solution from a nucleation teflon tube below the surface.

Three crystals are visible; a tiny one at 3 o'clock, the longest one (whose growth rate was measured) at 4 o'clock, and one growing downward at 5 o'clock. The two vertical lines (a, b) at the left are the plumes of depleted solution.

Growing crystals appear dark, because the picture is printed from Plus-X Reversal 16 mm movie film. 3.0 M, $\Delta T = 4.3°$ C.

a) 3.0 M, ΔT = 4.3° C,
d = 0.16 cm, R = 0.02 cm s^{-1}.

b) 3.0 M, ΔT = 7.7° C,
d = 1.7 cm, R = 0.2 cm s^{-1}.

c) 2.5 M, ΔT = 7.2° C,
d = 0.6 cm, R = 0.1 cm s^{-1}.

d) 2.5 M, ΔT = 8.9° C,
d = 1.8 cm, R = 0.2 cm s^{-1}.

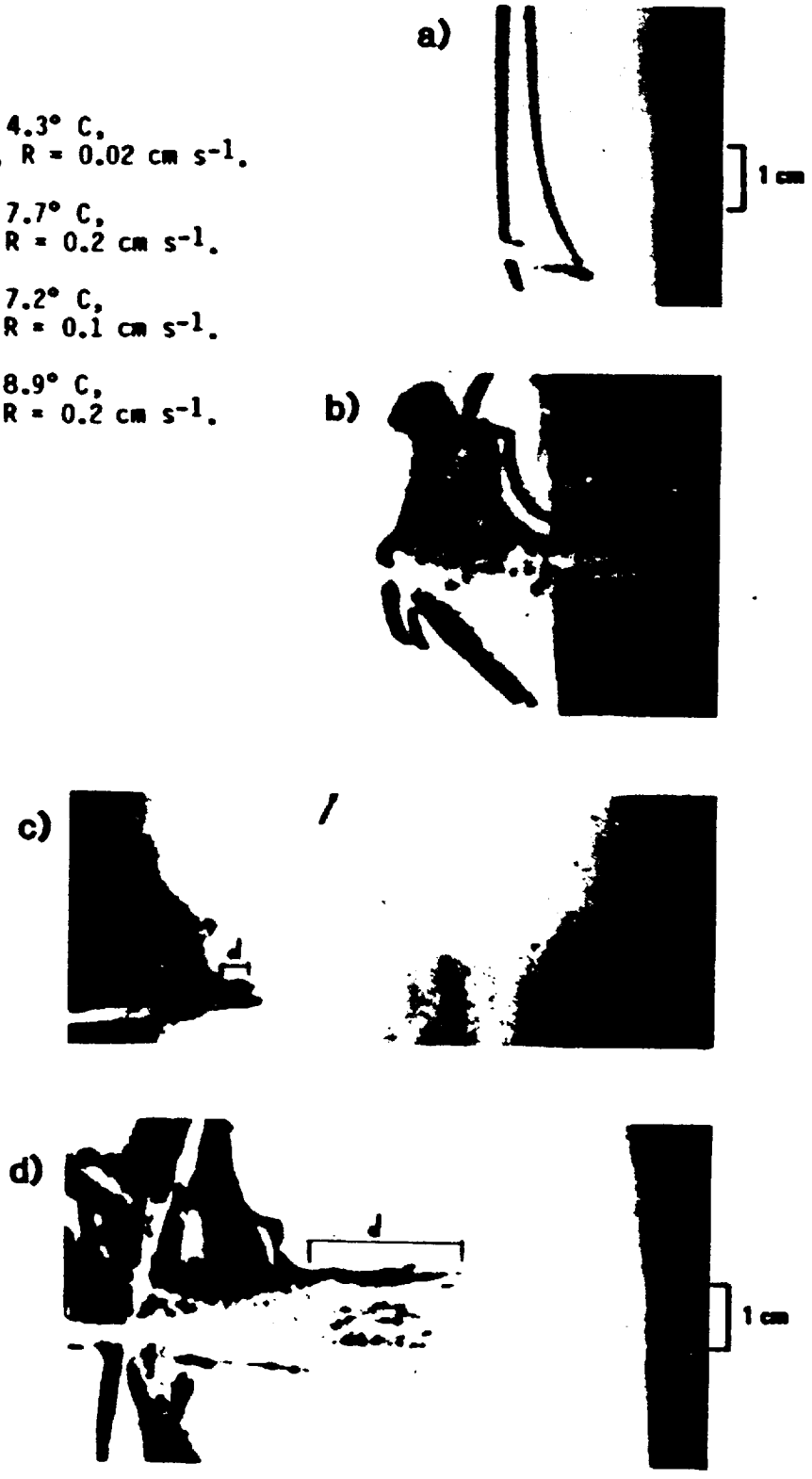

Fig. 18: Comparison of Characteristic Length, d, with Supercooling and Concentration sodium sulfate decahydrate.

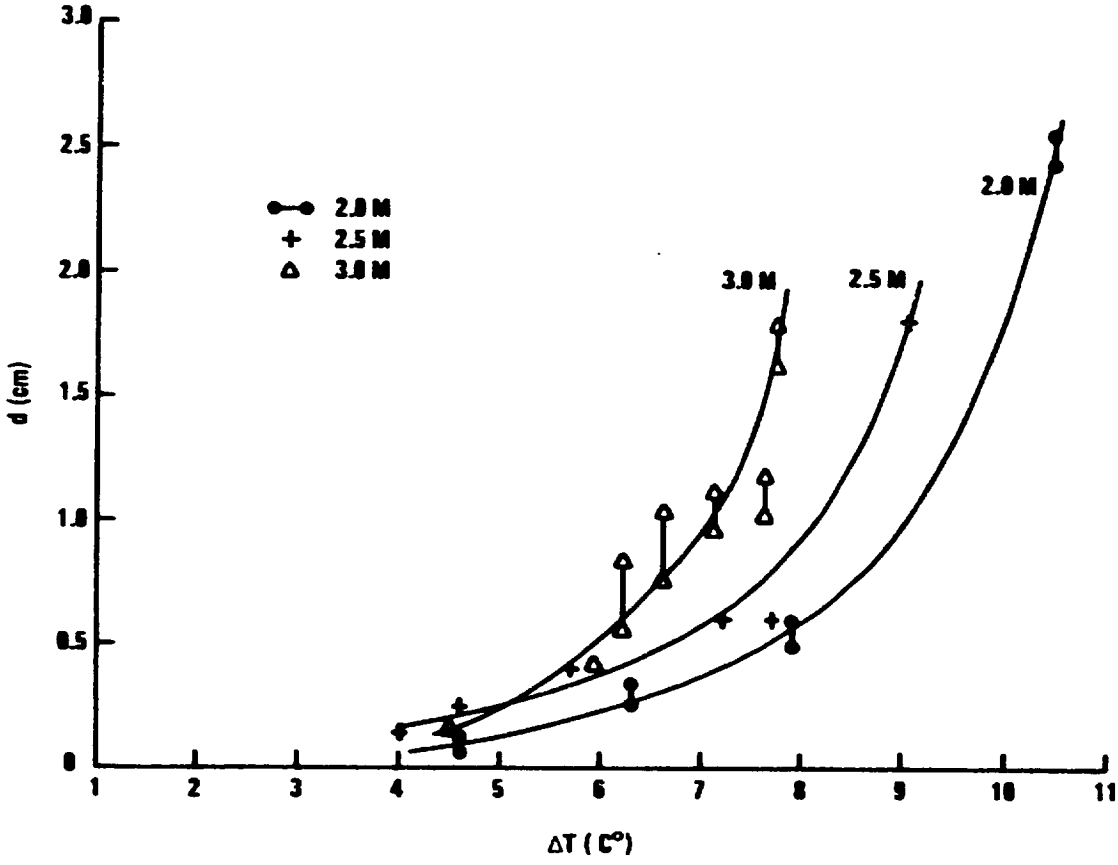

Fig. 19a Relation of characteristic length and supercooling for plume detachment for a crystal of sodium sulfate decahydrate growing horizontally.

slower whereas those growing downwards grow faster. Downward growth differs from horizontal growth by x 1.5 (3 M, 4.3° supercooling). The sequence in a Mach Zender interferometer shows a plume rising from a growing tip, the interference pattern around the tip indicating that the initial plume is quite narrow - 0.2 mm (Fig. 19b).

Further insight into the plume-crystal interaction can be obtained by moving the growing crystal through the solution. The plume bends back from the moving crystal, but is now almost a straight line, the accelerating region being shorter (Fig. 20, 21). These photographs clearly show rising plumes from each crystal tip, with additional plumes rising from sideways growing crystals behind the leading crystal. The precise geometry is difficult to determine from a single photograph. The starting plume vortex can be clearly seen in Figs. 20a, b, c.

ii. Crystallization of Ice from NaCl solution.

Similar experiments were carried out with ice in supercooled NaCl solution. No effect of convection could be seen M < 0.2, nor in pure water or pure D_2O. Experiments were carried out for 0.2, 0.5, 1.0 M and also sea water which showed downward convection as NaCl is rejected preferentially at the growing ice-solution interface from horizontal growing dendrite tips (Fig. 22). The starting plume vortices can be clearly seen (a-c). Notice that the plume oscillates downstream from the moving crystal (f-h). The convection plume is not so clear as in sodium sulfate solution, however the general characteristics are similar. Under stationary conditions, there is a greater detachment distance, and as the crystal is moved, the plume is bent back from the moving crystal, and remains attached.

iii. Role of ventilation on growth.

In both cases, sodium chloride and sodium sulfate, the plume velocity once detached from the crystal is independent of crystal transport velocity, as would

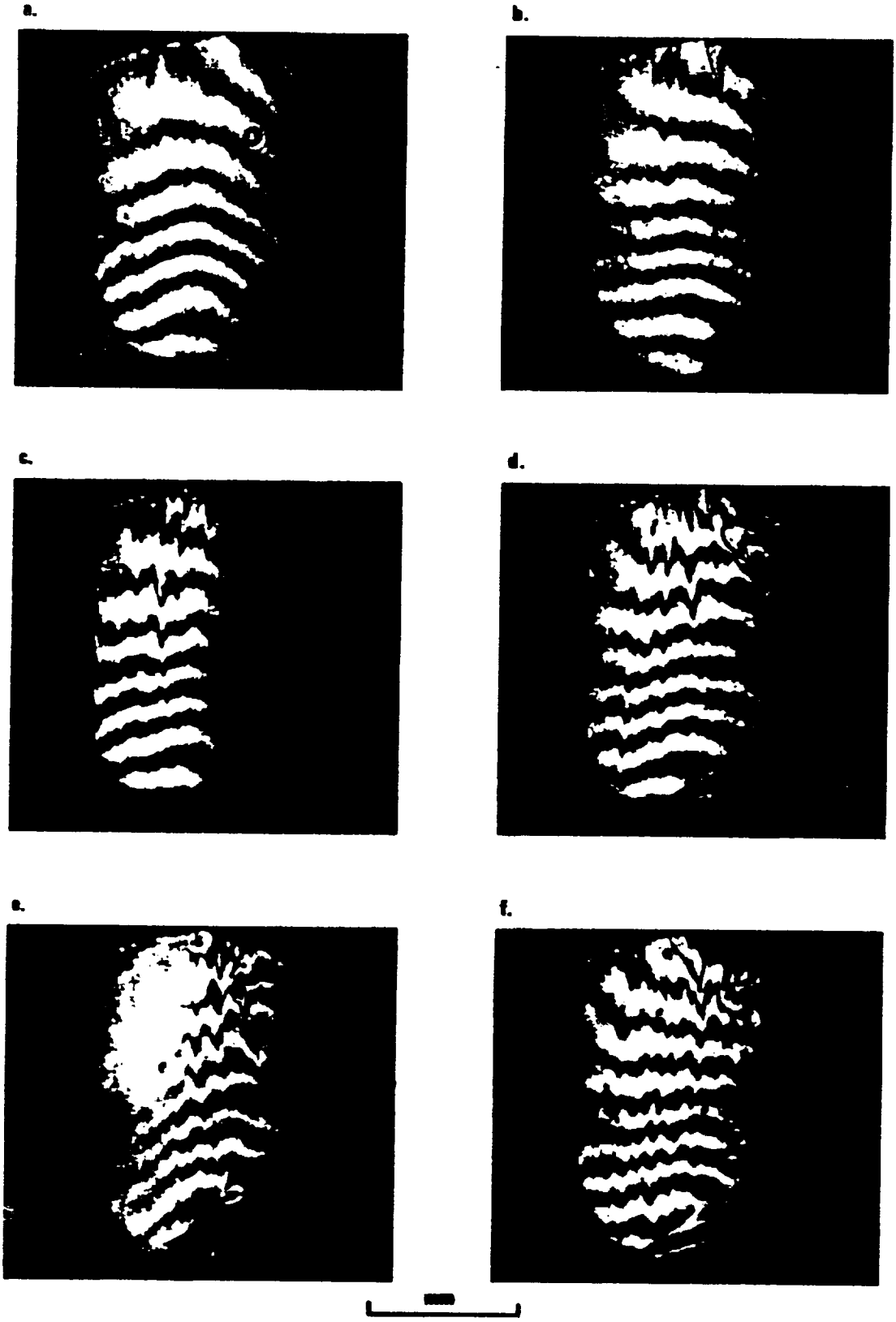

Fig. 19b Mach Zender interferogram of 2 M. Na_2SO_4 - 10 H_2O crystals growing in solution, 1 g. at supercooling 2.4°C. This shows a low density plume rising some 3 mm behind the growing tip, indicating a higher concentration on both sides (a, b). An instability (soliton) moves down the crystal (e) to be released towards the tip (f).

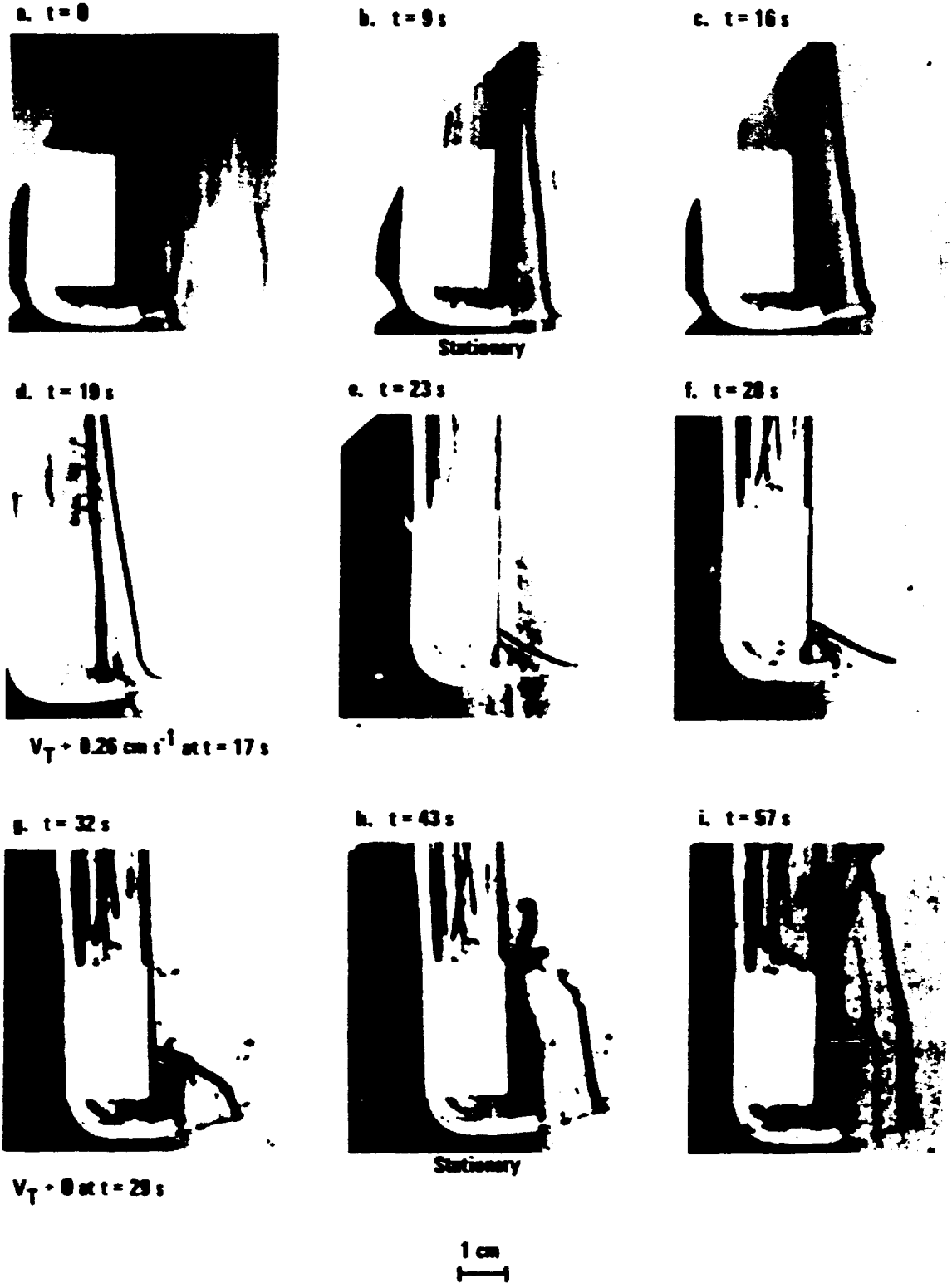

Fig. 20 Plume from a moving crystal in 1.0 M Na_2SO_4 solution. Supercooling ΔT = 5.5° C. Crystal moved left to right at 0.26 cm s^{-1} between t = 17 s and t = 29 s.

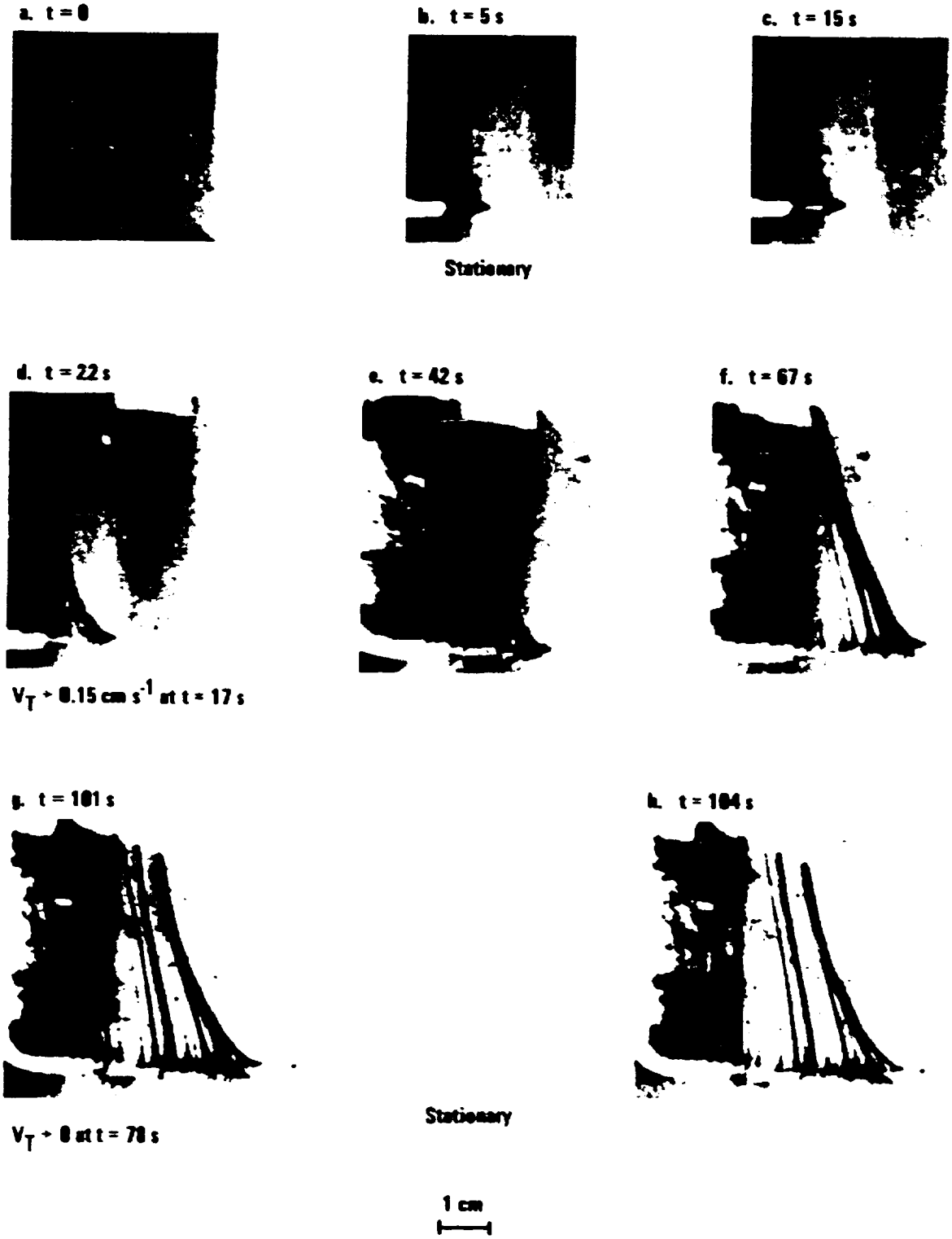

Fig. 21 Plume from a moving crystal in 2.5 M Na_2SO_4 solution. Supercooling ΔT = 4.8° C. Crystal moved left to right at 0.15 cm s^{-1} between t = 17 s and t = 78 s. a, b, c show the starting plume.

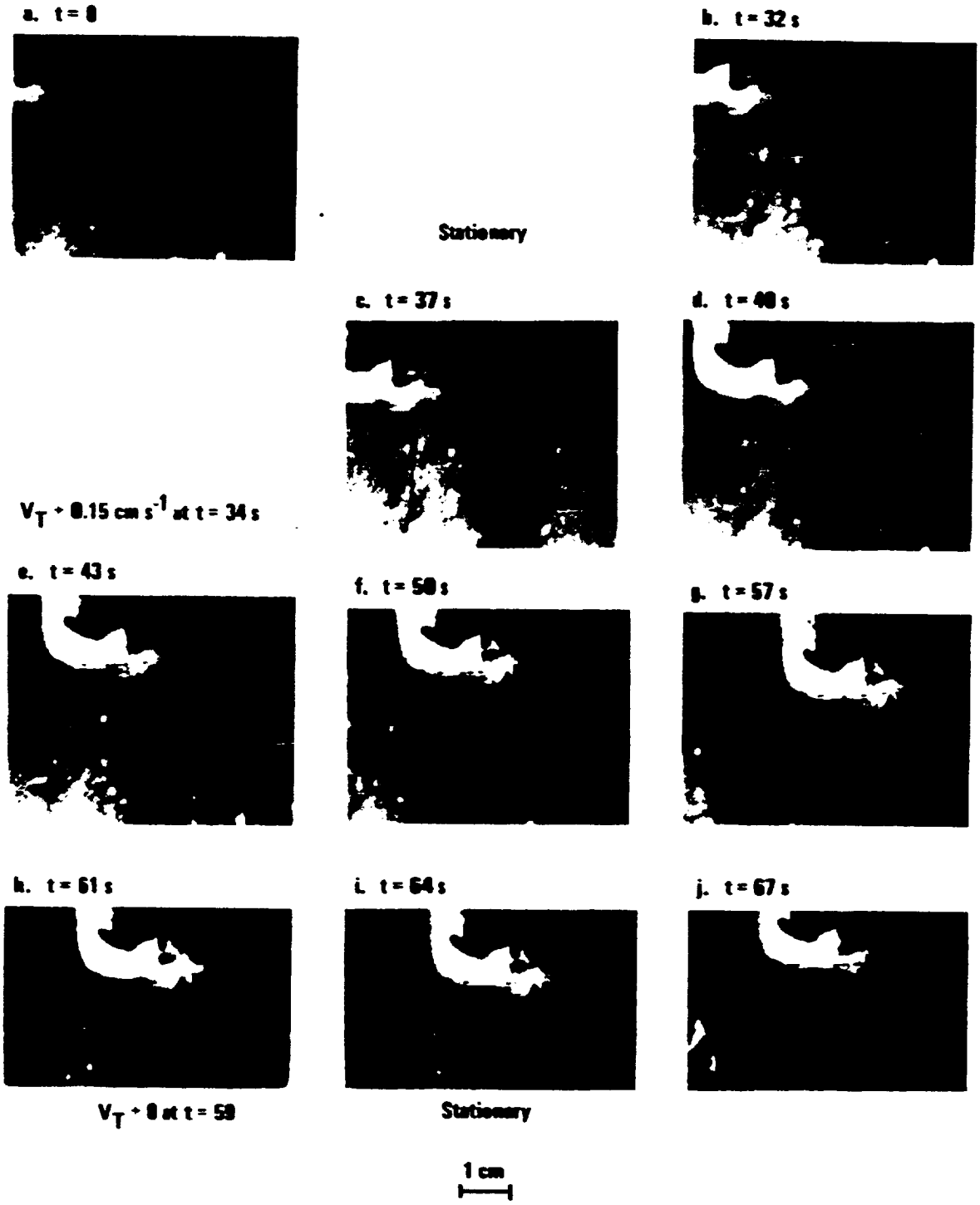

Fig. 22 Successive stages of plume behavior of ice crystals growing in 1.0 M NaCl solution. Supercooling ΔT = 0.5° C. Crystal moved left to right at 0.15 cm s^{-1} between t = 34 s and t = 59 s.

be expected. The crystal growth rate increases with transport velocity, and also with supercooling. Crystal tip dimensions are apparently smaller with increased supercooling and transport rate, but could not be accurately measured in the experiments because of the long working distance. Fig. 23 shows crystal growth velocity and convective velocity for decahydrate crystals at different molarities for a given supercooling, under stationary conditions. Both growth rates and convective velocities increase with supercooling and become equal at a critical value of supercooling, between 6 and 7° C. Moving the crystal increases growth rate, but at higher supercooling has less effect. Fig. 24 shows the effect of moving crystal at 0.15 cm s^{-1} through a 2.5 M solution, giving an increase in growth velocity compared with the stationary case. The convective velocity increase is not significant. Convective velocity, and crystal growth velocity for ice growth in various concentrations of sodium chloride solution and sea water (Figs. 25 to 28). Here also convective velocity and growth velocity increase with supercooling and become equal at supercooling between 1 and 2°C. It is convenient to use a log-log plot to display the effects Fig. 29 shows growth and convective velocity for 1, and 2 M sodium sulfate solution for a transport velocity of 0.26 cm s^{-1}, Fig. 30 for 2.5 M solution with 0.15 cm s^{-1} transport velocity, Fig. 31 shows comparable results for sodium chloride. The effect of transport velocity on growth is shown in Fig. 32 for a supercooling of - 5.5° C for sodium sulfate solutions, Fig. 33 for supercooling of 1, 2° for sodium chloride solutions. There is no significant effect of transport on convective velocity in either case. Crystal growth velocities have been extrapolated back to - 0.1°C cm s^{-1}. This demonstrates a possible effect of a given convective velocity on growth, which would be slower if the crystal grew in low g.

It is evident from these results that there exist a region of supercooling where low gravity and the absence of convection could lead to different growth

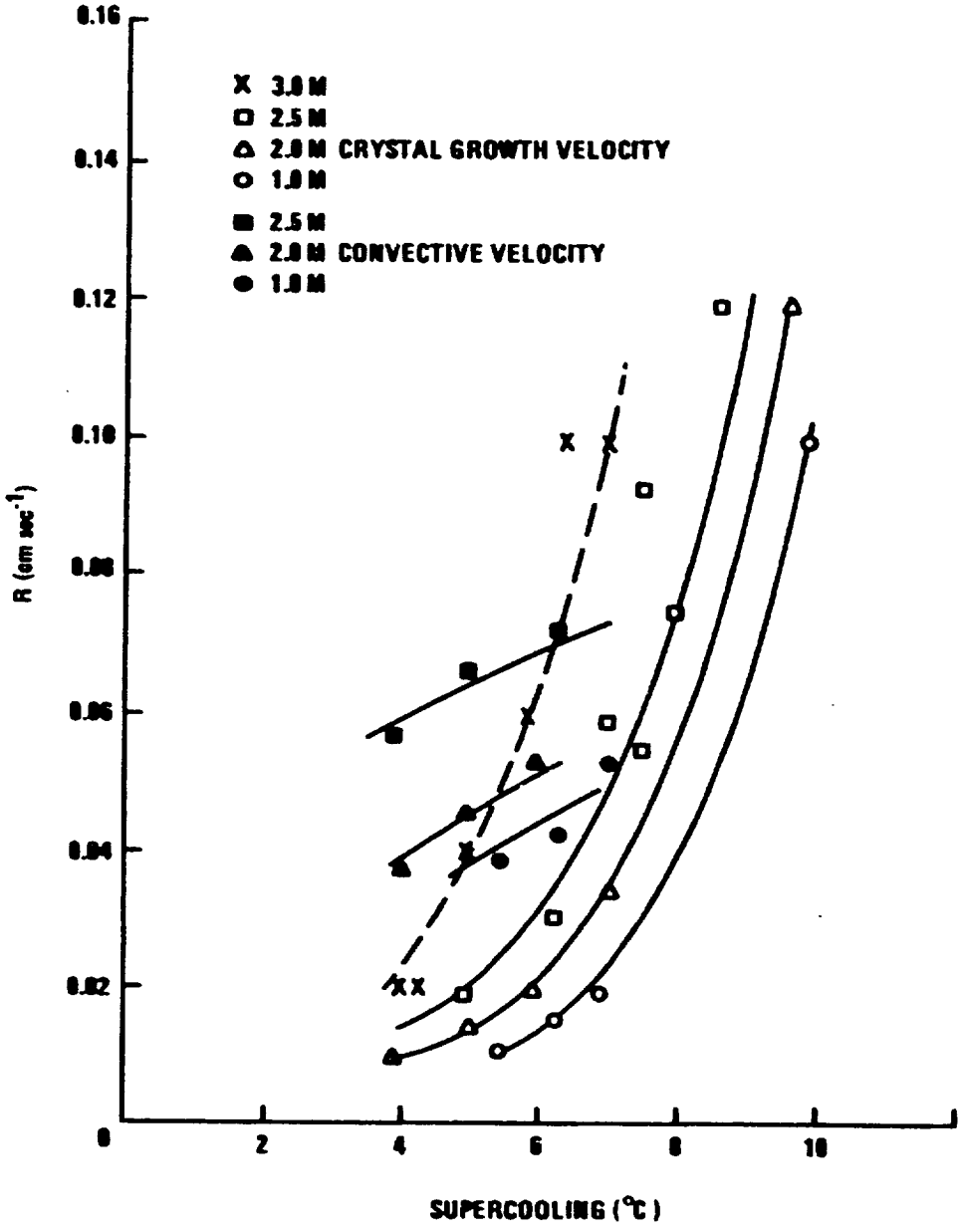

Fig. 23 Growth and convective velocity as a function of supercooling in Na_2SO_4 solution for a stationary crystal at different molarities. Convective velocity at 3 M not available.

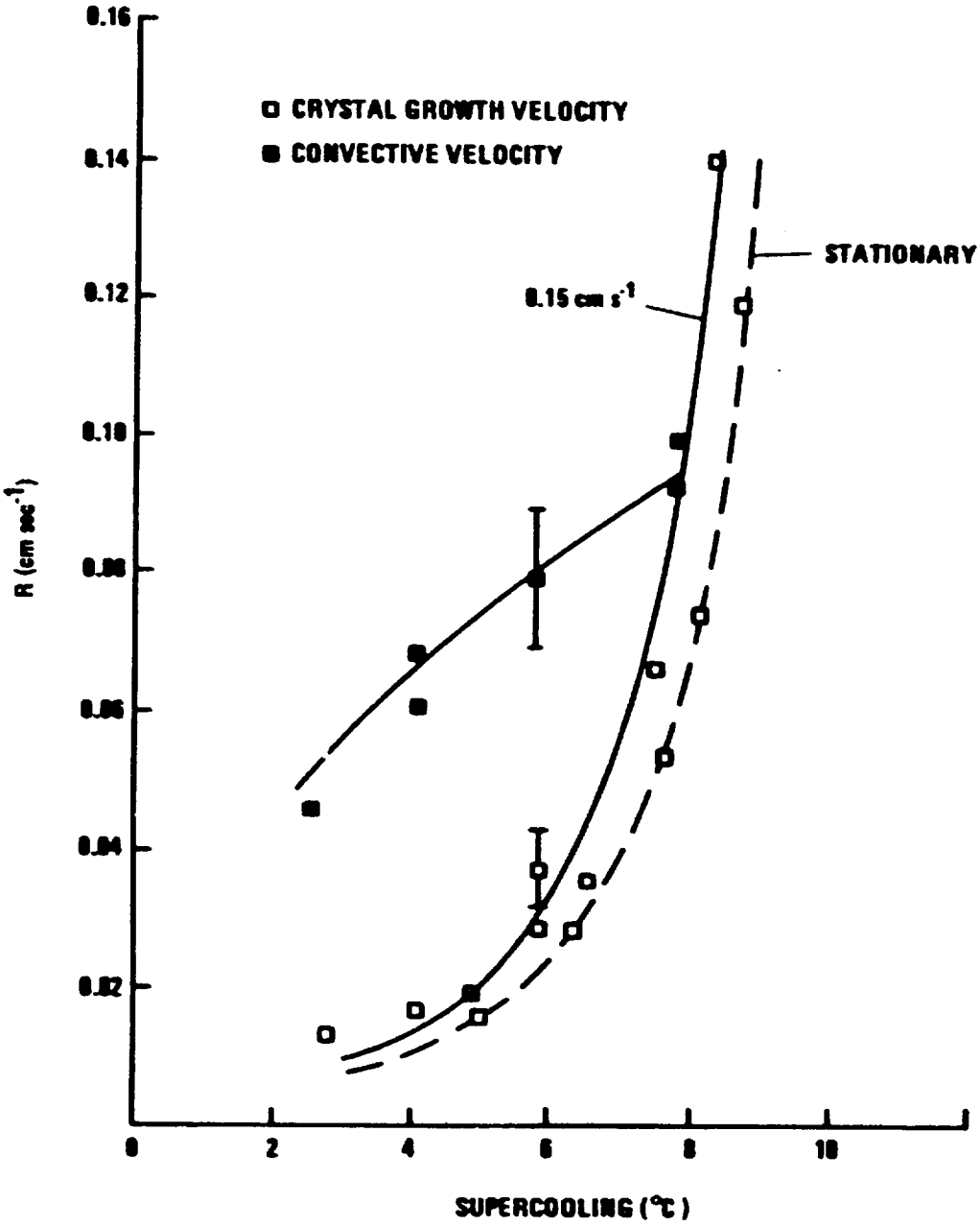

Fig. 24. Growth and convective velocity for $Na_2SO_4.10H_2O$ crystals in 2.5 M Na_2SO_4 supersaturated solution as a function of supercooling, moved at a velocity V_T = 0.15 cm s^{-1} through the solution.

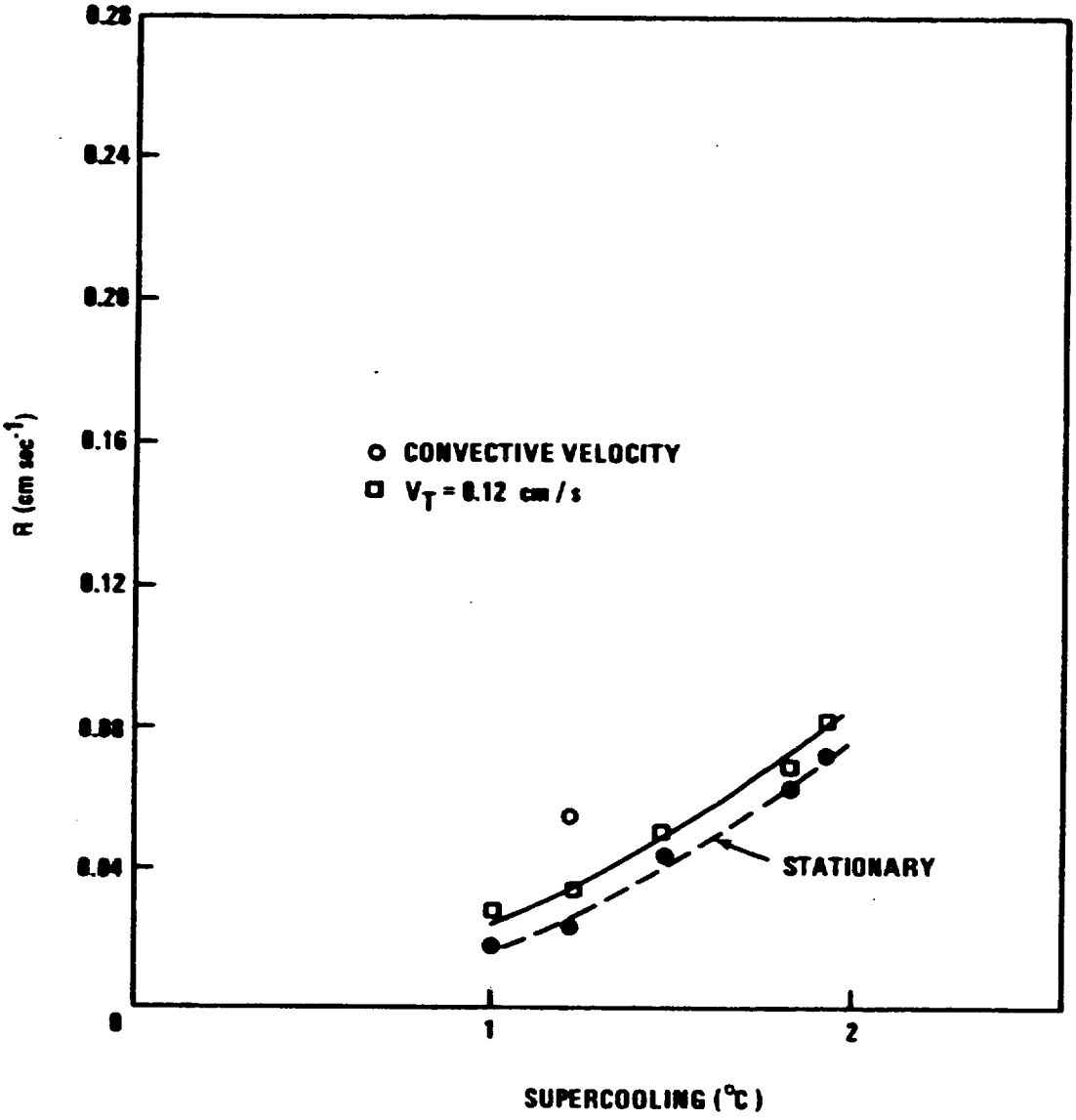

Fig. 25 Ice crystal growth under stationary and 0.12 cm s^{-1} transport velocity in 0.2 M NaCl solution.

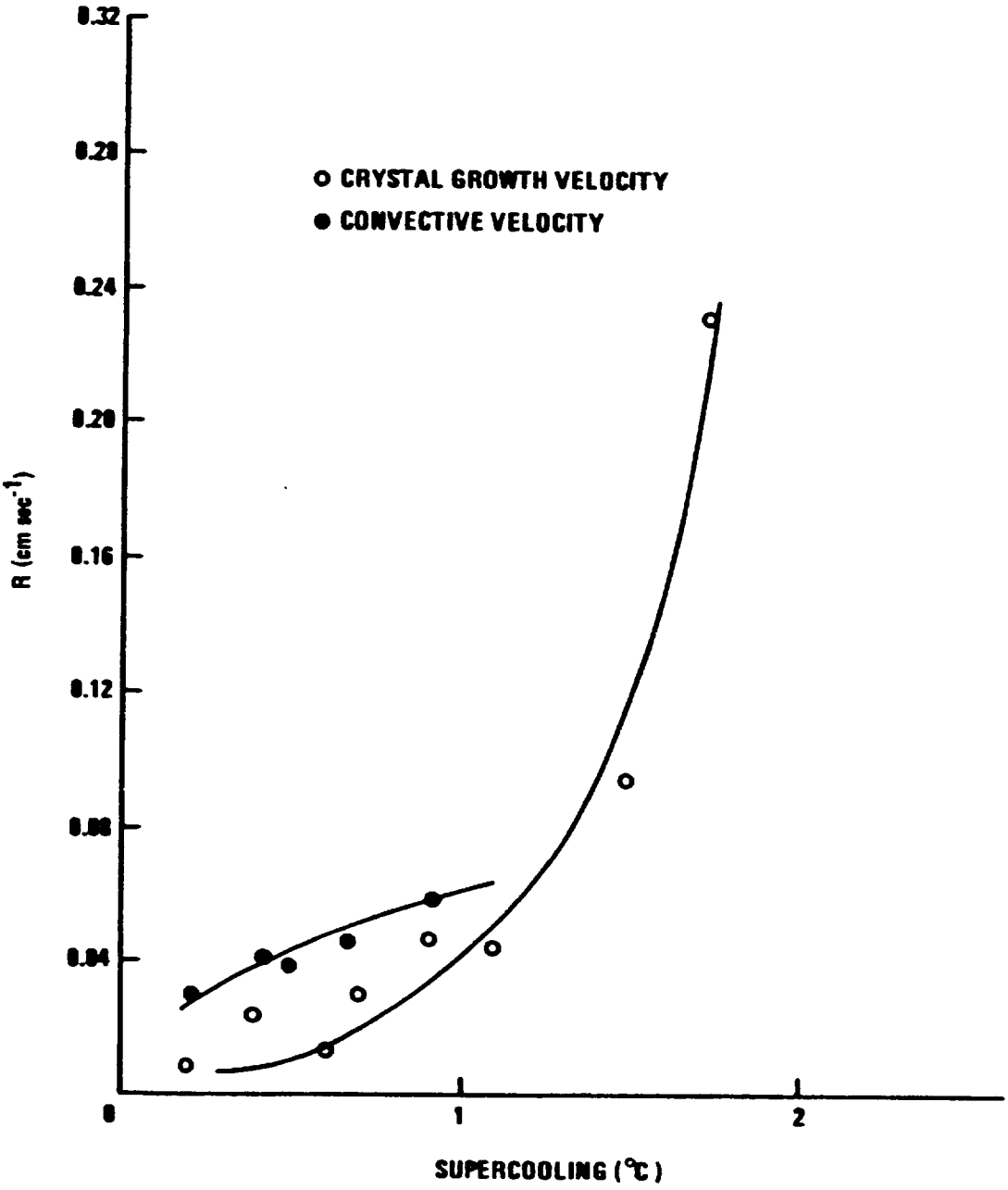

Fig. 26 Growth and convective velocity for ice in 0.4 M NaCl supercooled solution as a function of supercooling. Transport velocity V_T = 0.17 cm s^{-1}.

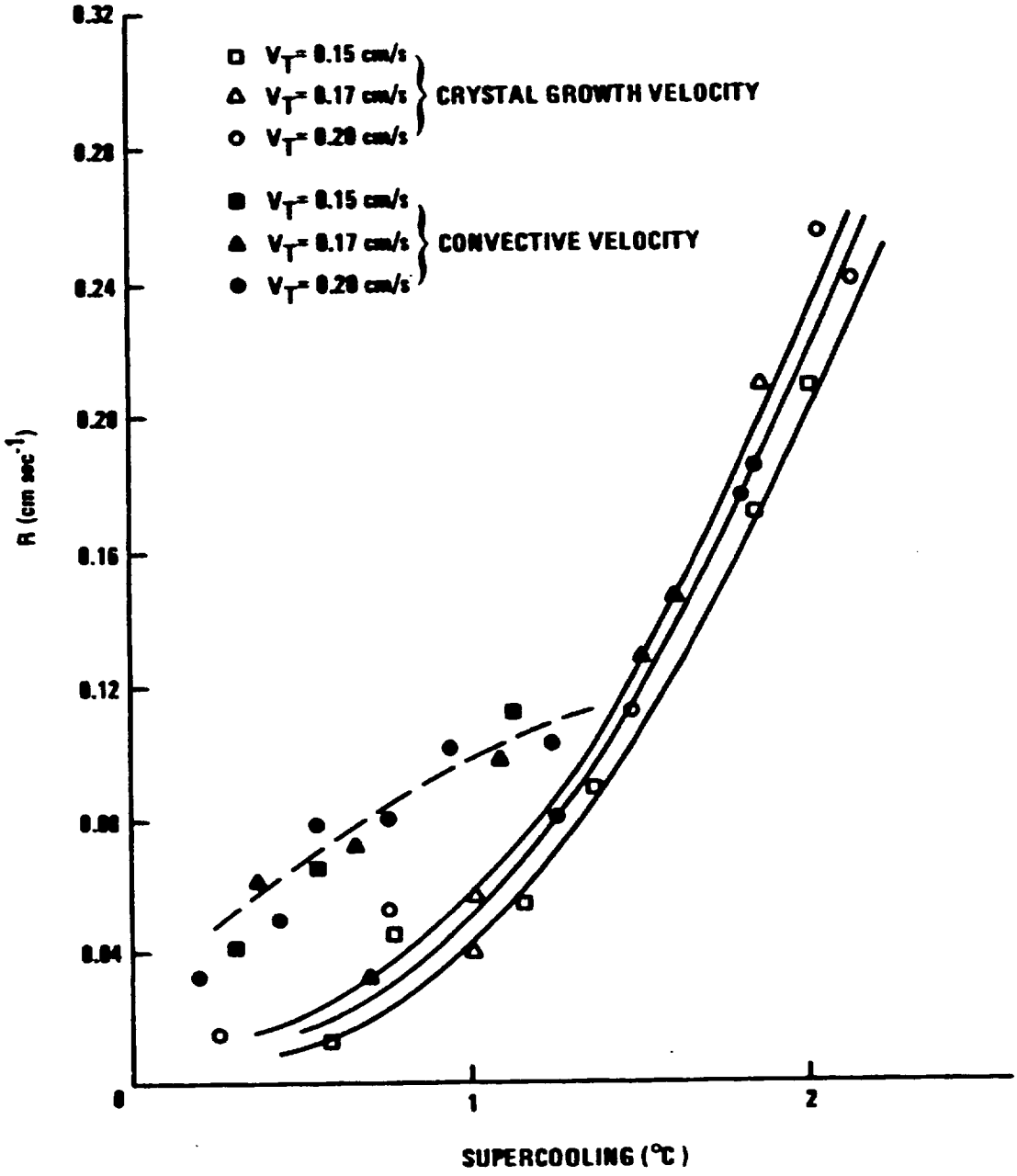

Fig. 27 Growth and convective velocity for ice in 1.0 M NaCl supercooled solution determined by supercooling and transport velocity.

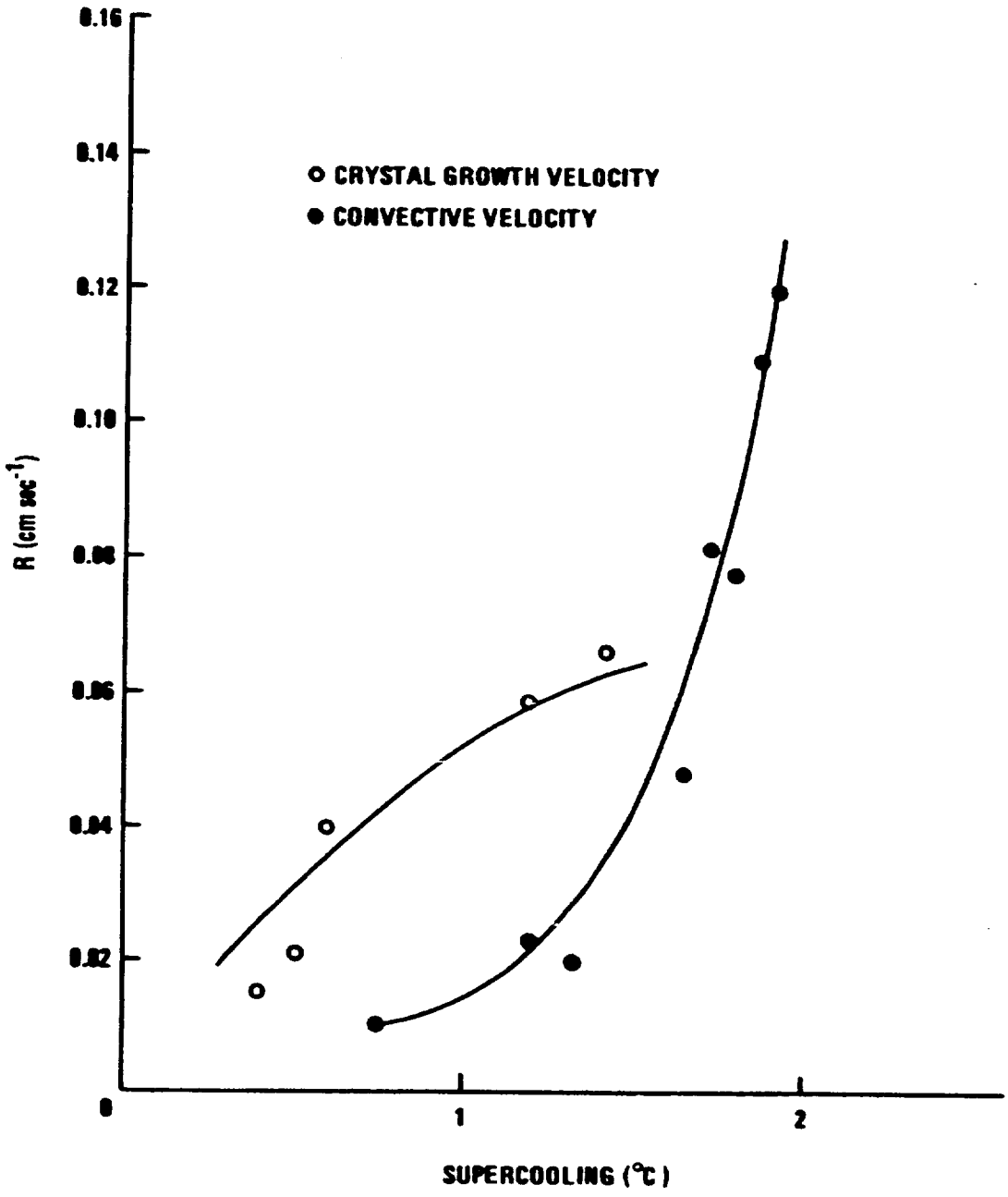

Fig. 28 Growth and convective velocity for ice in supercooled sea water as a function of supercooling at transport velocity $v_T = 0.15$ cm s^{-1}.

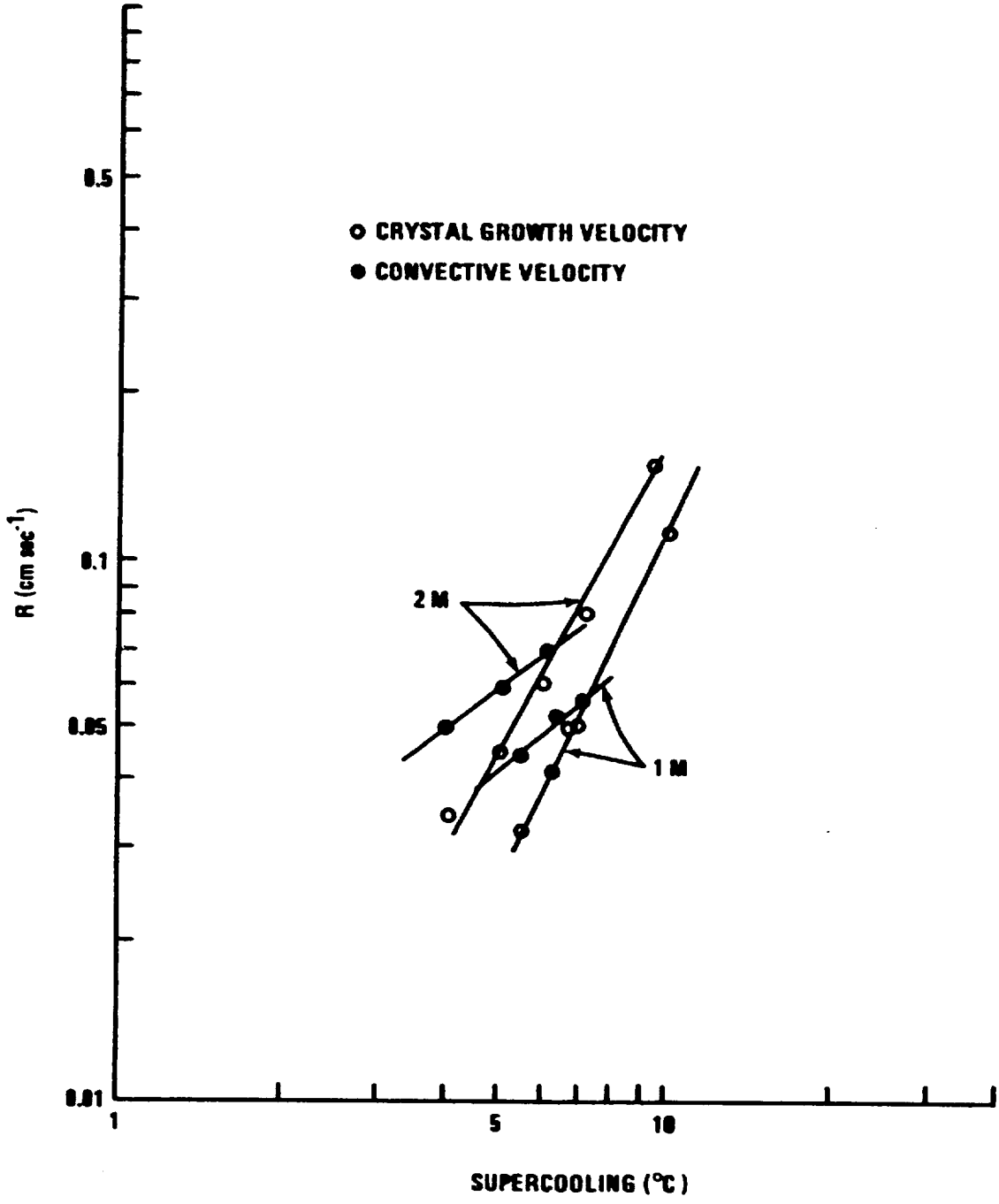

Fig. 29 Growth and convective velocity for 1.0 M and 2.0 M sodium sulfate solution. Transport velocity V_T = 0.26 cm s^{-1}.

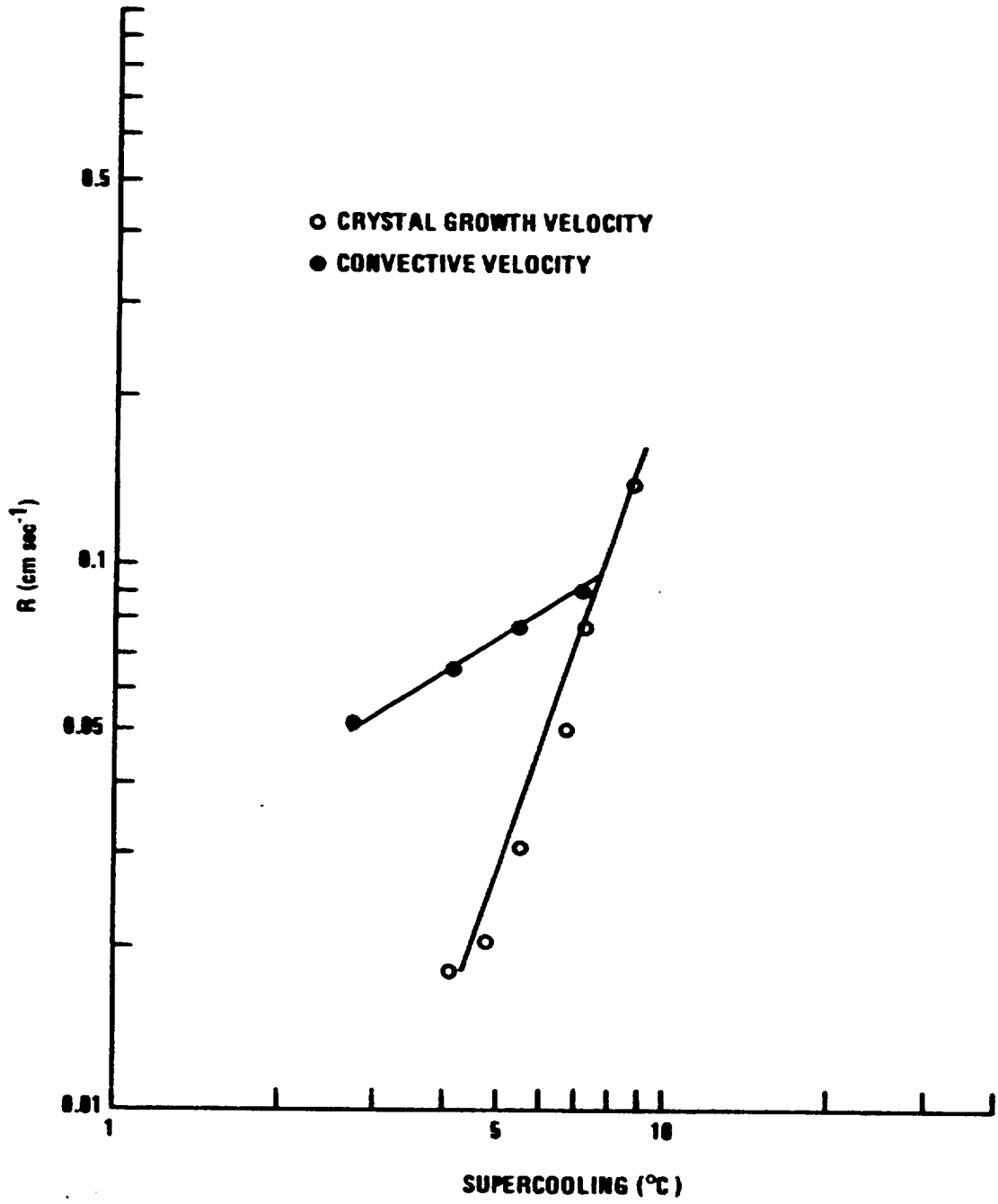

Fig. 30 Growth and convective velocity for sodium sulfate 2.5 M solution. Transport velocity V_T = 0.15 cm s^{-1}.

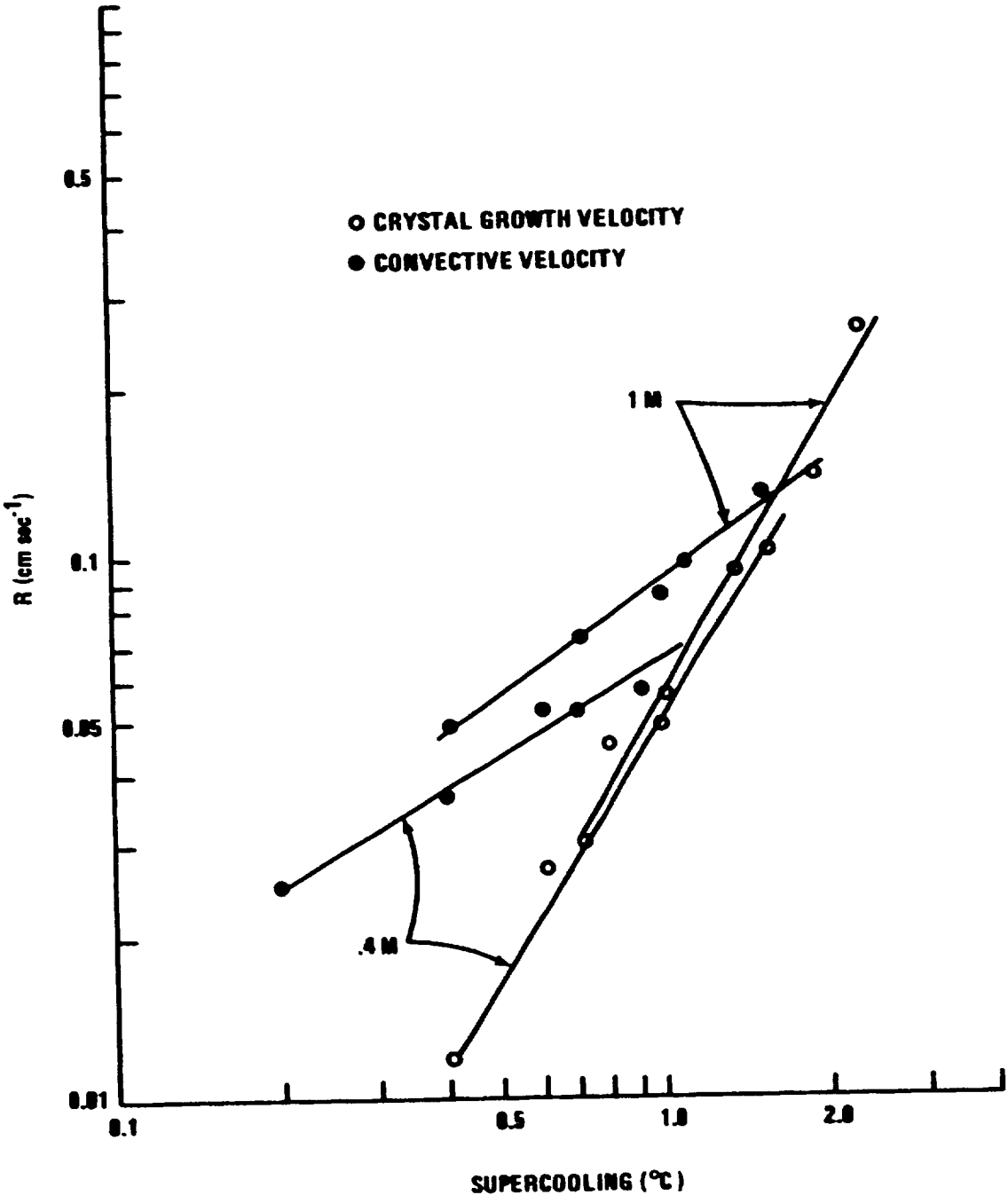

Fig. 31 Ice growth and convective velocity for 0.4 M and 1.0 M NaCl solution. Transport velocity V_T = 0.15 cm s^{-1}.

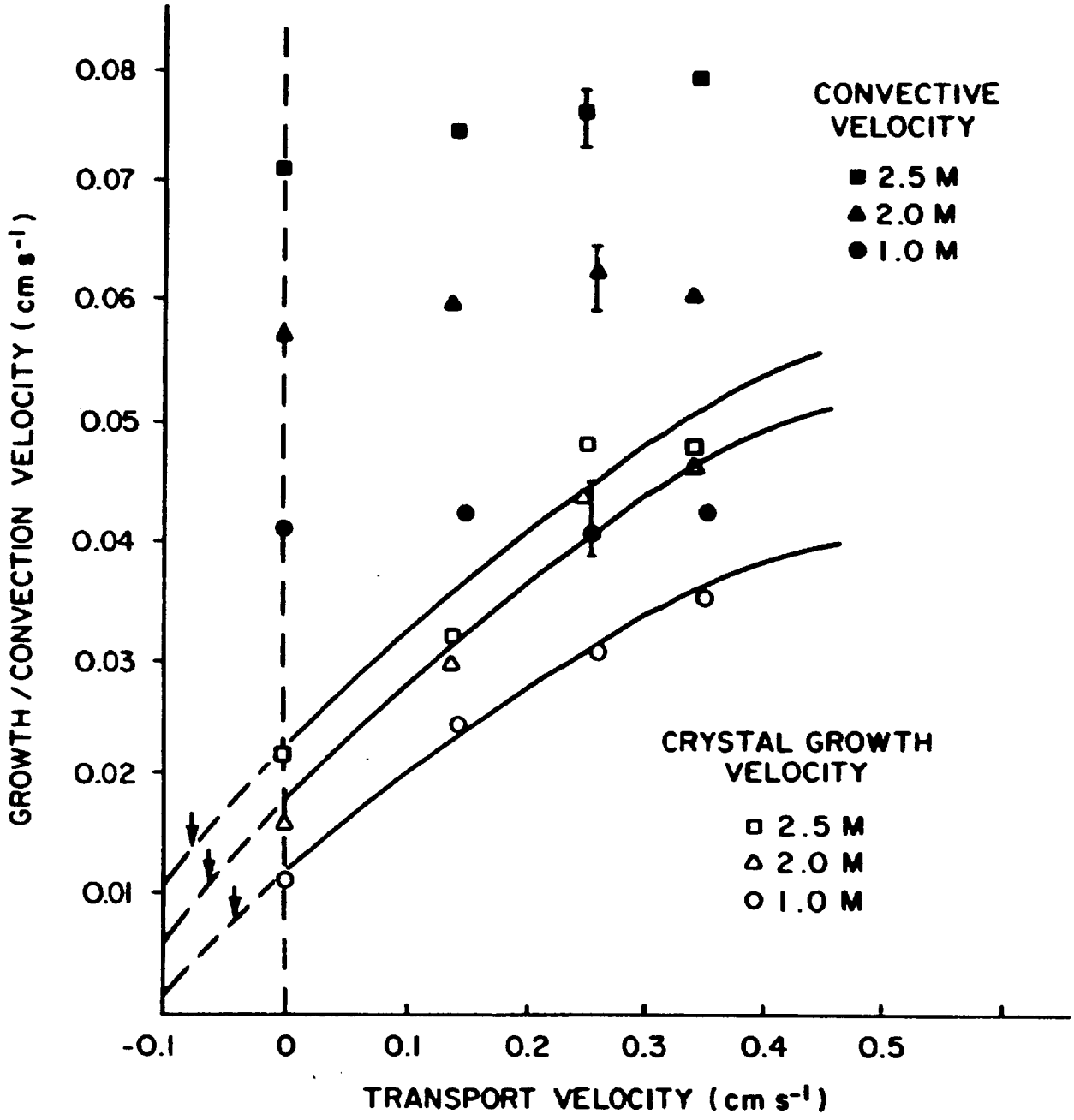

Fig. 32 Growth and convective velocity as a function of crystal transport velocity for different molarities, sodium sulfate decahydrate supercooling 5.5° C. Arrows indicate expected growth rate in low g in absence of convection observed in 1.0 g.

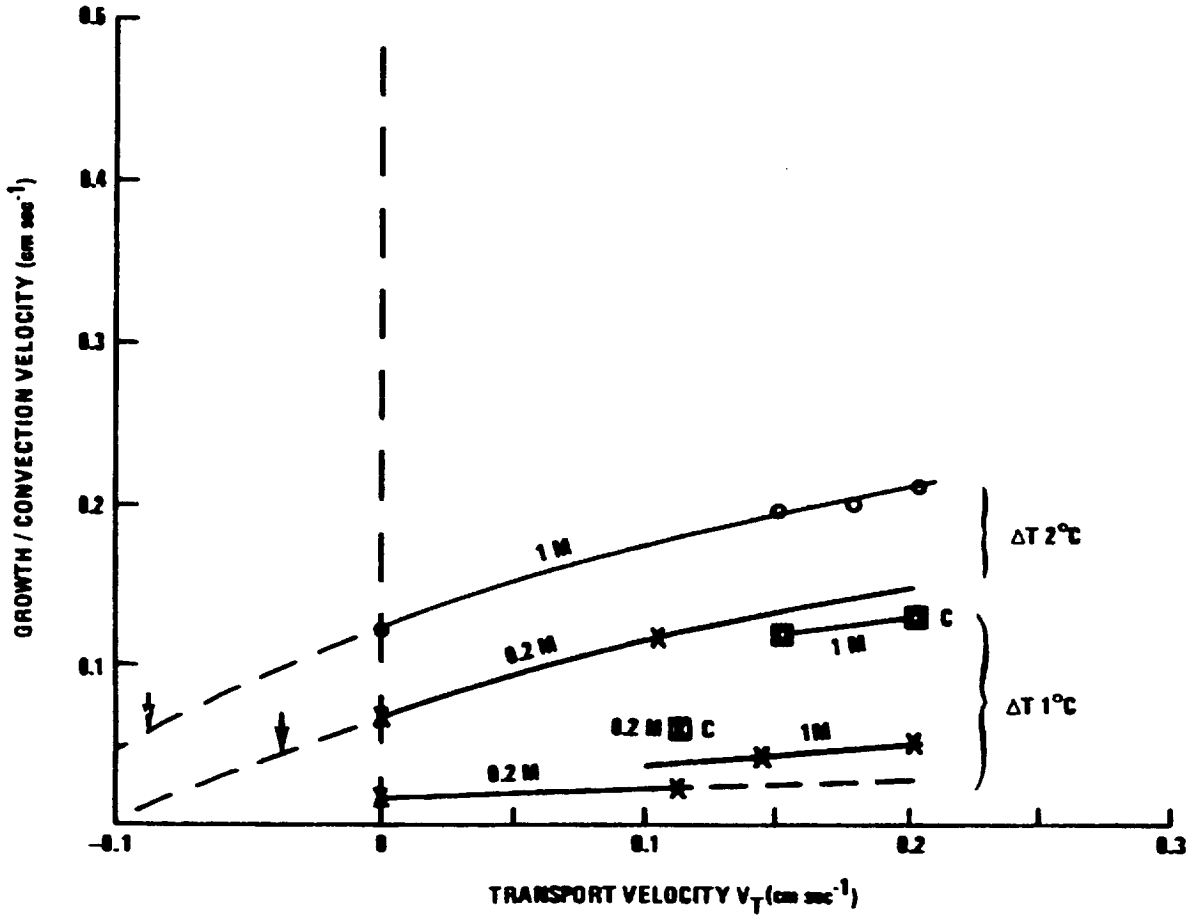

Fig. 33 Ice crystal growth rate and convection velocities at different transport velocity for NaCl solution, 0.2 M and 1.0 M. Arrows indicate expected growth rate in low g in absence of convection observed in 1.0 g.

rates. For both substances growth rates and convection rates become equal at a critical supercooling; for both substances there exists a temperature where the difference between convection rate and growth rate is a maximum. This decreases with ventilation and eventually disappears for U ~ 0.04 cm s^{-1} (decahydrate) and U ~ 0.08 cm s^{-1} (Ice in NaCl). For both substances relationships of Fig. 32, 33 can be used to predict growth rates in low g (arrowed) in the absence of kinetic effects.

b. Low gravity experiments: design criteria.

The results discussed above delineate optimum situations for finding an effect of low g on growth. It is immediately evident from Fig. 24, 28 that increasing transport velocity increases crystal growth rate; specifically an increase from zero (ie., natural convective velocity) to 0.12 cm s^{-1} increases the linear growth velocity by between a factor of 1.5 and 2. Similarly, it appears evident that at higher transport velocities that the growing tip is well ahead of the naturally convecting plume (Fig. 19, 22) so that no effect would be expected.

An effect would however be expected for stationary crystals where convective velocities are <u>less</u> than the crystal growth velocity, and greater than a velocity which, within the experimental error of (Fig. 32), would give a measurable increase because of the self-induced motion - say, 0.02cm s^{-1}. Hence, if such experiments were carried out under low g, it would be expected to see a decrease in growth velocity below that shown in Fig. 32 to a value equivalent to a transport velocity of between -0.05 and -0.1 cm s^{-1}.

The low g studies were designed to investigate the crystallization velocity of solution, both ice in NaCl and decahydrate from solution with supercooling about 1/2 - 1° C and 3 - 4° C respectively. These supercoolings give growth rates between 100 and 200 μm s^{-1} in both cases, which would be expected to be reduced by about a factor of 0.5 under low g if the extrapolations of Fig. 24 are valid.

One further consideration of the low g experiment is the rapidity with which such natural convection will die out. This has already been discussed (Table 1, p. 25) for a crystal of tip dimension 0.1cm, $\tau \sim \frac{0.1^2}{0.01}$ = 1 s for pure water and ~ 0.1 s for sodium sulfate solution with $\nu \sim 0.1$ (Fig. A3). Thus the deceleration of the convection on entering low g and its acceleration on reaching high g should be readily observable. The next section shows that this is indeed the case.

c. Crystallization under varying gravity.

i. Sodium sulfate decahydrate.

Fig. 34 shows the interferograms from a sequence from 10^{-3} g to > 1.2 g. For crystallization of decahydrate at 21.8°C, equivalent to a supercooling of 5.0°C. A buoyant plume was emitted from the capillary tip just prior to entry into low g; this remained almost unchanged as crystals grew (a - g). A crystal moved, possibly by surface tension effects, into the field of view pointing downwards halfway through the parabola. With pullout, this convective plume accelerated (h - z) and, at the same time, two convective plumes (2, 3, fig 34k) detached from the horizontally growing crystal and accelerated upwards (j - m: these eventually merge). Meanwhile, a crystal (C, fig 34h) began growing vertically downwards, as g increased presumably responding to a vertical plume rising past its tip - this plume is not however seen in the interferometer as it appears too narrow in vertical flow. The diffusion distance of solute during the course of the experiment is ~ $\sqrt{D \times t}$. With $D = 10^{-5}$ cm^2 s^{-1} this gives a distance of 100 μm in 10 s which is barely resolved by the Mach Zender optics. It is noted that there exists sharp gradients across the rising plume which persist for > 10 s (a-g). Compare crystals D, E (fig 34t). Measurements of the crystal growth velocity are shown in Fig. 35. The horizontally oriented crystals (A, B, Fig. 34h) change little in growth rate during the change of gravity. The reason for this is apparent from the position of the convective plume;

Fig. 34 (a-x) Crystal growth and convection in 2.3 M sodium sulfate solution. Nucleation was achieved by inserting a decahydrate crystal into the tube. Initial equilibrium temperature 27.0°C; initial supercooling 5.1°C giving $\Delta n_\lambda = 0.06$ ($\lambda = .6328$ μm) (from Fig. A4).

Photography of a growing crystal began in low gravity (a), continued for ~ 17 s at g ~ 0.05 ± .02 (with variability due to atmospheric turbulence) and then continued as g increases to > 1.2 g. Growth rates are given for crystal A, B, C, h in Fig. 35.

A plume of low density had emerged from the capillary (k, l) and is essentially stationary during low g, but accelerated upward as g increased. Two other plumes rise from the horizontal crystals as gravity increases k 2, 3. The main set of fringes are from monochromatic light (0.6328 μm) with fringe spacing and detail in uniform density resulting from inhomogenities in the container and the angular offset of the mirrors. The close fringes shown at the bottom of the cell results from the curvature of the glass. Narrow diffraction fringes occur around all regions of sharp discontinuity, and are ignored in this analysis.

Sequence 1: a - p shows crystal growth and plume development going from low to high g.

Sequence 2: q - x shows plume development in high g, decreasing on entry into low g.

The boundary layer around the downward oriented crystal D(t) remains unchanged from high g to low g, but increases as g increases (w, x). The boundary layer around the slant crystal E(t) decreases in thickness as the tip convection decreases and finally ceases in low g.

Crystals still move around under low g presumably because of capillary effects.

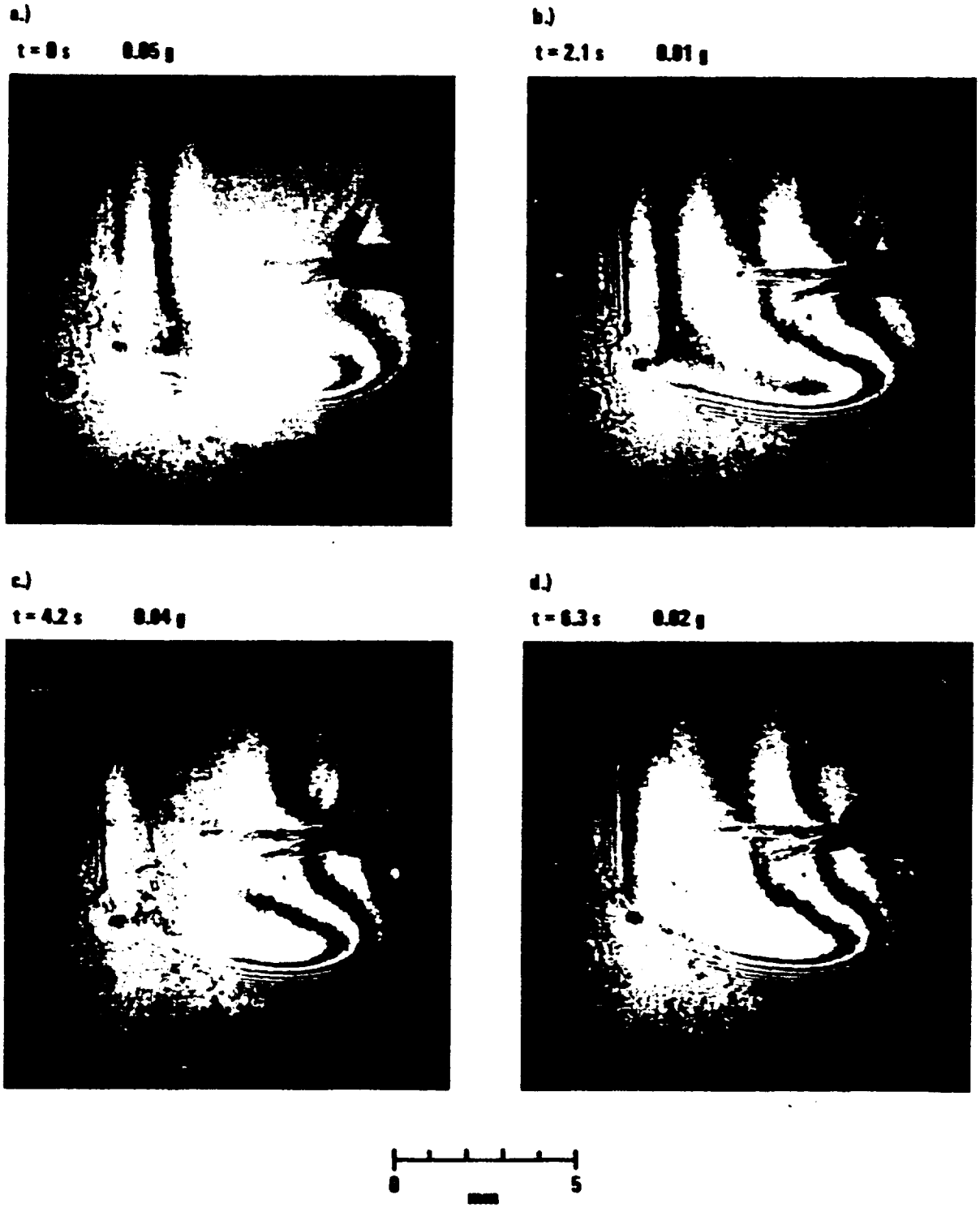
a.)
t = 0 s
0.85 g
b.)
t = 2.1 s
0.81 g
c.)
t = 4.2 s
0.84 g
d.)
t = 6.3 s
0.82 g
0
5
mm

e.)

t = 8.4 s 0.84 g

f.)

t = 10.5 s 0.84 g

g.)

t = 14.0 s 0.84 g

h.)

t = 15.4 s 0.87 g

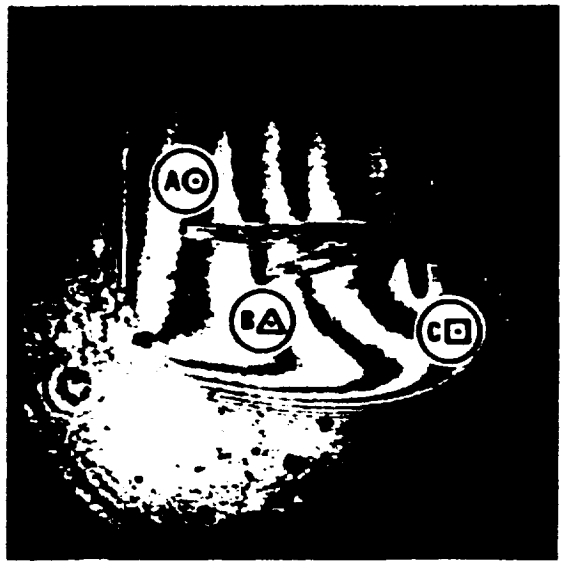

i.)
t = 16.1 s 0.13 g

j.)
t = 16.8 s 0.4 g

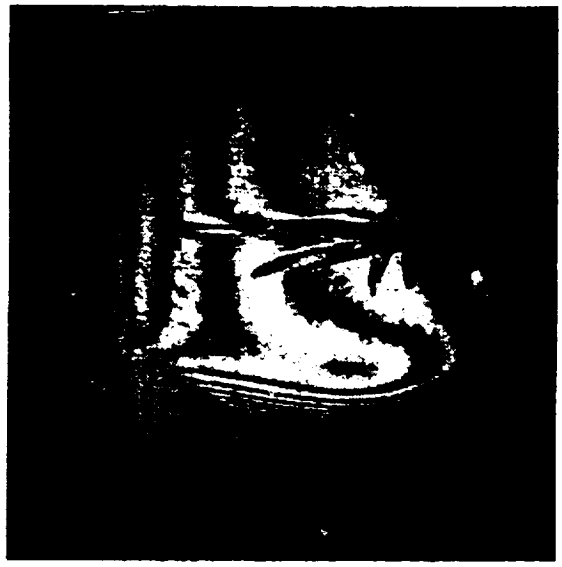

k.)
17.5 s 0.52 g

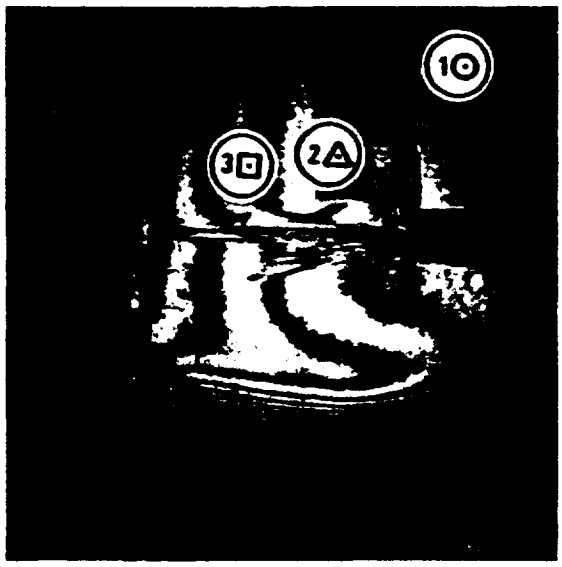

l.)
18.2 s 0.71 g

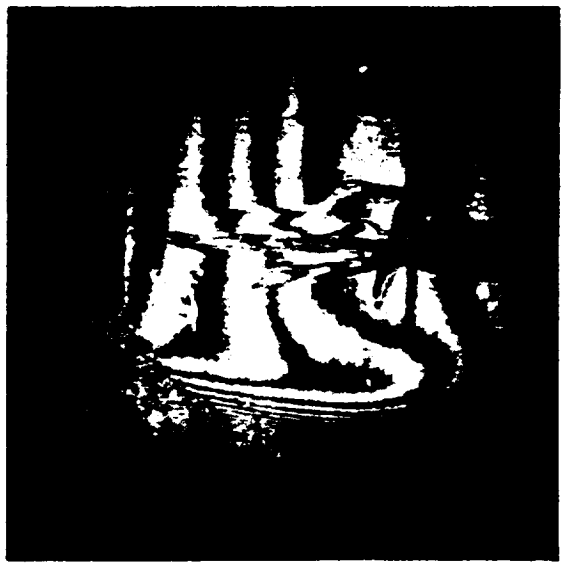

m.)

t = 18.9 s 0.87 g

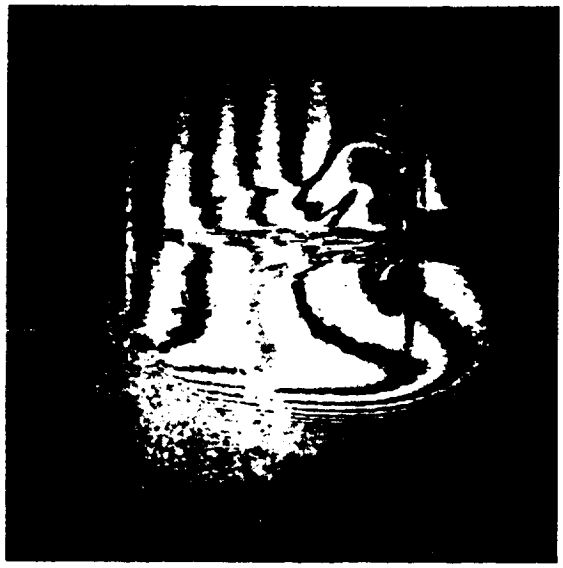

n.)

t = 19.6 s 1.8 g

o.)

t = 20.3 s 1.1 g

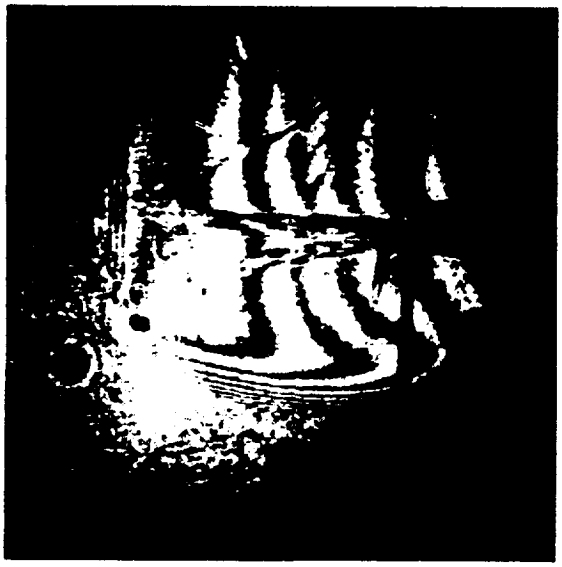

p.)

t = 21.0 s 1.2 g

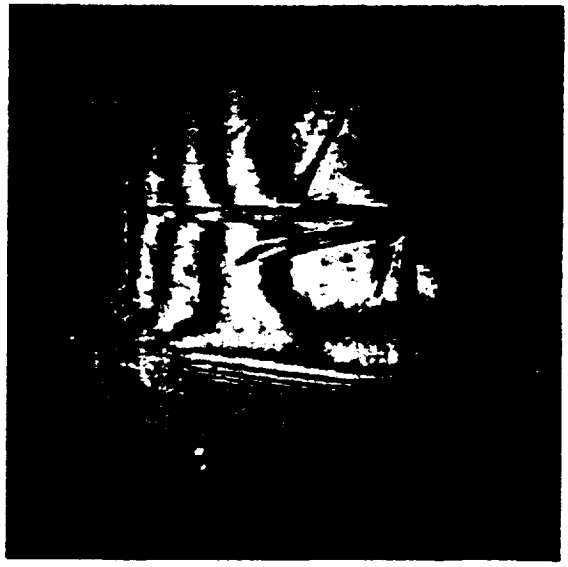

q.)
t = 67.9 s >1.2 g

r.)
t = 68.6 s >1.2 g

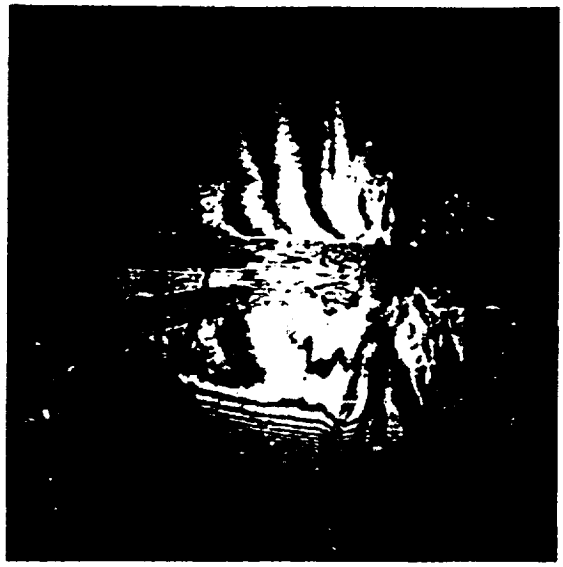

s.)
t = 73.5 s 0.86 g

t.)
t = 74.9 s 0.89 g

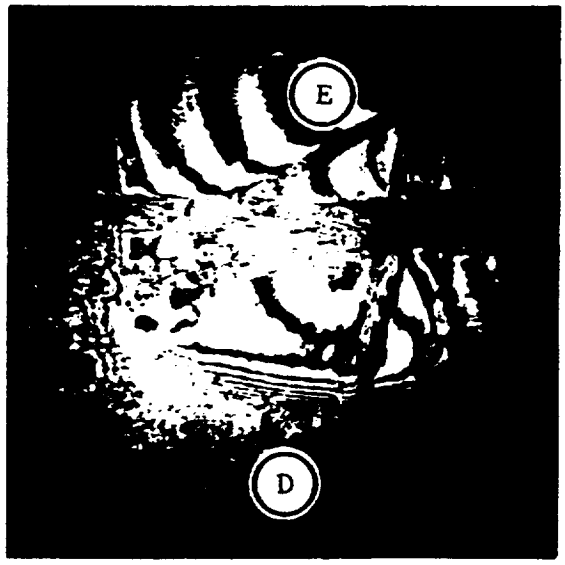

u.)

t = 79.1 s 0.84 g

v.)

t = 88.9 s 0.81 g

w.)

t = 91.7 s 0.81 g

x.)

t = 93.1 s 0.51 g

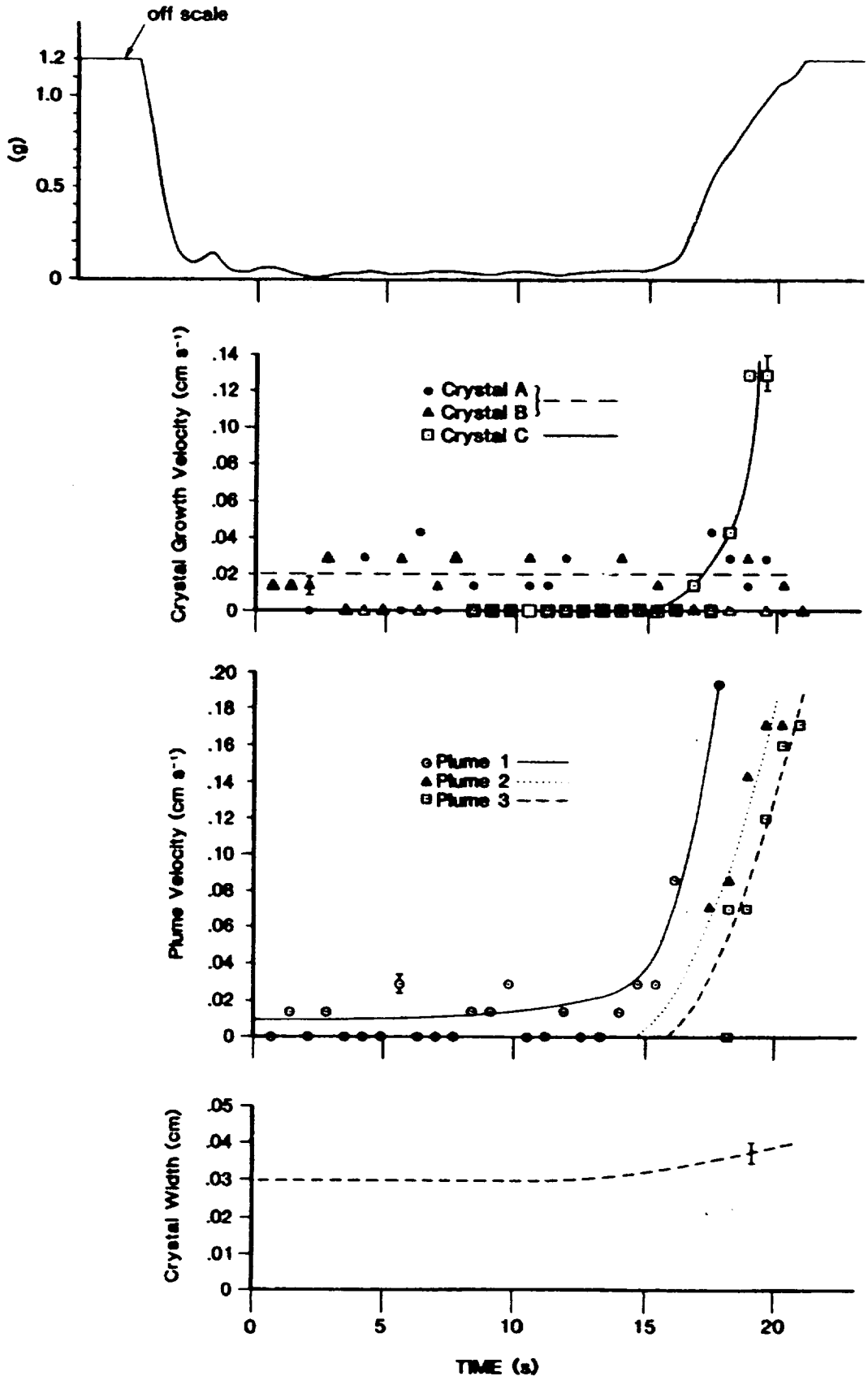

Fig. 35 Crystal growth rates and plume rise velocity during gravity change from low to high. Data from Fig. 34, A,B,C,h; 1, 2, 3, k

it detaches from the leading tip of the crystals. By contrast, the vertically oriented crystal (C, Fig. 34h) accelerates in growth rate as g increases from 0.01 to 0.2 to 0.4, to a value of 0.186 $\pm$ .005 cm s^{-1} at 1.0 g. The width growth rate of the crystal does apparently change as the convective plume rises back from the tip (Fig.35). The tip of the convection accelerates as it rises with the vertically moving plume accelerating more quickly than the elongated plumes from the horizontal crystals, although the maximum velocities recorded (0.2 cm s^{-1}) are comparable. Similarly, a buoyant vortex ring generated by growth from a fallen crystal persists as it rises, (Fig. 36, 37a). The isolated vortex ring rises somewhat slower than the tip of a starting plume from a newly initiated source (Fig. 37b, c). It is clear from the figures that there is a stilling time of a few seconds as gravity changes, and that once low g is attained, diffusion over the period of observation is slow. The wakes visible in Fig. 36 show persistence over tens of seconds, which is consistent with the low diffusion rates of solute. Under controlled conditions, this would provide an ideal way of measuring diffusion coefficients completely uninfluenced by motion. This technique would similarly provide opportunity for verifying theoretical concepts of plume and vortex ring motion, since inertial effects can be separated completely from buoyancy effects under low g. It is emphasized that in these photographs the line of sight dimension giving rise to the refractive index difference is unknown, so that we need to interpret the optical path differences in terms of the geometry of the system - a vortex ring with minimum density in a doughnut and a plume with minimum density in the center as a sausage being an incomplete, transient vortex ring at the rising tip.

The second parabola some 50 seconds later shows additional crystals growing from the container wall; in this case with quite distinct facets (Fig. 34 g-k). The temperature had risen 1° over this period, giving a lower supersaturation. Following the second parabola several new convective plumes appeared rising with comparable velocity.

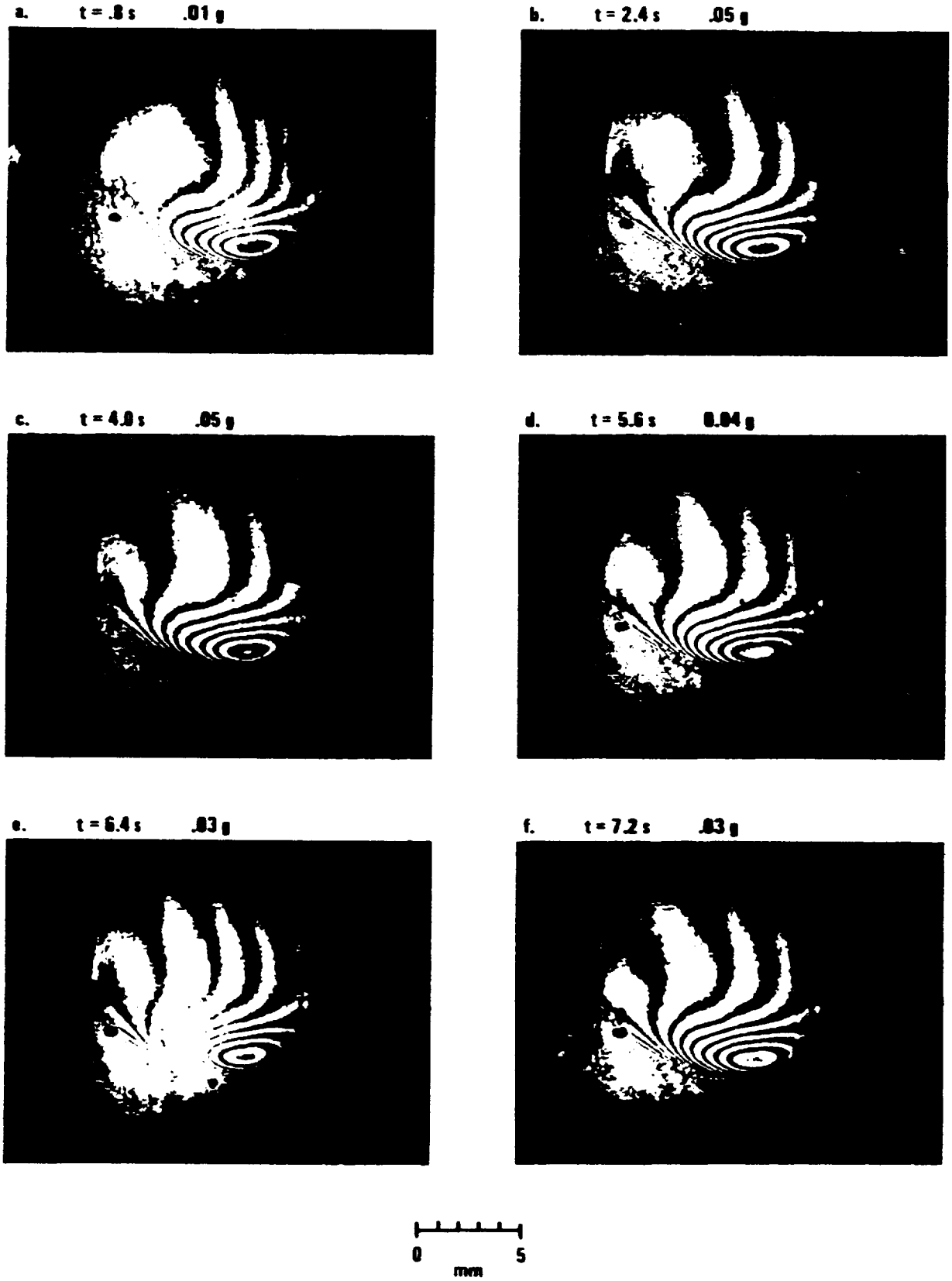

Fig. 36 A bouyant plume which emerged from the nucleation tube in high g remains almost stationary in low g (a - i), accelerates as g increases (j - l). A vortex ring is created from a fallen crystal (out of the field of view) rises as g increases (m - n). Initially a wake is evident, but is not apparent at a later stage (s,t). u-z shows a further sequence with different internal structure. Supercooling 2. 5°C.

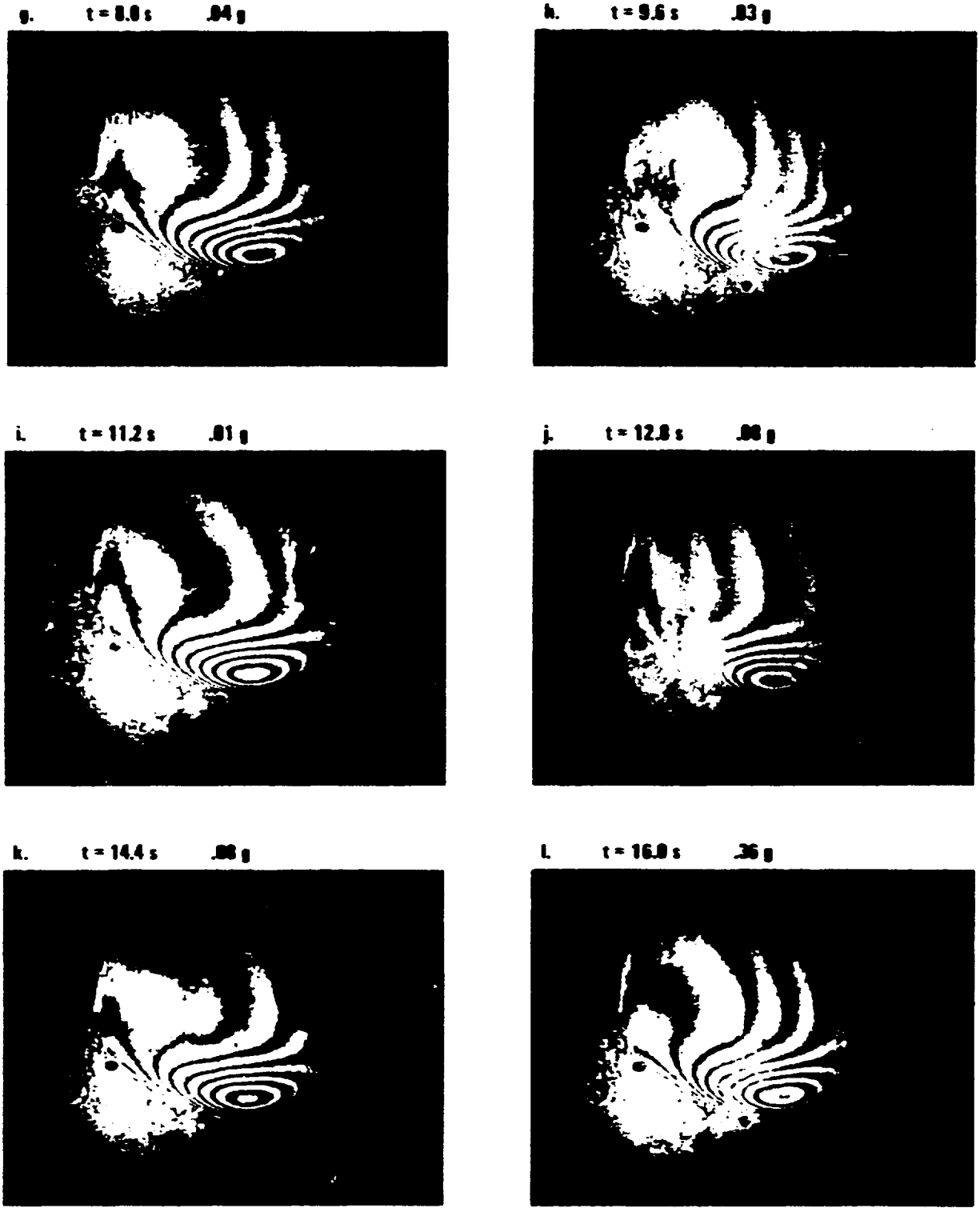
g. t = 8.8 s .84 g
h. t = 9.6 s .83 g
i. t = 11.2 s .81 g
j. t = 12.8 s .88 g
k. t = 14.4 s .88 g
l. t = 16.8 s .36 g
0
5
mm

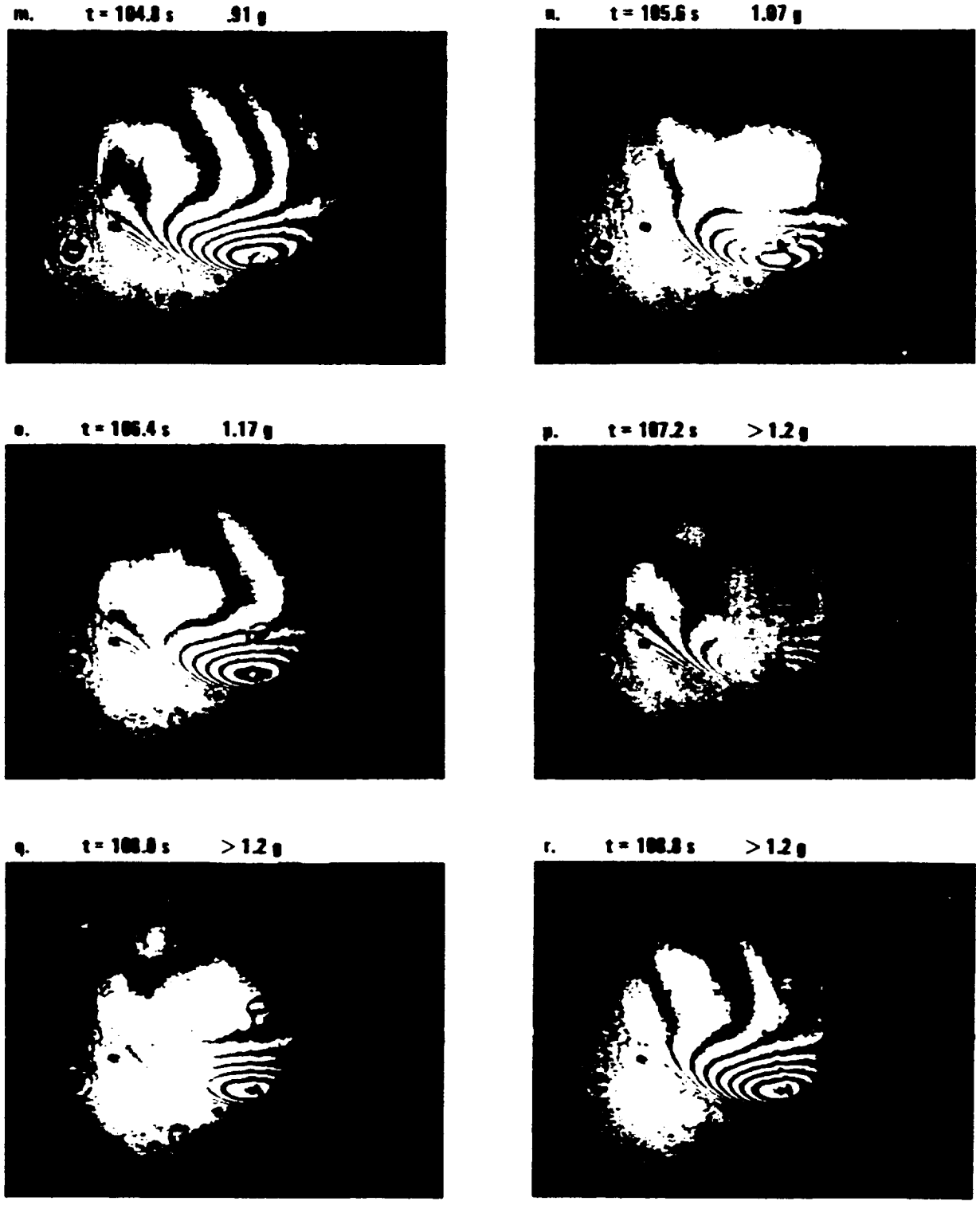
m. t = 104.8 s .91 g
n. t = 105.6 s 1.07 g
o. t = 106.4 s 1.17 g
p. t = 107.2 s > 1.2 g
q. t = 108.0 s > 1.2 g
r. t = 108.8 s > 1.2 g
0
5
mm

s. t = 108.6 s >1.2 g

t. t = 118.4 s >1.2 g

u. t = 196.0 s > 1.2 g

v. t = 196.8 s > 1.2 g

w. t = 197.6 s > 1.2 g

x. t = 198.4 s > 1.2 g

y. t = 199.2 s > 1.2 g

z. t = 200.0 s > 1.2 g

(a)

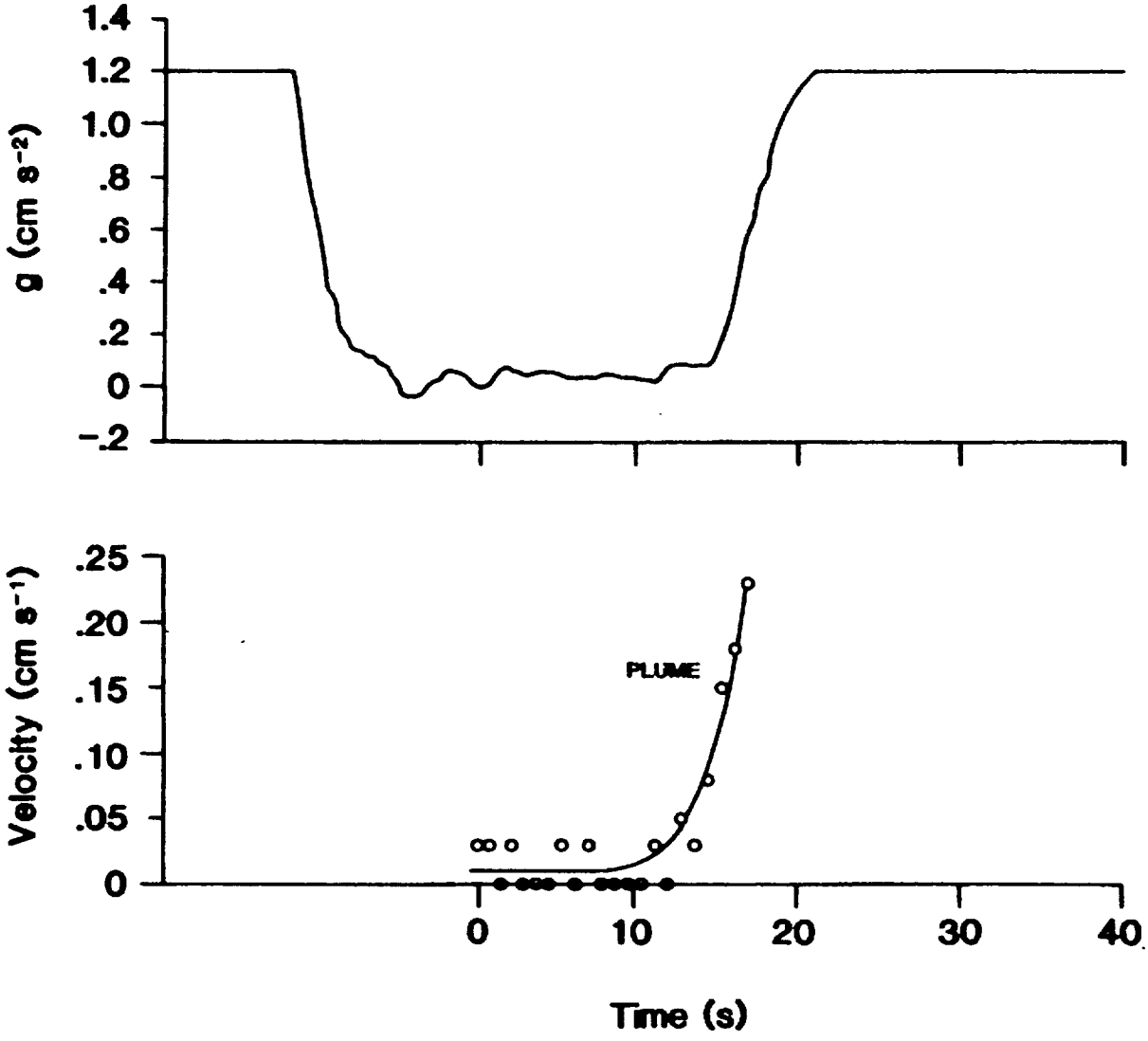

Fig. 37 a, b, c Velocity of the plume and vortex ring in Fig. 36a related to gravity. There is an apparent decrease of vortex ring velocity as it rises, in both cases. g magnitude is not available in this region.

(b)

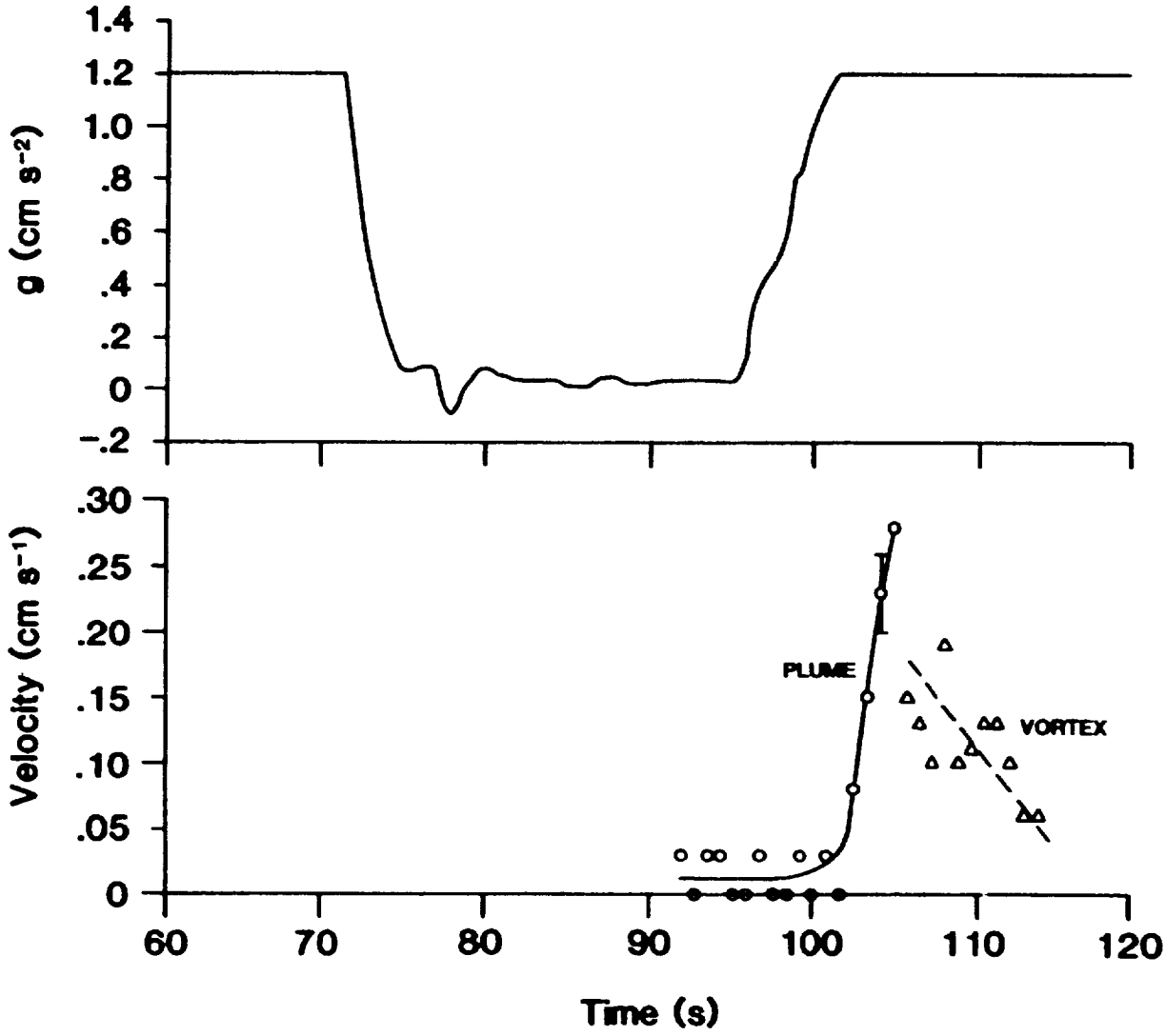
1.4
1.2
1.0
.8
.6
.4
.2
0
-.2
g (cm s⁻²)
.30
.25
.20
.15
.10
.05
0
Velocity (cm s⁻¹)
PLUME
VORTEX
60
70
80
90
100
110
120
Time (s)

(c)

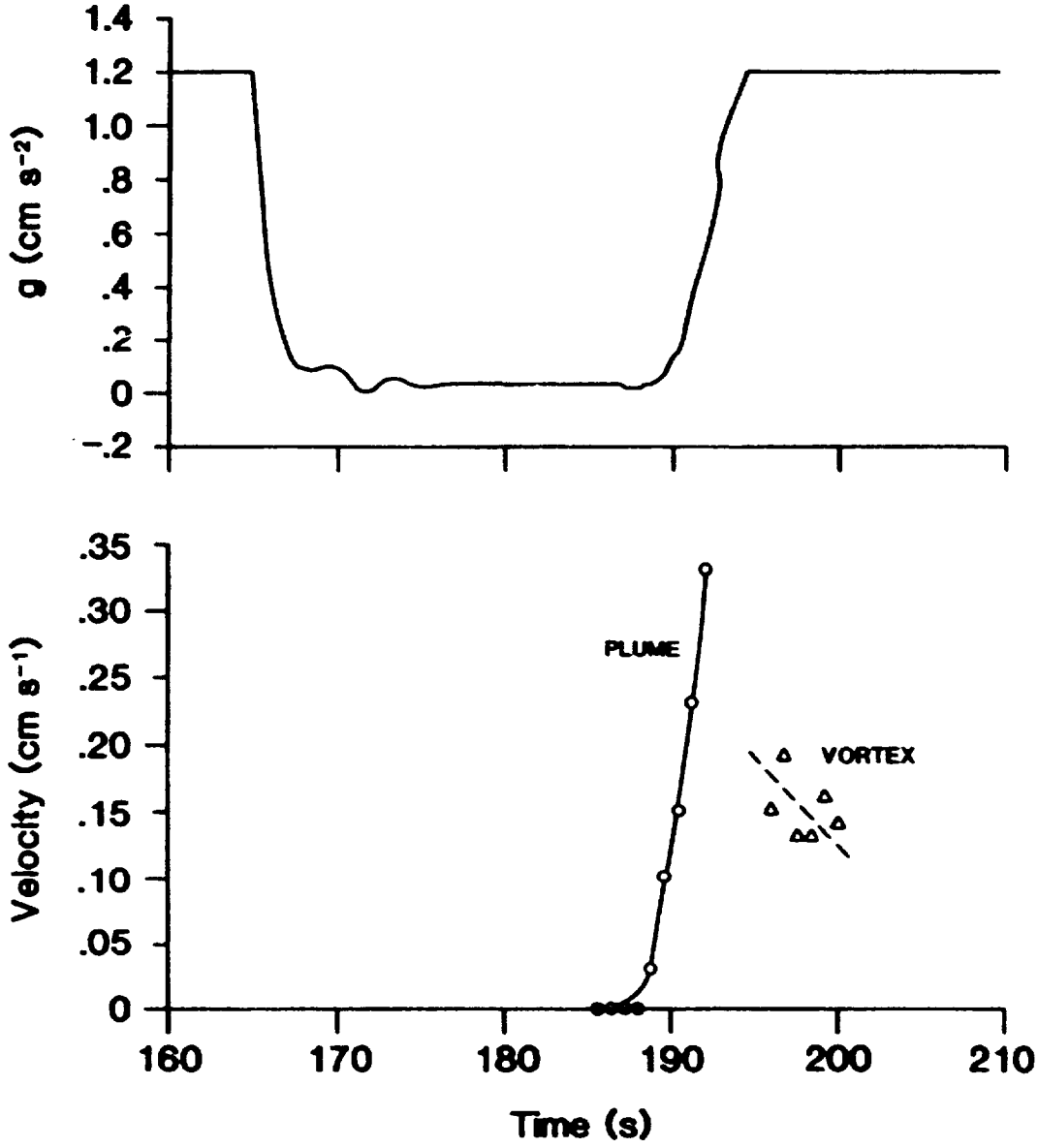
1.4
1.2
1.0
.8
.6
.4
.2
0
-.2
g (cm s⁻²)
.35
.30
.25
.20
.15
.10
.05
0
Velocity (cm s⁻¹)
PLUME
VORTEX
160
170
180
190
200
210
Time (s)

C-2

Further into the crystallization process a more general fluid motion became evident on the scale of the cell itself as can be seen from the displacement of fringes towards the edge of the cell away from the individual crystals.

ii. Ice in supercooled sodium chloride.

Visible convection does not usually occur from the tips of ice dendrites growing either horizontally or vertically; there is apparently no direct effect even in high g. This is somewhat at variance with the plume shown in the laboratory study in Fig. 22. Such a plume was obtained only infrequently in the laboratory study, as opposed to the sodium sulfate plume which occurred in every case and may be related to some accident of the dendrite structure or motion. However, once the initial dendrites have grown, there appears to be a secondary growth which is more effective in giving rise to high density salt solution which sinks from the spongy ice/solution mixture, and is clearly shown in the interferograms (Fig. 38). This begins some 10 s after the initial growth (in low g) and requires a somewhat longer period to begin flow following the transition from low to high g. (Fig. 39). A comparable sequence is shown in Fig. 40. On one occasion such a descending plume in high g gave rise to extensive nucleation of small ice crystals as it accelerated downward (Fig. 41). The plume extended downward some 2 cm from the nucleating site. Crystals subsequently rose under their own buoyancy although the initial mass retained its identity. The lack of distortion in the interferogram shows that the diffusion of solute from the crystal plume is negligible.

It follows that in general there are two distinct convection regimes associated with dendrite growth in solution. Type I, (as with sodium sulfate decahydrate) convection takes place from the individual dendrite, and has the capability of increasing the tip growth velocity with increasing orientation of growth direction towards the gravity direction.

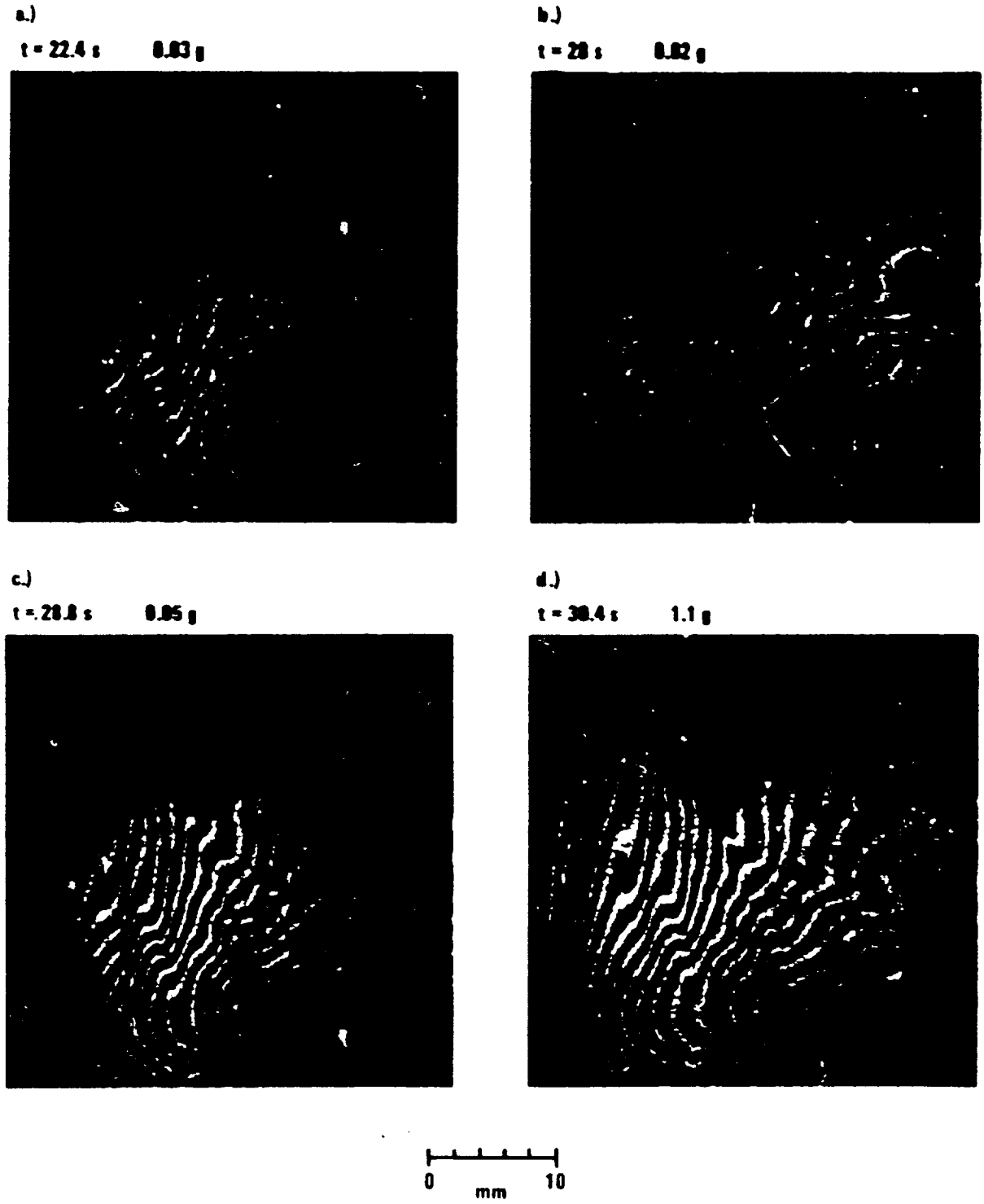

Fig. 38 A downward growing ice crystal in 6.0% 1.07M NaCl (ΔT = 1.3° C) gives no convective plume in low g and takes 13 s to initiate a downward convective plume in high g. The crystal rotates and grows slightly faster on entry into high g.

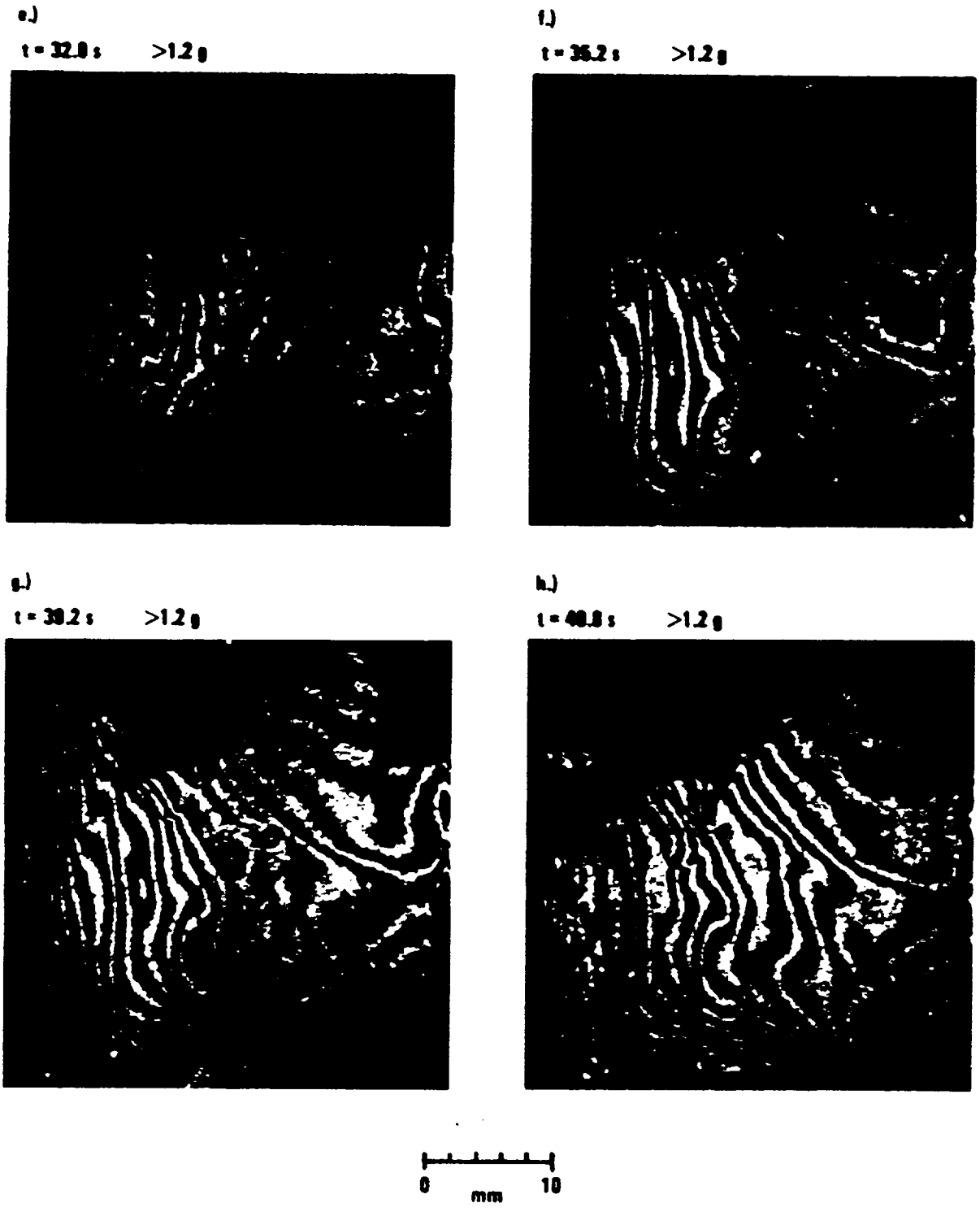
e.)
t = 32.8 s >1.2 g
f.)
t = 35.2 s >1.2 g
g.)
t = 39.2 s >1.2 g
h.)
t = 40.8 s >1.2 g
0
mm
10

i.)

t = 43.2 s >1.2 g

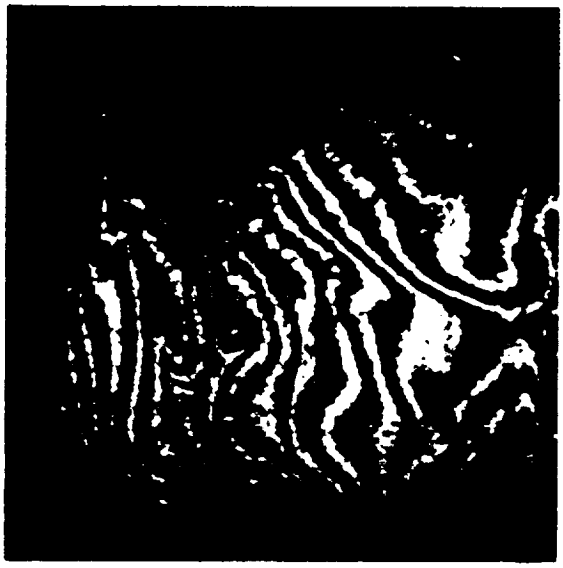

j.)

t = 46.4 s >1.2 g

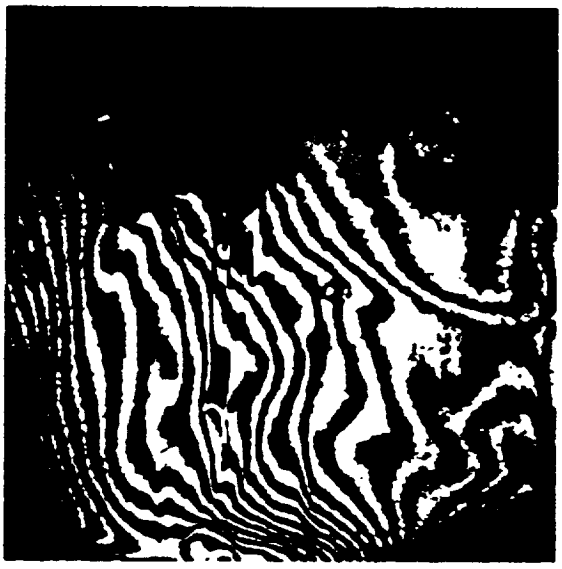

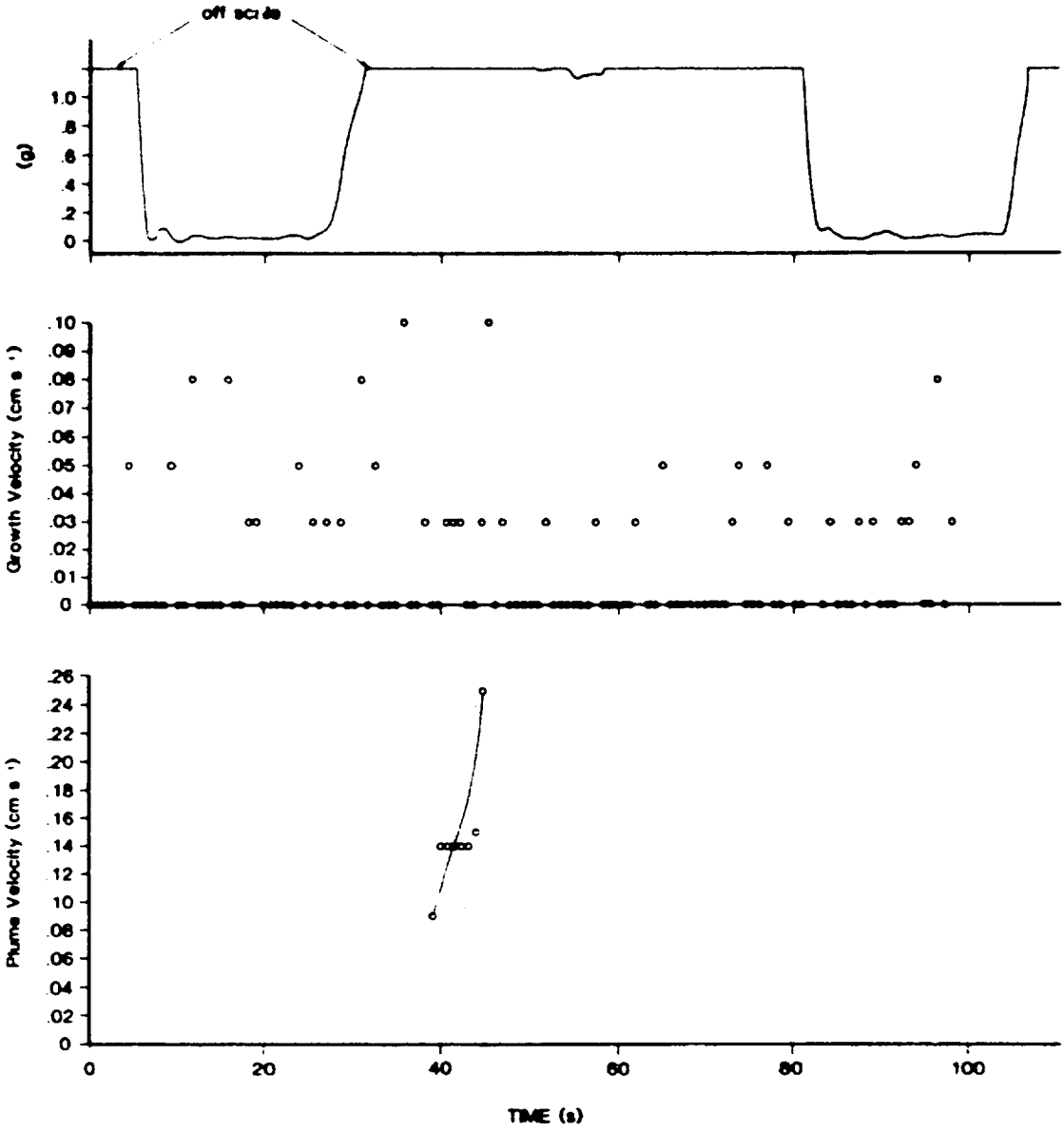

Fig. 39 Growth velocity of the downward oriented dendrite (Fig. 37) is unrelated to g. The plume of high concentration NaCl solution takes ~ 10 s before leaving the dendrite mush.

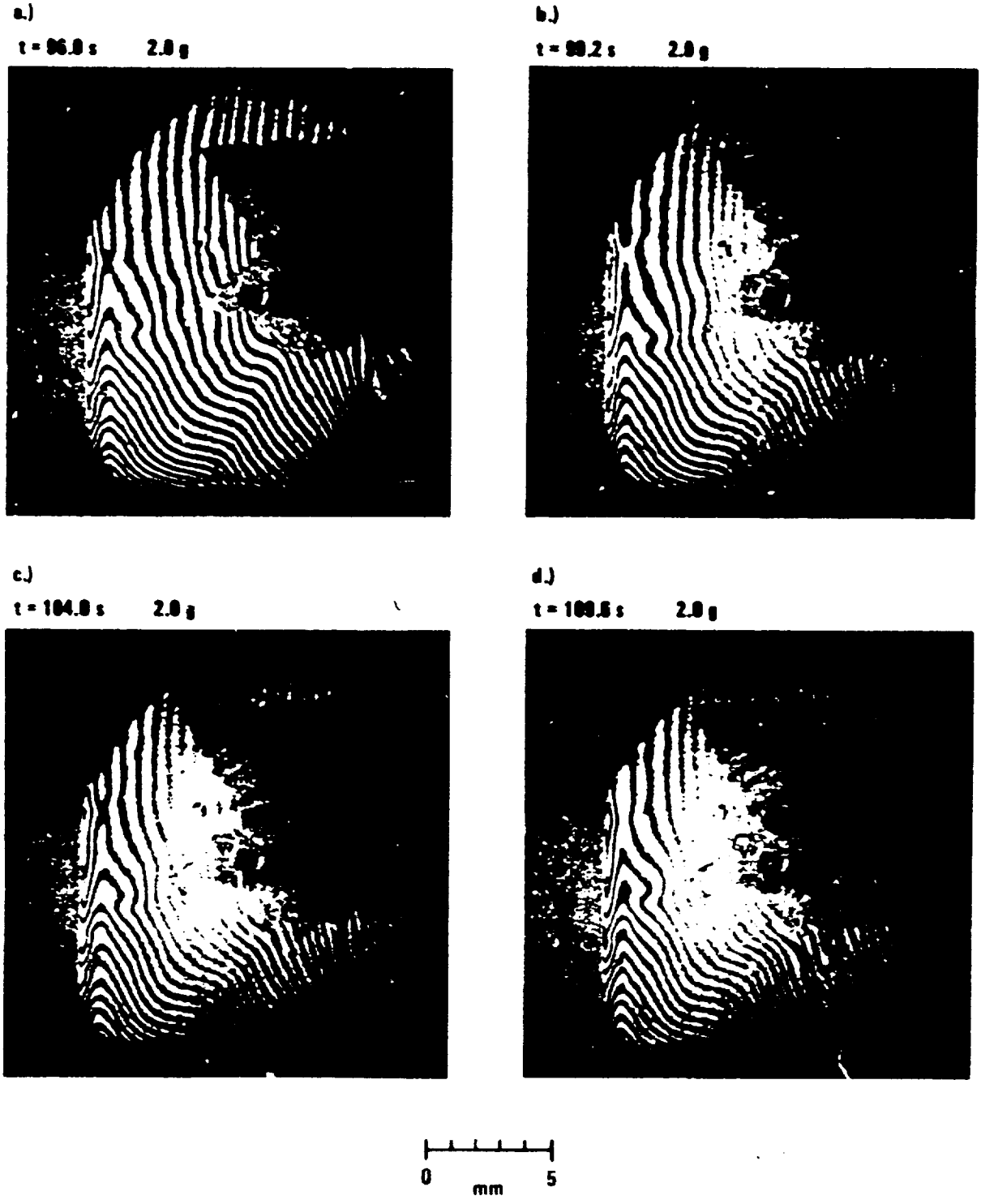

Fig. 40 Influence of high gravity on plume convective velocity and growth rate of a horizontally growing ice dendrite in 6.0% 1.07M NaCl. Supercooling 1.1°C.

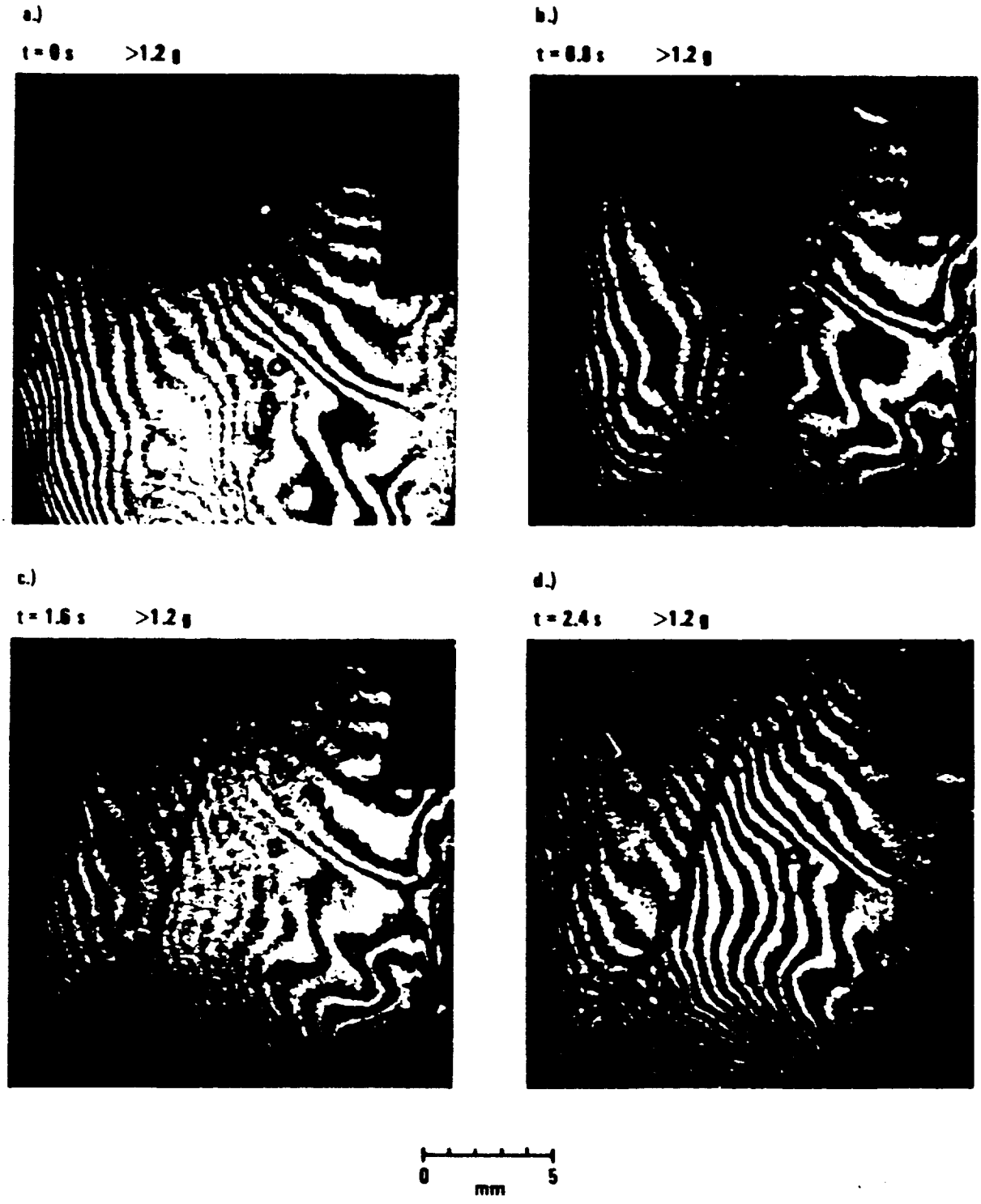

Fig. 41 Nucleation and growth of convective plume transported crystals. NaCl solution 6.0% 1.07M supercooling 1.3° C. The crystals nucleate along the plume injected downward from the capillary tube after the initial nucleation (a, b). As they grow they rise (g > 1.2 in each case), the crystal line becoming unstable. The higher density fluid is apparently carried along with the crystals and does not have time to drain.

e.)
t = 3.2 s >1.2 g

f.)
t = 4.8 s >1.2 g

g.)
t = 4.8 s >1.2 g

h.)
t = 5.6 s >1.2 g

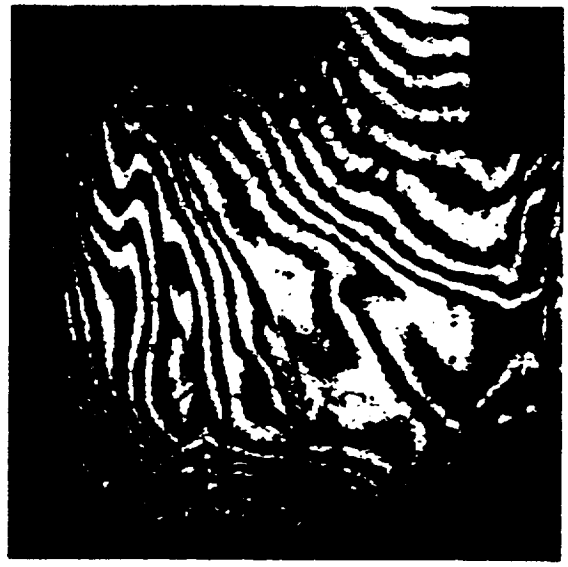

Type II on the other hand as with ice in sodium chloride, fails to initiate convection until well after the dendrite growth front has passed, irrespective of the orientation. Convection eventually begins from the bulk of the dendrite mass in definite drainage channels, leading to laminar descending plumes.

The time constant for convection in the first case is subjected to an increasing diffusion boundary layer thickness which detaches as its dimension becomes large enough (the criterion for convection, R_a is proportional to d^3); in the second case the reason appears to be residual crystallization in the crystal mesh rejecting further solute until the bouyancy is sufficiently large to produce convection. This crystallization persists over an extended period of time for sodium sulfate, giving rise to local motion in the crystal interstices and results in a slow crystallization consistent with the slow increase of temperature.

Significant questions remain concerning the rate of mass crystallization of an isolated given volume of solution, and the physics of the process of crystallization, recrystallization and Ostwald ripening over times long compared with the initial growth of dendrites following nucleation.

Influence of ventilation on crystal growth velocity

It is evident that increase of ventilation increases crystal growth velocities both for solution and vapor phase growth. The functional dependence on velocity reflects a complex series of physical processes. It is necessary to distinguish between these cases where the crystals retain a faceted periphery with unchanging aspect ratio - this appears to be the case for $NaNO_3$ investigated by Kirkova and Nikolaeva (1983) and for sodium decahydrate, Chen et al., 1979 - from those cases where the crystal aspect ratio changes, and in turn from those cases there comes sprout to give dendrites or needles. In the former case, growth rate increases, initially linearly with velocity to a maximum value, for ventilation between 5 and 15 cm s^{-1} increasing with supersaturation. This can

be interpreted as a reduction of the boundary layer thickness such that the crystallization process is dominated entirely by kinetic effects and the surface supersaturation approaches that of the environment. In the latter case, for ice from the vapor in air the velocity dependence found by both Keller and Hallett (1982) and Alena and Hallett (1987) shows a velocity dependence which increases slowly at first and approaches $v^{1/2}$ only at velocities > 10 cm s^{-1} where heat/mass transfer dominate (see Miksch, 1969; Cantor et al, 1972). These changes are associated with the transition of a thick crystal to a thinner crystal to needle or dendrite sprouts, and shares comparable behavior, only with different geometry for column → needles and plates → dendrites.

The supersaturation dependence of growth rate shows a similarly complicated behavior, as the shape of the crystal changes. A satisfactory theory is difficult to formulate, since the physical processes responsible for these transitions are evidently related to changing surface kinetic processes at different places on the crystal in relation to fluid motion. A picture can be hypothesized, that, as the local supersaturation increases, a transition from defect growth to corner surface nucleation occurs - the absence of defects for growth of ice plates gives evidence for this. With supersaturation or ventilation increase, surface nucleation begins at corners where local supersaturation is greatest; growth can still occur as facets should layers propogate rapidly to the facet center. There comes a critical supersaturation where layers fail to complete and hopper crystals form; the extreme case is the needle or dendrite which completely lack facets at the tip.

The local supersaturation effectively increases as ventilation velocity increases. The transition plates → column shown in Fig. 14 under low supersaturation shows a kinetic effect which would be expected to be influenced by low velocities in 1 g and require higher supersaturation in low g. The growth rates are much too slow for this observation in the KC 135 environment, and would require the longer periods available in the Shuttle or space station.

This can be quantatively analyzed as follows:

Enhancement of growth by ventilation results from a thinning of the boundary layer, the effect subsequently related to the ratio of the momentum/thermal boundary layer (Prandtl number) and the momentum/diffusion boundary layer. In a gas these are comparable; in a water solution these rates are 13 and 1600 respectively; hence the transport of heat and solute are controlled by the velocity profile. Empirically, this gives, for a sphere; (Pruppacher and Klett, 1978) enhanced transport by the factor shown in Table 4.

In low g, the velocities of transport and convection in solution are ~ 0.2cm s^{-1} and tip radii ~ 100 μm, so that the transport dependence is right in the transition regime between U and $U^{1/2}$. For growth from the vapor, for falling crystals at 20-40 cm s^{-1}, the regime is clearly $U^{1/2}$. In the diffusion chamber, between 0 and 2 g (Fig. 13) the linear crystal growth rate approximately doubles. This implies a convection or an imposed velocity of ~ 2 cm s^{-1} ($U^{1/2}$ dependence) (assuming a $U^{1/2}$ dependence a tip dimension of 100 μm and $\nu = 0.25$ cm^2 s^{-1} at 800 mb). In one g this would be equivalent to 1.4 cm s^{-1} (transfer $\propto g^{1/2}$) and it remains a question as to whether such a velocity would effect a habit change if persisting for a long period - for example, would columns in one g at 1.4 cm s^{-1} convective ventilation grow as plates in low g at zero ventilation?

9. OVERALL CONCLUSIONS.

These experiments, although limited in scope by the short low gravity time (~20 s) in a KC 135 parabola, lead to some intriguing questions. There appears to be a real effect in growth rate of ice dendrites from the vapor, with higher g forces giving faster growth. There is a definite effect in convection around sodium decahydrate dendrites in solution, but not around ice dendrites in NaCl solution. There is an effect in convection in interstices of a crystal-

TABLE 4

	mass:	$1 + 0.11\ Sc^{2/3}\ Re$	$0.78 + .31\ Sc^{1/3}\ Re^{1/2}$
	heat:	$1 + 0.11\ Pr^{2/3}\ Re$	$0.78 + .31\ Pr^{1/3}\ Re^{1/2}$
solution	mass:	$1 + 87\ U$	$.78 + 8.7\ U^{1/2}$
solution	heat:	$1 + 3.5\ U$	$.78 + 1.8\ U^{1/2}$
air	mass:	$1 + 0.05\ U$	$.78 + 0.2\ U^{1/2}$
air	heat:	$1 + 0.06\ U$	$.78 + .24\ U^{1/2}$ $(U\ cm\ s^{-1})$

$$1.4 > Sc^{1/3}\ Re^{1/2} > 1.4$$

Transition velocity criteria for a sphere:

		1 mm	100 mm
for solute in water,	$U < 0.05\ cm\ s^{-1}$ (mass)		$.0[illegible]\ cm\ s^{-1}$
	$U < 0.24\ cm\ s^{-1}$ (heat)		$.1\ cm\ s^{-1}$
for water vapor in air,	$U < 3.8\ cm\ s^{-1}$ (mass)		$1.0\ cm\ s^{-1}$
	$U < 1.8\ cm\ s^{-1}$ (heat)		$.5\ cm\ s^{-1}$

Enhancement of transport vapor in air and solute in water with ventilation for a sphere, as influenced by the transport velocity.

lizing mush, related to pore size. Generally, some indication of convective effects can be assessed from Gr > 10. Under the conditions of these experiments, Re < 100, plume equilibrium rise is laminar, although starting plumes may be oscillatory.

The KC-135 is an ideal environment for semi-quantitative laboratory bench type of experiments where the time frame is long enough, since we can obtain immediate comparison of the effect of low (.05) g and high (2) g on growth and convection. These experiments are however limited by short time, and the turbulence level of the aircraft under typical clear air conditions ($\pm$ 0.05 g).

Many questions remain on the nature of convection on the systems studied. Whilst it appears evident that dendrites and needles growing from either solution or vapor have a moleculary rough interface, the growth mode of the faceted crystals under low supersaturation is still unclear. The presence of defects (screw dislocations) may be important for growth under these conditions and needs to be investigated. Equally important, the role of slow convection in enhancing local supersaturation, may be important in the crystallization processes, since under these conditions growth rate is proportional to the square of the supersaturation. These questions are of a fundamental nature, and apply to the growth of any crystal.

The transition to growth rate proportional to supersaturation once a critical value for surface nucleation is reached may also be influenced by low flow velocity. This is suggested by the ground based experiments on habit change of ice growth from the vapor at low supersaturation. These are relevant to solidification of a bulk sample (a metal casting) where both initial dendrite growth, secondary crystallization by dendrite motion in the resulting overall convection and final crystallization of the aggregate are all important. Each stage is influenced by the presence of a gravitational field and the resulting fluid flow.

In the absence of kinetic considerations, the adiabatic thermal behavior of a supercooled solution for ice crystallization or hydrate crystallization would be identical. The base equations (1, 2) show that the thermal wave spreads out more quickly from the crystal than the concentration wave, which is controlled by the low diffusivity of the ions in solution. The observed crystallization rates are rapid, so that beyond a few degrees supercooling a laboratory sized sample would be solidified to a fraction consistent with its initial supercooling - ~ 6% for the case of ice supercooled by 5°C. The observations show that the temperature rise to near the equilibrium point in either case for ice is instantaneous - within the response time of the measuring system (< 0.1 s). By contrast the response time for the sodium sulfate is much slower. This is consistent with a kinetic effect, implying that there are no barriers to ice crystallization - we know that growth in the "a" axis direction is not limited by kinetics. By contrast, we have evidence that decahydrate crystallization is limited by kinetics at supercooling less than 1-2° C. It follows that initial crystallization in the former case proceeds until the equilibrium temperature is reached to less than 0.1°C within the time resolution of the temperature measurement; in the second case lower non-kinetic limited growth proceeds until the supercooling is ~ few °C, beyond which kinetic limitations are rate limiting and the temperature rises more slowly.

These considerations lead to the following conclusions:

- For dendritic and slower (faceted) growth, convection rates are important in impurity segregation under quite specific conditions. These depend on crystal kinetics, density excess, initiation of convection, and the fluid thermal and diffusion properties.
- Convection is important in vapor growth in changing kinetics under conditions typical of the atmosphere; it is only important in ice growth in solutions at small supercooling and long times.

- Convection is only important in sodium sulfate growth at moderate supercooling and under these conditions segregation and defect structure could be significantly influenced by lack of convection in low g.
- Dendrite tip crystallization is influenced by convection in some systems; this effect can be removed under low g. For these not so influenced, single narrow filaments uninfluenced by convection can be produced in the ground laboratory by withdrawing the dendrite tip at the crystallization velocity. The technique may not be possible for a system exhibiting tip convection, when an extended low g environment may be advantageous and allow large dendrite width at lower supercooling to be produced. The role of electromagnetic damping needs to be investigated in this situation.
- Inhibition of secondary crystals in larger systems by removal of collision breeding in a non-convecting low g environment can significantly influence complete solidification of a melt; crystal rearrangement by surface tension effects would become dominant.
- The low g environment is valuable for differentiating between buoyant and inertial effects in ideal fluid flow systems such as vortex ring propagation or plume tip rise.

An ideal growth arrangement for such studies will require not only the uniform low g of space but the capabilities of high g (by a centrifuge) for comparative purposes. The comparative effect of the high/low g on KC135 have demonstrated the utility of changing g in a controlled way. Future plans for space-station material science and fluid mechanics studies need to take these criteria into account.

REFERENCES

Alena, T. and J. Hallett, 1987: Column-needle transition of ice crystal growing from the vapor. (In preparation).

Bennema, P., 1969: The importance of surface diffusion for crystal growth from solution. J. Crystal Growth, 5, 29-43.

Cantor, B. and A. Vogel, 1977: Dendritic solidification and fluid flow. J. Crystal Growth, 41, 109-123.

Carruthers, J.R., 1976: Origins of convective temperature oscillation in crystal growth melts. J. Crystal Growth, 32, 13-26.

Chen, P.S., P.J. Shlichta, W.R. Wilcox and R.A. Lefever, 1979: Convection phenomena during the growth of sodium chlorate crystals from solution. J. Crystal Growth, 47, 43-60.

Curtis, B.J. and J.P. Dismukes, 1972: Effects of natural and forced convection in vapor phase growth systems. J. Crystal Growth, 17, 128-140.

Daley, S.F., 1984: Frazil ice dynamics CRREL Monograph 84-1, p. 46.

Estrin, J., 1975: Secondary nucleation due to fluid forces on a polycrystalline mass of ice. A I Ch E. J., 21, 392-395.

Evans, L.F., 1973: The growth and fragmentations ice crystals in an electric field. J. Atmos. Science, 30, 657-664.

Eisenberg, D. and W. Kauzmann, 1969: The structure and properties of water. Oxford, Univ. Press.

Fang, Q.T., M.E. Glicksman, S.R. Coriell, G.B. McFadden and K.F. Bolsvert, 1985: Convective influence on the stability of a cylindrical solid-liquid interface. J. Fl. Mech., 151, 121-140.

Garabedian, H. and R.F. Strickland-Constable, 1974: Collision breeding of ice crystals. J. Crystal Growth, 22, 188-192.

Gilmer, G.H. and P. Bennema, 1972: Simulation of crystal growth with surface diffusion. J. Appl. Physics, 43, 1347-1360.

Gilpin, R.R., 1976: The influence of natural convection on dendritic ice g wth. J. Crystal Growth, 36, 101-108.

Glicksman, M.E., 1984: Free dendritic growth. Materials Science and Eng. 65, 45-55.

Glicksman, M.E., G.B. McFadden, S.R. Coriell, R.F. Bolsvert and Q.T. Fang, 1984: Morphological stability in the presence of fluid flow in the melt. Met. Trans., 15A, 2117.

Glicksman, M.E. and P.W. Voorhees, 1985: Thermal measurement of Ostwald ripening kinetics in partially crystallized mixtures. J. Crystal Growth, 72, 599-615.

Glicksman, M.E., S.R. Coriell and G.B. McFadden, 1986: Interaction of flows with the crystal melt interface. Am. Rv. Fl. Mech., 18, 307-335.

Gonda, R. and M. Komabayasi, 1971: Skeletal and dendritic structures of ice crystals as a function of thermal conductivity and vapor diffusivity. J. Met. Soc., Japan, 49, 32-42.

Hallett, J., 1964: Experimental studies of the crystallization of supercooled water. J. Atmos. Sci., 21, 671-682.

Hallett, J., 1968: Nucleation and growth of ice crystals in biological systems. Published in Low Temperature Biology of Foodstuffs, 23-52, Pergamon Press, Oxford.

Hallett, J., 1984: How snow crystals grow. American Scientist, 72, 582-589.

Hallett, J., 1987: Faceted snow crystals. J. Opt. Soc. Am., 4, 581-588.

Hallett, J. and B.J. Mason, 1958: The influence of temperature and supersaturation on the habit of ice crystals grown from the vapor. Proc. Roy. Soc., A247, 440-453.

Hallett, J. and E. Wedum, 1978: Influence of convection on free growth of dendrite crystals from solution. UAH/NASA Workshop on Fluids Experiment System. The Univ. of Alabama - Huntsville. p.211-224.

Hallett, J., N. Cho, C. Fought, G. Keyser, R. Purcell, C. Saunders and A. Tomana, 1982: Concept and implementation of ice crystal growth and drop freezing experiments in a low gravity environment. Final Report: NASA NAS8-32977.

Harrison, K. and J. Hallett, 1986: On the freezing of supercooled aqueous solution and atmospheric chemical reactions. Preprints, Conference on Cloud Physics, Snowmass, CO, Sept. 22-26, p.C67-C70.

Holder, D.W. and R.J. North, 1956: Schlieren methods. NARA/AGARDOGRAPH V25, Part I.

Huang, S.C. and M.E. Glicksman, 1981a: Fundamentals of dendritic solidification I. Steady state tip growth. ACTA Met., 29, 701-715.

Huang, S.C. and M.E. Glicksman, 1981b: Fundamentals of dendritic solidification II. Development of sidebranch structure. ACTA Met., 29, 717-734.

Humphries-Owen S.P.F., 1949: Crystal growth from solution. Proc. Roy. Soc., A197, 218-237.

Huppert, H.E. and M.G. Worster, 1985: Dynamical solidification of a binary melt. Nature, 314, 703-707.

Katz, J.L. and P. Mirabel, 1975: Calculation of supersaturation profiles in thermal diffusion chambers. J. Atmos. Sci., 32, 646-652.

Keller, V., C.Y. McKnight and J. Hallett, 1979: Growth of ice discs from vapor and the mechanism of habit change of ice crystals. J. Crystal Growth, 49, 648-664.

Keller, V. and J. Hallett, 1982: Influence of air velocity on the habit of ice crystal growth from the vapor. J. Crystal Growth, 60, 91-106.

Kikuma, I. and A. Vogel, 1977: Dendritic solidification and fluid flow. J. Crystal Growth, 41, 109-125.

Kirkova, E. and R. Nikolaeva, 1983: Influence of the flow velocity supersaturation and temperature on the crystal growth from solutions. Crys. Res. and Tech., 18, 743-754.

Kirshenbaum, I., 1959: Physical properties and analysis of heavy water. McGraw Hill.

Knight, C., 1971: Breeding of crystal nuclei by classical nucleation: Theory of some observations and experiments. J. Crystal Growth, 11, 201-217.

Kurz, W. and D.J. Fisler, 1987: Dendrite growth at the limit of stability. ACTA Met., 29, 11-20.

Laxmanan, V., 1985a: Dendritic solidification I. ACTA Met., 33, 1023-1035.

Laxmanan, V., 1985b: Dendritic solidification II. ACTA Met., 33, 1037-1049.

Laxmanan, V., 1985c: Dendritic solidification III. ACTA Met., 33, 1475-1480.

Luten, D.B., 1934: The refractive index and density of solutions of D_2O in H_2O. Phys. Rev., 45, 163.

Mason, B.J., 1971: The physics of clouds. Oxford Univ. Press.

Mehu, A., R. Abjean and Johannin-Gilliert, 1966: Measure comparative des indices de refraction l'eau legere et de l'eau lounge a different temperatures. Application a la measure de concentrations des solution de H_2O - D_2O. J. Chem. Phys., 63, 1569-1574.

Miksch, E.S., 1969: Solidification of ice dendrites in flowing supercooled water. Trans. Metallurgical Soc. of AIME, 245, 2069-2072.

Mullins, W.W. and R.F. Sekerka, 1963: Morphological stability of a particle growing by diffusion or host flow. J. Appl. Physics, 34, 323-329.

O'Hara, M. and R.C. Reid, 1973: Modelling crystal growth rates from solution. Prentice Hall, Inc.

O'Hara, S. and W.A. Tiller, 1967: On the mechanisms of crystal multiplication during solidification in the presence of fluid motion. Trans. Metallurgical Soc. of AIME, 239, 497-501.

Ovinko, D.E., G.A. Alfinser and W.V. Moshov, 1974: Kinetics and shape of crystal growth from its melt for substances with low L/KT value. J. Crystal Growth, 26, 233-238.

Owen, R.B., 1982: Interferometry and holography in a low-gravity environment. Appl. Optics, 21, 1349-1355.

Powers, D.J., S.C. Colbeck and K. O'Neill, 1985: Thermal convection in snow. CRREL Report 85-9, p.70.

Pruppacher, H. and J.D. Klett, 1978: Microphysics of clouds and precipitation. Reidel Publishing Co.

Reid, R.C. and T.K. Sherwood, 1966: The properties of gases and their liquids. Second Ed. McGraw Hill.

Ryan, B.F., E.R. Wishart and D.E. Shaw, 1976: The growth rates and densities of ice crystals between -3 and -21°C. J. Atmos. Science, 33, 842-850.

Schaefer, R.J., M.E. Glicksman and J.P Ayers, 1975: Dendritic crystallization in succinonitrile; impurity effects. Phil. Mag., 32, 725-743.

Schnepple, W., L Vandenberg and N. Skinner, 1987: Spacelab 3 vapor growth experiment. p.12-15 NASA publ. 2622a.

Tewari, S.N. and V. Laxmanan, 1987: A critical examination of dendrite growth models; a comparison of theory with experimental data. ACTA Met., 35, 175-183.

Tilton, L.W. and J.K. Tugler, 1938: Refractive index and dispersion of distilled water for visible radiation at temperatures 0 to 60°C. J. Res. Nat'l. Bur. Standards, 20, 419-477.

Turner, R.S., 1973: Bouyant convection. Cambridge University Press, p. 215.

Vlahakis, J.G. and A.T. Burduhn, 1974: Growth rate for ice crystal in flowing water and salt solution. AlCh.E.J., 20, 581-587.

Acknowledgement

This report includes results from work carried out under a previous NASA contract NAS8-32977 as well as the new results from the present contract NAS8-34605. The experiments under variable gravity were sponsored by NASA Headquarters Microgravity Science and Applications Division.

The KC-135 aircraft work was carried out under the direction of Robert Shurney of Marshall Space Flight Center, whose help was vital to the success of the project. Parts of this report are included in the Ph.D dissertation of Dr. N. Cho, and the M.S. theses of K. Harrison, A. Lord and E. Wedum in the Department of Physics, University of Nevada, Reno.

APPENDIX

Physical properties of solutions.

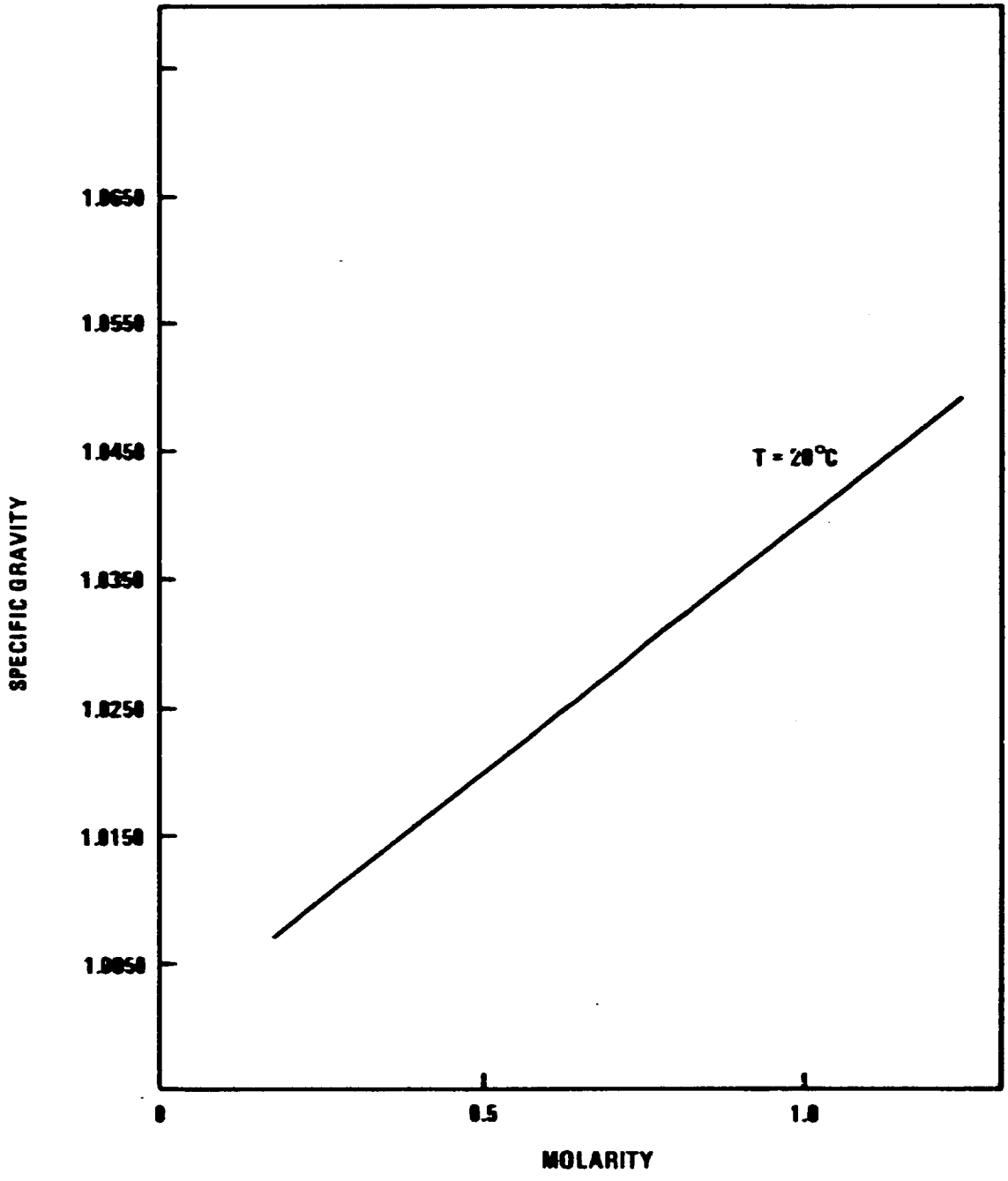

A-1 Specific gravity - molarity for sodium chloride solution.

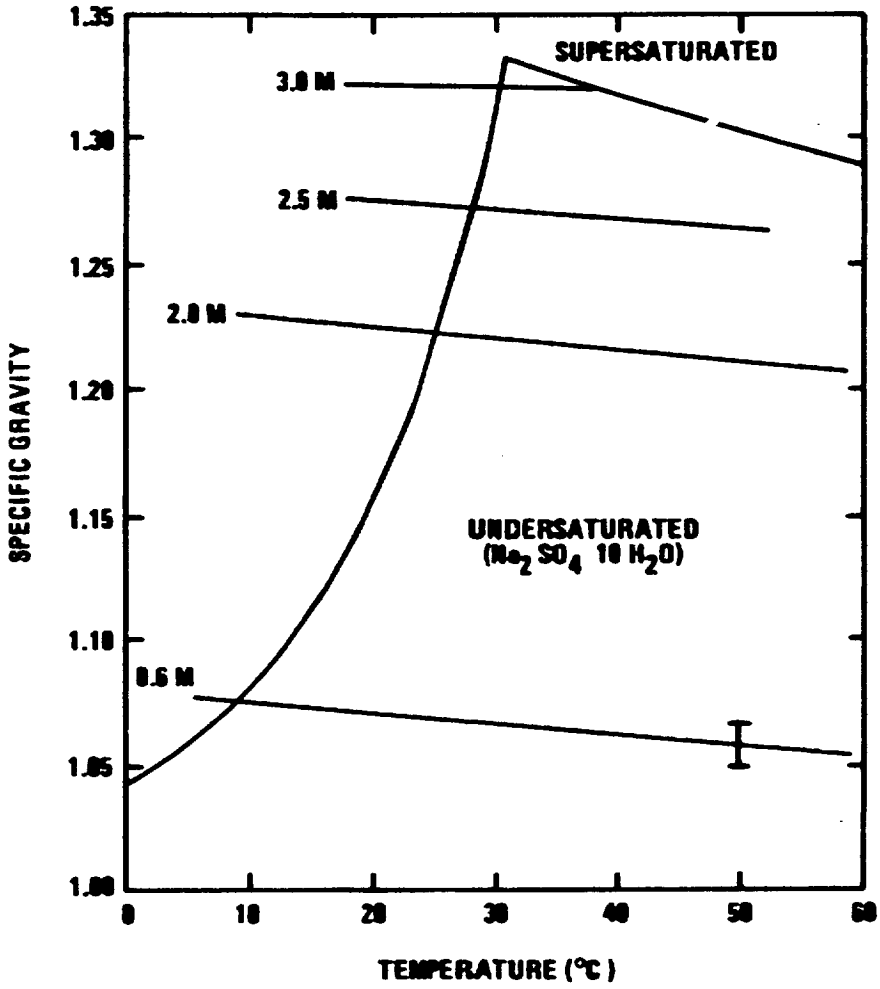

A-2 Specific gravity - molarity for different temperatures of sodium sulfate solutions. The curved lines are equilibrium for the decahydrate and the anhydrite.

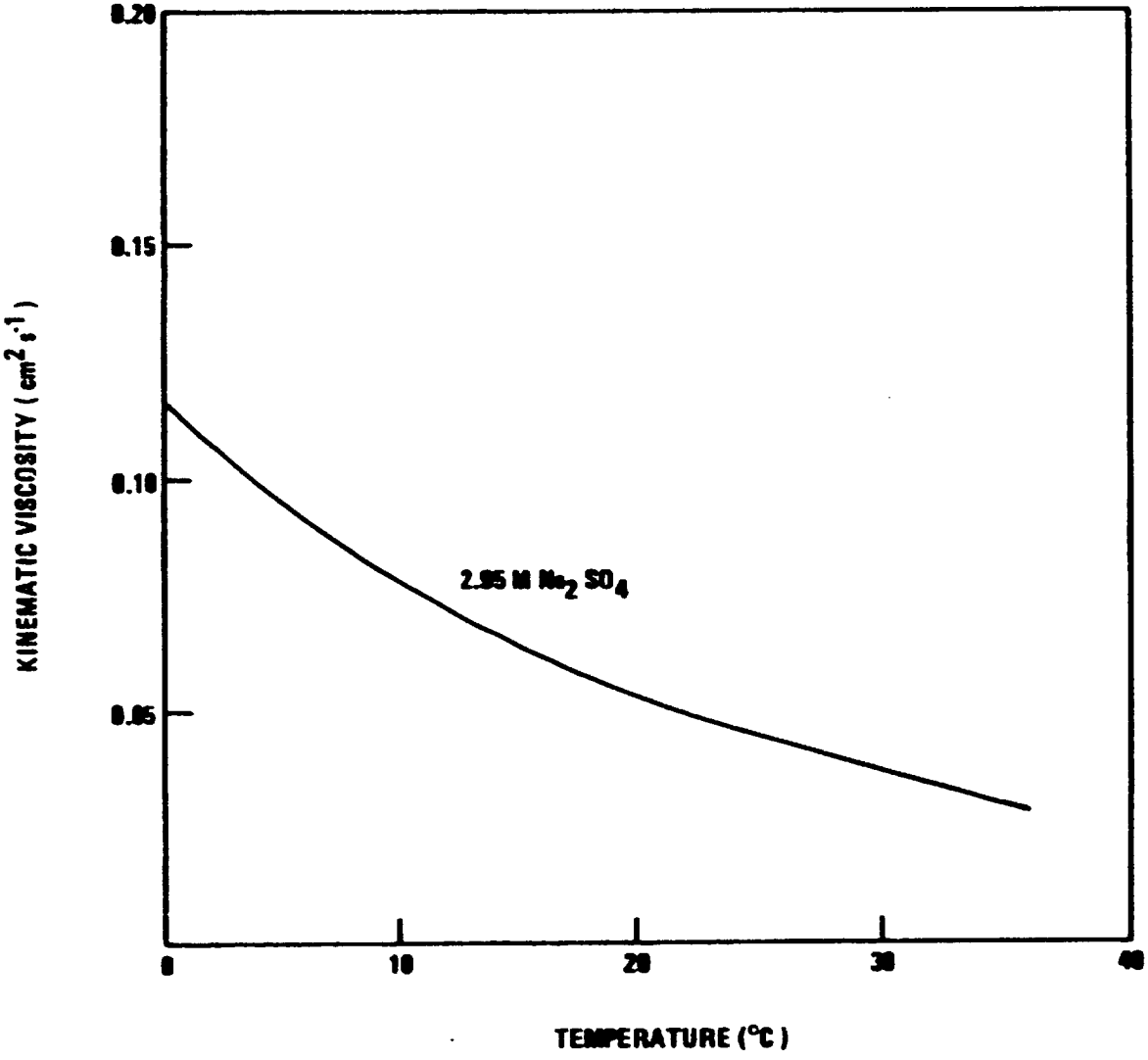

A-3 Temperature dependence of the Kinematic viscosity of 2.95 M sodium sulfate solution.

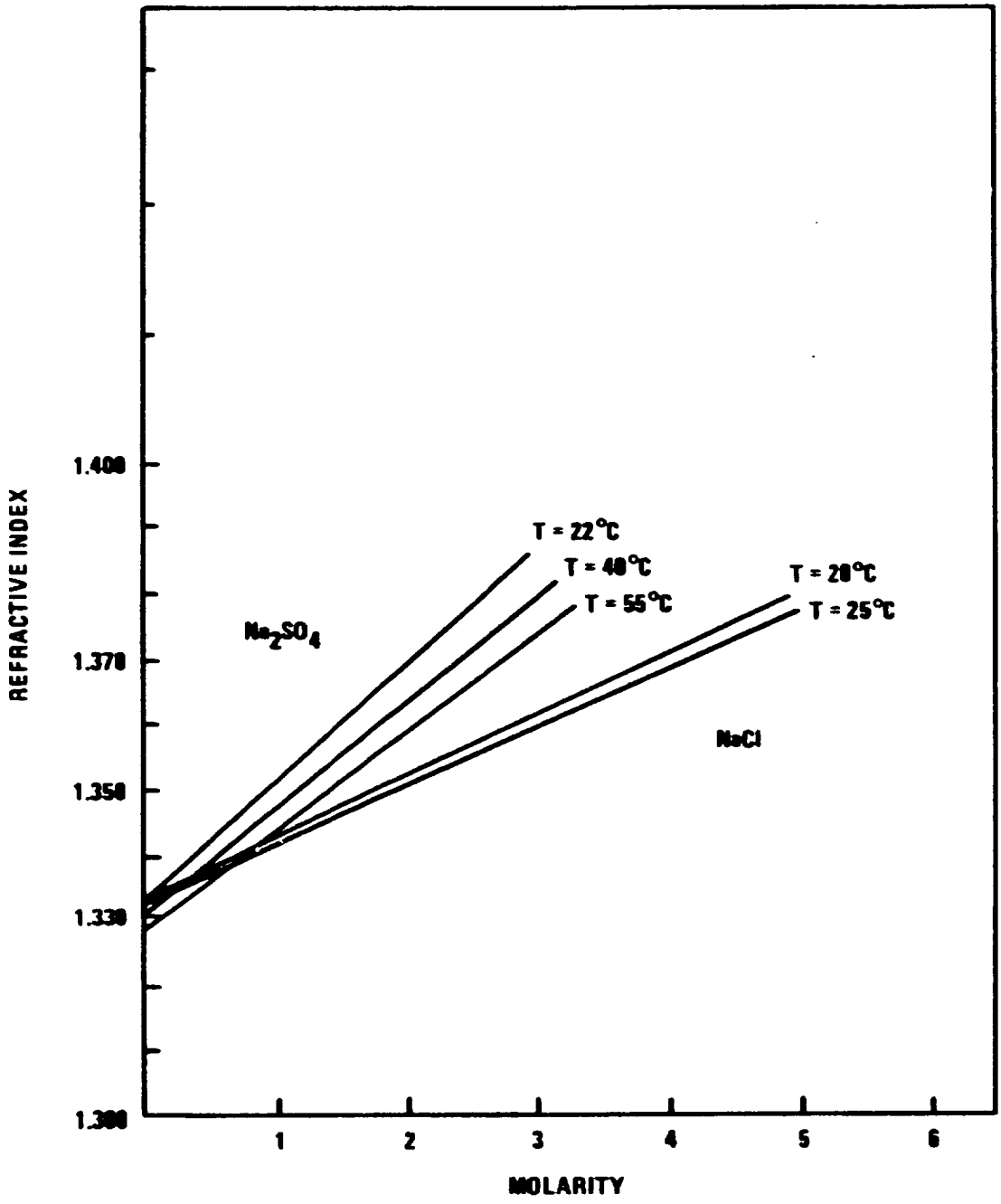

A-4 Refractive index for sodium sulfate and sodium chloride solutions.

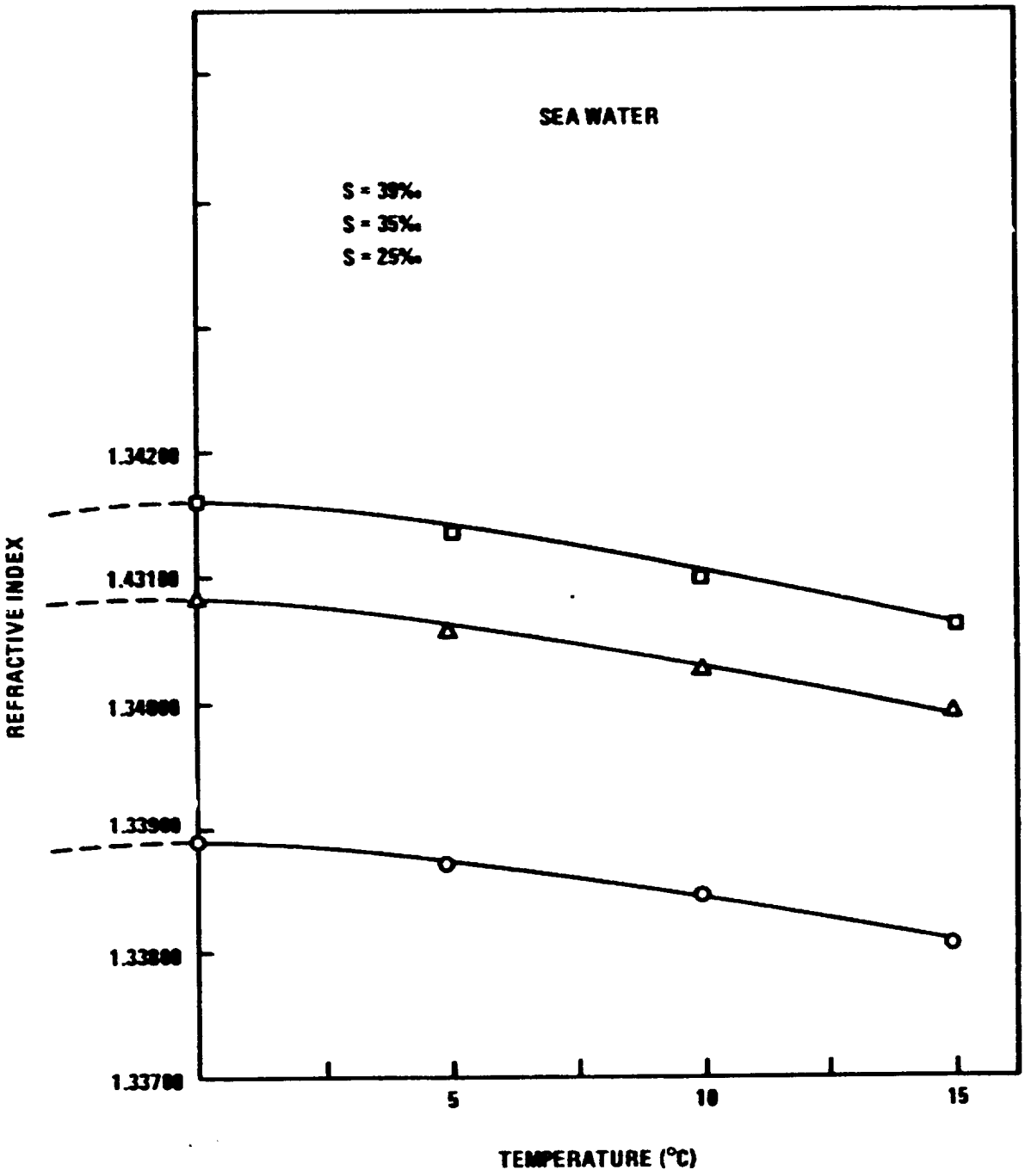

A-5 Temperature dependence of refractive index for sea water.

Figure Captions

Fig. 1. a, b Containers for investigating crystallization of uniformly supercooled liquids. Nucleation is achieved by injecting a cold wire or a seed crystal into the narrow plastic tube. The larger container (b) enables the growing crystal to be moved at a fixed velocity up to 0.5 cm s^{-1} relative to the liquid. Volume (a) 10 ml, (b) 100 ml.

Fig. 2a Thermal diffusion chamber for ice crystal growth from vapor under controlled temperature, and supersaturation.

Fig. 2b Thermal diffusion chamber for ice crystal growth from vapor under controlled temperature, and supersaturation. Typical temperature and supersaturation profiles
A 0.59°C mm^{-1} B 0.47°C mm^{-1} C 0.37°C mm^{-1}

Fig. 2c The dynamic chamber for controlled ventilation at velocities up to 1/2m s^{-1}.

Fig. 3a Schlieren optical system for investigation of crystal growth in solution.

Fig. 3b Mach Zender interferometer for KCl35 solution growth study.

Fig. 4 Growth condition in a vapor with variable carrier gas diffusivity. Conduction dominates in the absence of a carrier gas, and the crystal surface temperature approaches that for a vapor pressure at the environmental temperature. When diffusion dominates (carrier gas at high pressure) the crystal and environment are almost isothermal.

Fig. 5 Increase of Temperature with Time during Adiabatic Crystallization of Sodium Sulfate decahydrate from solution. Trace of temperature recorded by thermocouple shown in Fig. 1a. Crystallization appeared complete after 2 minutes, but final temperature was not reached until 4 minutes later.

Fig. 6 Increase of temperature following adiabatic crystallization of ice from NaCl solution. Note that the initial temperature of the solution is 0.25°C below that of the equilibrium temperature of the original solution; resulting from solute rejection during ice crystal growth.

Fig. 7 Cross section of static diffusion chamber for ice crystal growth in air or helium at controlled pressure.

Fig. 8 Chamber filling and flushing connections.

Fig. 9 Layout of static diffusion chamber for ice crystal growth from the vapor. It is mounted in palette ready for KC135 parabolic trajectory flights.

Fig. 10 Vertical and lateral g component during low g KC135 parabola and high g pullout. The effect of turbulence along the flight path gives g uncertainty $\pm$ 0.05 in low g and 1.8 $\pm$ 0.1 in high g with lateral turbulence effects $\pm$ 0.05 g.

Fig. 11 Ice crystals growing in the static diffusion chamber at temperature - 5° C, ice supersaturation 40% in helium at 500 mb pressure.

Fig. 12 Linear growth velocity of ice crystals in helium for different pressures.

Fig. 13 Growth of ice crystals in helium (500 mb) showing lower growth rate in low g and higher growth rate in high g.

Fig. 14a, b Habit dependence of ice growth from the vapor in air on supersaturation at - 5°C. Initial growth: 12% over ice giving a column; later growth : 1% over ice giving a plate (a); final growth at 5% over ice to give a hollow column (b).

Fig. 15 Refractive index of water shows a flat maximum just below the equilibrium fusion point H_2O, and just above for D_2O. In either case, the difference was not great enough to give visible effects in the Schlieren system.

	Temperature of maximum density	Melting point	Temperature of maximum refractive index
H_2O	+4°C	273.15°C	-2
D_2O	+11°C	276.97°C	+7

Fig. 16 Phase diagram for sodium sulfate - H_2O solution. Point A represents conditions of a supersaturated solution, 2.2 M; supercooled by 6.9°C. On nucleation, crystals grow with a driving force equivalent to the intersection of the horizontal line with the equilibrium, ΔM = 0.8 M

Fig. 17 Sodium Sulfate Decahydrate Crystals Growing into Supersaturated Solution from a nucleation teflon tube below the surface.

Three crystals are visible; a tiny one at 3 o'clock, the longest one (whose growth rate was measured) at 4 o'clock, and one growing downward at 5 o'clock. The two vertical lines (a, b) at the left are the plumes of depleted solution.

Growing crystals appear dark, because the picture is printed from Plus-X Reversal 16 mm movie film. 3.0 M, ΔT = 4.3° C.

Fig. 18: Comparison of Characteristic Length, d, with Supercooling and Concentration sodium sulfate decahydrate.

a) 3.0 M, ΔT = 4.3° C,
d = 0.16 cm, R = 0.02 cm s^{-1}.

b) 3.0 M, ΔT = 7.7° C,
d = 1.7 cm, R = 0.2 cm s^{-1}.

c) 2.5 M, ΔT = 7.2° C,
d = 0.6 cm, R = 0.1 cm s^{-1}.

d) 2.5 M, ΔT = 8.9° C,
d = 1.8 cm, R = 0.2 cm s^{-1}.

Fig. 19a Relation of characteristic length and supercooling for plume detachment for a crystal of sodium sulfate decahydrate growing horizontally.

Fig. 19b Mach Zender interferogram of 2 M. Na_2SO_4 - 10 H_2O crystals growing in solution, 1 g. at supercooling 2.4°C.
This shows a low density plume rising some 3 mm behind the growing tip, indicating a higher concentration on both sides (a, b). An instability (soliton) moves down the crystal (e) to be released towards the tip (f).

Fig. 20 Plume from a moving crystal in 2.5 M Na_2SO_4 solution.
Supercooling ΔT = 4.8° C. Crystal moved left to right at 0.15 cm s^{-1} between t = 17 s and t = 78 s.
a, b, c show the starting plume.

Fig. 21 Plume from a moving crystal in 1.0 M Na_2SO_4 solution.
Supercooling ΔT = 5.5° C. Crystal moved left to right at 0.26 cm s^{-1} between t = 17 s and t = 29 s.

Fig. 22 Successive stages of plume behavior of ice crystals growing in 1.0 M NaCl solution. Supercooling $\Delta T = 0.5°$ C. Crystal moved left to right at 0.15 cm s^{-1} between t = 34 s and t = 59 s.

Fig. 23 Growth and convective velocity as a function of supercooling in Na_2SO_4 solution for a stationary crystal at different molarities. Convective velocity at 3 M not available.

Fig. 24 Growth and convective velocity for $Na_2SO_4.10H_2O$ crystals in 2.5 M Na_2SO_4 supersaturated solution as a function of supercooling. Moved at a velocity V_T = 0.15 cm s^{-1} through the solution.

Fig. 25 Ice crystal growth under stationary and 0.12 cm s^{-1} transport velocity in 0.2 M NaCl solution.

Fig. 26 Growth and convective velocity for ice in 0.4 M NaCl supercooled solution as a function of supercooling. Transport velocity V_T = 0.17 cm s^{-1}.

Fig. 27 Growth and convective velocity for ice in 1.0 M NaCl supercooled solution determined by supercooling and transport velocity.

Fig. 28 Growth and convective velocity for ice in supercooled sea water as a function of supercooliing at transport velocity V_T = 0.15 cm s^{-1}.

Fig. 29 Growth and convective velocity for 1.0 M and 2.0 M sodium sulfate solution. Transport velocity V_T = 0.26 cm s^{-1}.

Fig. 30 Growth and convective velocity for sodium sulfate 2.5 M solution. Transport velocity V_T = 0.15 cm s^{-1}.

Fig. 31 Ice growth and convective velocity for 0.4 M and 1.0 M NaCl solution. Transport velocity V_T = 0.15 cm s^{-1}.

Fig. 32 Growth and convective velocity as a function of crystal transport velocity for different molarities, supercooling 5.5° C. Arrows indicate expected growth rate in low g in absence of convection observed in 1.0 g.

Fig. 33 Ice crystal growth rate and convection velocities at different transport velocity for NaCl solution, 0.2 M and 1.0 M. Arrows indicate expected growth rate in low g in absence of convection observed in 1.0 g.

Fig. 34 (a-x) Crystal growth and convection in 2.3 M sodium sulfate solution. Nucleation was achieved by inserting a decahydrate crystal into the tube. Initial equilibrium temperature 27.0°C; initial supercooling 5.1°C giving $\Delta n_\lambda = 0.06$ ($\lambda = .6328$ μm) (from Fig. A4).

Photography of a growing crystal began in low gravity (a), continued for ~ 17 s at g ~ 0.05 ± .02 (with variability due to atmospheric turbulence) and then continued as g increases to > 1.2 g. Growth rates are given for crystal A, B, C, h in Fig. 35.

A plume of low density had emerged from the capillary (k, l) and is essentially stationary during low g, but accelerated upward as g increased. Two other plumes rise from the horizontal crystals as gravity increases k 2, 3. The main set of fringes are from monochromatic light (0.6328 μm) with fringe spacing and detail in uniform density resulting from inhomogenities in the container and the angular offset of the mirrors. The close fringes shown at the bottom of the cell results from the curvature of the glass. Narrow diffraction fringes occur around all regions of sharp discontinuity, and are ignored in this analysis.

Sequence 1: a - p shows crystal growth and plume development going from low to high g.

Sequence 2: q - x shows plume development in high g, decreasing on entry into low g.

The boundary layer around the downward oriented crystal D(t) remains unchanged from high g to low g, but increases as g increases (w, x). The boundary layer around the slant crystal E(t) decreases in thickness as the tip convection decreases and finally ceases in low g.

Crystals still move around under low g presumably because of capillary effects.

Fig. 35 Crystal growth rates and plume rise velocity during gravity change from low to high. Data from Fig. 34, A,B,C,h; 1, 2, 3, k

Fig. 36 A bouyant plume which emerged from the nucleation tube in high g remains almost stationary in low g (a - i), accelerates as g increases (j - l). A vortex ring is created from a fallen crystal (out of the field of view) rises as g increases (m - n). Initially a wake is evident, but is not apparent at a later stage (s,t). u-z shows a further sequence with different internal structure. Supercooling 2. 5°C.

Fig. 37 a, b, c Velocity of the plume and vortex ring in Fig. 36a related to gravity. There is an apparent decrease of vortex ring velocity as it rises, in both cases. g magnitude is not available in this region.

Fig. 38 A downward growing ice crystal in 6.0% 1.07M NaCl (ΔT = 1.3° C) gives no convective plume in low g and takes ~ 13 s to initiate a downward convective plume in high g. The crystal rotates and grows slightly faster on entry into high g.

Fig. 39 Growth velocity of the downward oriented dendrite (Fig. 38) is unrelated to g. The plume of high concentration NaCl solution takes ~ 10 s before leaving the dendrite mush.

Fig. 40 Influence of high gravity on plume convective velocity and growth rate of a horizontally growing ice dendrite in 6.0% 1.07M NaCl. Supercooling 1.1°C.

Fig. 41 Nucleation and growth of convective plume transported crystals. NaCl solution 6.0% 1.07M supercooling 1.3° C. The crystals nucleate along the plume injected downward from the capillary tube after the initial nucleation (a, b). As they grow they rise (g > 1.2 in each case), the crystal line becoming unstable. The higher density fluid is apparently carried along with the crystals and does not have time to drain.

Appendix - Figure Captions

A-1 Specific gravity - molarity for sodium chloride solution.

A-2 Specific gravity - molarity for different temperatures of sodium sulfate solutions. The curved lines are equilibrium for the decahydrate and the anhydrite.

A-3 Temperature dependence of the Kinematic viscosity of 2.95 M sodium sulfate solution.

A-4 Refractive index for sodium sulfate and sodium chloride solutions.

A-5 Temperature dependence of refractive index for sea water.